THE
PHYSICAL REVIEW
A Journal of Experimental and Theoretical Physics Established by E. L. Nichols in 1893
VOL. 58, NO. 7 OCTOBER 1, 1940 SECOND SERIES

Further Investigations of the Air Mass Effect on Cosmic-Ray Intensity

D. H. LOUGHRIDGE AND PAUL F. GAST
University of Washington, Seattle, Washington
(Received July 29, 1940)

The existence of an effect upon cosmic-ray intensity at the boundaries separating different types of air masses is clearly established by the results of these observations, and has lately received additional confirmation from the work of Nishina, Sekido, Simamura, and Arakawa.* This effect is evidently of the type postulated by Blackett to explain the seasonal variation in cosmic-ray intensity, although in this case both temperatures and pressures in the upper air contribute to the change. Work is now in progress to compare cosmic-ray intensities with the daily meteorological sounding balloon records which have recently become available.

INTRODUCTION

WHEN Blackett[1] introduced his explanation of the temperature effect of cosmic rays, he suggested that it might be possible to correlate variations in cosmic-ray intensity with the structure of cyclonic depressions. The authors have previously reported[2] in a brief note some experimental results bearing on this problem. However, the results reported there were subject to considerable uncertainty because of the small number of individual cases reported. Therefore, the present investigation was undertaken to put the experimental findings on a firmer footing and also to include in the present report a more complete description of the meteorological phenomena involved.

It is well known[3] that cyclones in temperate latitudes generally have associated with them sharp boundaries across which there is a marked variation in meteorological variables, especially temperature and humidity. These are the so-called fronts. The upper portion of Fig. 1 gives a cross section in an east-west plane of a typical warm front. The warm air on the left is running up over the denser cold air on the right along the surface of discontinuity. The whole system has a net west to east motion. Sounding balloon

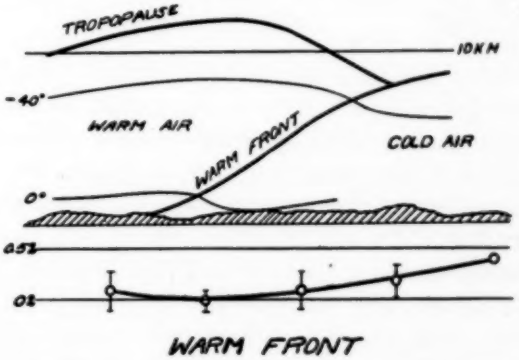

FIG. 1. Cross section of a typical warm front and the mean intensity curve for cosmic rays observed at the passage of such a front. It is to be emphasized that the warm front is a generalized one and does not represent the exact conditions under which the measurements are carried out.

* Y. Nishina, Y. Sekido, H. Simamura and H. Arakawa, Phys. Rev. **57**, 1050 (1940) and Phys. Rev. **57**, 663 (1940).
[1] P. M. S. Blackett, Phys. Rev. **54**, 973 (1938).
[2] D. H. Loughridge and P. F. Gast, Phys. Rev. **56**, 1169 (1939).
[3] See for example: Namias *Air Mass Analysis* (Milton, Massachusetts, 1938); Humphreys *Physics of the Air* (McGraw-Hill, Philadelphia, 1930); or any modern text on meteorology.

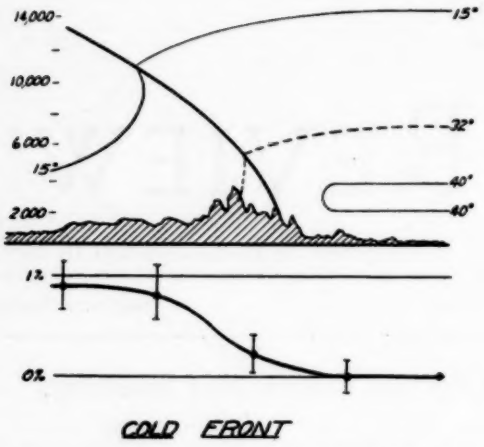

FIG. 2. Cross section of typical cold front with the intensity curve for cosmic rays below.

flights[4] have shown that these primary disturbances as such do not extend into the stratosphere but that there are secondary disturbances produced in that region. These disturbances consist essentially in an upward shifting of the base of the stratosphere with the arrival of warm air masses below and a corresponding downward shift with the arrival of cold air. These shifts are manifested by changes in pressure and temperature in the stratosphere with the passage of a front below. If one assumes the laws of a perfect gas to hold for the air in this region, and further assumes the usual exponential decrease of density with height, then one obtains, as was previously pointed out[2] the following expression for the shift in height of a layer of given density

$$Z_1-Z_0=\frac{RT}{Mg}\ln\frac{(P_1T_0)}{(P_0T_1)},$$

where Z indicates height of the layer and the subscripts 0 and 1 refer to the initial and final values of the variables. Experimental values of pressure, temperature, etc., give values of Z_1-Z_0 ranging from 500 to 1000 meters at an altitude of from 14 to 16 km. Smaller changes would be expected at higher altitudes. This is just such a shift as Blackett requires for his "temperature effect." The change of intensity at the earth's surface being given by

$$dI/I=-dZ/L,$$

where L is the mean range of the mesotrons. This investigation was undertaken to determine experimentally whether such an effect existed.

APPARATUS

The apparatus consisted of a high-pressure ionization chamber, of the Carnegie model C type,[5] shielded by 12 cm of lead. This apparatus was mounted in a specially constructed, thermally insulated, deck house aboard the *M. S. Northland* traveling between Seattle, Washington and Juneau, Alaska. The apparatus was originally put in service to determine the latitude effect between these two points. For the investigation of the air mass alone, a permanent location ashore would have perhaps been preferable.

EXPERIMENTAL PROCEDURE

The apparatus gave hourly values of the ionization produced by cosmic rays. This value was then reduced to a standard barometric pressure of 30 in. of Hg by applying a linear correction obtained by fitting a straight line to the intensity *versus* barometer data obtained at a fixed latitude over a long period.[6] This correction amounted to -4.5 percent per inch of Hg. Six hourly means were then computed from these corrected values. The intensity in the vicinity of all the barometric lows was next investigated. The intensity for the six-hour period in which the lowest barometer occurred was noted, as well as the intensities for

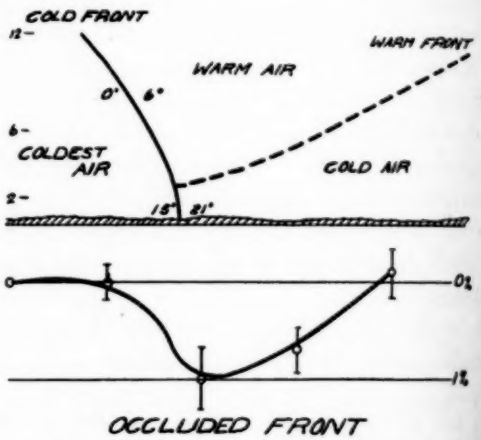

FIG. 3. Cross section of a typical occluded front with cosmic-ray intensity curve below.

[4] J. Bjerknes, Geofys. Pub. 9 No. 9 (1933) and J. Bjerknes and E. Palmen, Geofys. Pub. 12, No. 2 (1937).

[5] A. H. Compton, E. O. Wollan and R. D. Bennett, Rev. Sci. Inst. 5, 415 (1934).

[6] P. S. Gill, Phys. Rev. 55, 1151 (1939).

the two six-hour periods just preceding and the two just following the low. The time at which the low occurred and the position of the ship were also noted. The weather maps for these times were then consulted at the Seattle airport office of the U. S. Weather Bureau to determine what type of front, if any, was passing over the ship in each instance. The individual instances were thus sorted out into warm fronts, cold fronts, etc. A mean curve of cosmic-ray intensity *versus* time was then determined for each type of front.

Results

Of the 75 barometric lows investigated, 6 were warm fronts, 17 were cold, 34 were occlusions, 13 contained no fronts, and 5 involved more than a single front passing the apparatus in the 30-hour period investigated (five six-hour periods). These five were not included in the following results. The results are given in Figs. 1 through 4. Figure 1 shows the results for warm fronts, the upper portion, as mentioned before, gives a vertical section of the atmosphere, whereas the lower curve shows the change in cosmic-ray intensity as we pass from the cold to the warm air. Since the individual fronts occurred at different times of the year and were thus subject to the "seasonal" effect as well as to other world-wide changes in intensity, individual variations occurred at different general levels of intensity. In computing the mean curve and the probable errors, the individual curves were shifted up or down until they all coincided at the point on the right. The probable errors were then computed in the usual way for the other points on the curve. It is to be noted, however, that they do not represent errors in the usual sense, since there is no reason to expect all individual fronts to produce the same variation.

Figure 2 gives the results for the 17 cold fronts observed. The upper portion of the figure contains a cross section of a typical cold front. The cold air on the left is driving under the warmer air on the right and as is the case with all the fronts the whole system has a west to east, or, in the figure, a left to right motion. The mean curve is computed in the same way as for the warm fronts.

In Fig. 3 an occluded front is represented in which a mass of warm air has been cut off, or

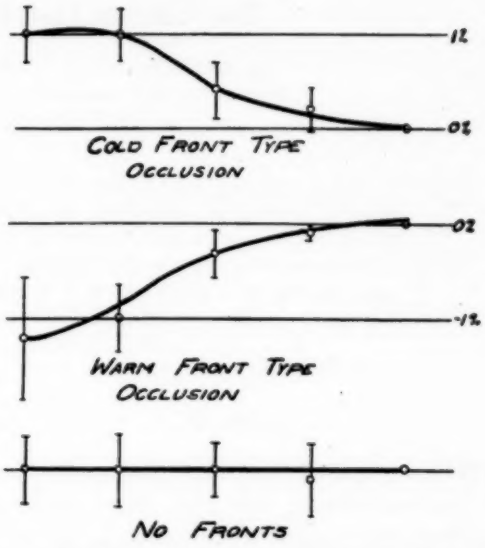

Fig. 4. The upper curve shows mean cosmic-ray intensity change at a cold front type occlusion, the center curve at a warm front type. The bottom curve gives mean intensity change at passage of low containing no fronts, showing that ordinary barometer correction is adequate in these cases.

"occluded," from the surface by colder air masses. The mean curve for fronts of this type of which there were 15 is shown in the lower portion of the figure. As is to be expected it shows a decrease when the warm air is overhead and a corresponding increase with the influx of the cold air. When an occluded front contains only a small pocket of warm air trapped by colder air below, the effect of the warm air is negligible and the change in intensity is mainly determined by whether the air following the front is colder or warmer than the air preceding. Curves for fronts of this type are shown in Fig. 4. The cold front type is the mean of 14 instances and the warm front type the mean of 5.

The lower curve in Fig. 4 shows the mean curve for the 13 lows which contained no fronts.

In conclusion, we wish to express our sincere appreciation to Dr. Arthur H. Compton for making available the apparatus and for helpful discussion of the results. Also we are indebted to the Northland Transportation Company for the use of space aboard their ship, to Mr. B. W. Joyce, First Officer of the *M. S. Northland* for careful attention to the apparatus, and finally to Mr. J. C. Smith and the staff of Seattle Airport Station of the U. S. Weather Bureau for their friendly cooperation.

The Carbon Isotopes of Mass Ten and Eleven

L. A. DELSASSO, M. G. WHITE, W. BARKAS, AND E. C. CREUTZ
Palmer Physical Laboratory, Princeton University, Princeton, New Jersey

(Received August 8, 1940)

C^{11} has been produced by two new reactions; namely, $B^{11}(p,n)C^{11}$ and $N^{14}(p,\alpha)C^{11}$. The upper limit of the positron spectrum of C^{11} has been measured in a cloud chamber and the value 0.95 ± 0.03 Mev obtained. A new isotope, C^{10}, has been produced by the reaction $B^{10}(p,n)C^{10}$. This nucleus has a disintegration period of 8.8 ± 0.8 sec. The upper limit of the positron spectrum was found to be 3.36 ± 0.1 Mev. A discussion is given of the relation which these measurements bear to the isobaric splitting and systematic properties of light nuclei.

INTRODUCTION

THE isotope C^{11} has been produced in several laboratories[1,2] by (p,γ), (d,n) and $(n,2n)$ reactions and is one of the best known of the light positron emitting nuclei. In a preliminary report[3] investigations of two additional processes producing C^{11} were described.

The accepted value[1] for the energy of C^{11}, namely, 1.15 Mev, was obtained under conditions where contamination by N^{13} was probable. This circumstance, together with the fact that the computed disintegration energy of C^{11} suggests a discrepancy, made it important to remeasure this quantity. Recent preliminary observations[4] of the threshold for the $B^{11}(p,n)C^{11}$ reaction likewise indicate that the C^{11} beta-radiation cannot be so energetic as previously supposed.

From the computations of Bethe[5] it appeared quite certain that C^{10} should be stable against disintegration into heavy particles. Because no nucleus of this type was known, and because of the importance of a knowledge of the period and disintegration energy of C^{10} for an understanding of the systematic properties of light nuclear systems, the problem of its production and study seemed to merit attention.

In this paper we report a measurement of the beta-ray energy of C^{11} and describe experiments in which C^{10} was produced and its period and disintegration energy measured.

EXPERIMENTAL

The reactions we have studied were induced by protons of energy up to 6.4 Mev from the Princeton cyclotron. Boron targets were prepared simply by pressing amorphous boron into pieces of clean sheet lead. This method has been found convenient for making targets of many materials which occur in powdered or crystalline form. No appreciable activity is induced in the lead itself.

Bombardments were made in an atmosphere of hydrogen in a chamber open at one end, but through which a sufficient flow of hydrogen was maintained from the other end to prevent air from coming in contact with the target. The beam entered the target chamber through a window of 0.4-mil aluminum. This arrangement permitted the removal of the target without delay, yet avoided contamination by the disintegration products of air. The hydrogen also helped to cool the target. As previously described,[3] bombardment of targets in air always yielded a contamination activity of C^{11} from $N^{14}(p,\alpha)C^{11}$ as well as F^{17} and F^{18} from the bombardment of oxygen. With the present arrangement the amount of contamination is negligible except with certain kinds of target materials which adsorb gases, or with very long bombardments.

Half-life measurements were made with electroscopes of the Lauritsen quartz-fiber type. The short period of C^{10} was determined, after some experimentation, by simultaneously photographing a stop watch dial and the projected

[1] Fowler, Delsasso and Lauritsen, Phys. Rev. **49**, 561 (1936).
[2] Crockcroft, Gilbert and Walton, Proc. Roy. Soc. **A148**, 225 (1935); H. R. Crane and C. C. Lauritsen, Phys. Rev. **45**, 497 (1934); Pool, Cork and Thornton, Phys. Rev. **52**, 239 (1937); Yost, Ridenour and Shinohara, J. Chem. Phys. **3**, 133 (1935).
[3] W. Barkas, Phys. Rev. **56**, 287 (1939).
[4] Haxby, Shoupp, Stephens and Wells, Phys. Rev. **57**, 567 (1940).
[5] H. A. Bethe, Phys. Rev. **54**, 436 (1938).

shadow of the fiber as it passed over a graduated scale. The photographs were taken at intervals of about one second. In the early work[3] on the bombardment of boron by protons the period of C^{11} was the only one which was definitely present. With higher energy protons and short bombardment times the additional short period expected of C^{10} appeared. Under the best conditions we have obtained C^{10} with an initial activity equal to that of C^{11}. It was found possible also to increase considerably the ratio of C^{10} to C^{11} activity by absorbing out much of the softer beta-radiation from C^{11} by interposing aluminum absorbers between the source and the electroscope.

The energy measurements of the beta-rays from C^{11} were carried out in a cloud chamber equipped with a well projecting through the glass top into the chamber. In the side of the well was a copper foil window with a surface density of 11.6 mg/cm². The chamber was filled with hydrogen and ethyl alcohol vapor. Tracks measured satisfied the following criteria: (a) no visible scattering, (b) at least 10 cm in length, (c) coming apparently from the source. The illumination in the chamber was confined to a region about one centimeter in depth so no correction for the component of momentum parallel to the field was necessary. Photographs were taken with a single Sept camera placed directly above the chamber. The developed photographs were reprojected through the same lens system and curvature of the tracks compared with a set of curves accurately drawn on white paper.

Our magnetic field intensity was determined fairly well by computation from the geometry of the Helmholz coils, and from flip coil measurements. A final accurate value was obtained by placing in the field the chamber of a 180° focusing beta-ray spectrometer and photographing the standard internal conversion lines from the active deposit of thorium. These lines have been carefully measured by Ellis[6] and more recently by Flammersfeld.[7] The field measurement is therefore referred directly to this discrete beta-ray spectrum.

[6] C. D. Ellis, Proc. Roy. Soc. **A138**, 318 (1932).
[7] A. Flammersfeld, Zeits. f. Physik **114**, 227 (1939).

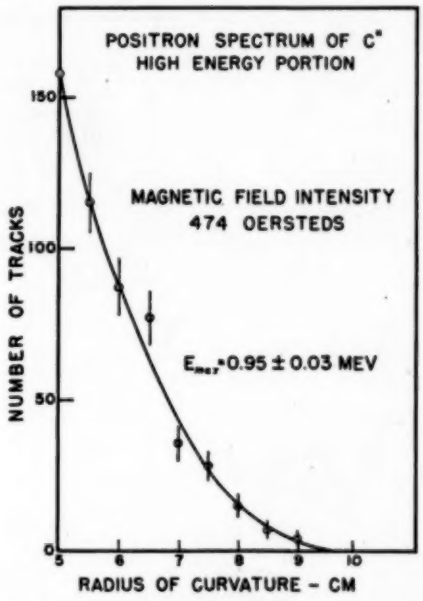

FIG. 1. Momentum distribution of the positrons from C^{11}. A cloud-chamber foil correction of 0.02 Mev has been added to the visually extrapolated upper limit.

The technique for measuring the C^{10} disintegration energy was as follows: The cloud chamber was placed about thirty feet away from the cyclotron at a lower level away from the stray magnetic field and rather well protected by earth from neutrons and gamma-rays. Targets were bombarded in the cyclotron for ten seconds, then placed in a brass capsule which fitted snugly into a pneumatic tube. In this way the target was delivered to the cloud chamber in about two seconds. The total time elapsed between the removal of the target from the beam until the cloud chamber expanded was about four seconds. Using a cycle of ten seconds between cloud-chamber expansions the target was, however, usually strong enough to be used for a second expansion. In spite of the aid of these improved techniques, however, a large amount of labor was required to accumulate the spectrum obtained. This is because only about one-fifth of the boron nuclei are those of B^{10}, and in addition the threshold for the (p,n) reaction in B^{11} is much lower than in B^{10} so that the beta-rays of C^{10} which extend above the energy distribution of those of C^{11} are relatively rare. About half the tracks obtained for C^{10} were photographed with air in the chamber. These electrons showed no essential difference in

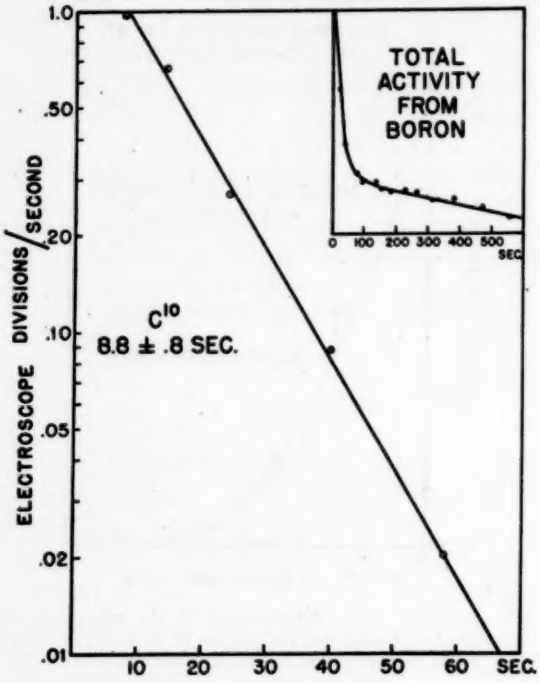

FIG. 2. A typical C^{10} decay curve. The insert curve shows to what extent it was necessary to allow for the C^{11} activity.

distribution from those photographed in hydrogen so the two sets of data were added together. Indeed, for such high energy electrons air is perhaps preferable to hydrogen because of the better definition of the tracks produced by slower diffusion of the droplets and greater ionization.

RESULTS

The accepted value[8] for the period of C^{11} is 21 minutes. We have made many incidental observations of this period, and this figure is near the mean of our experimental values. We cannot claim, however, accuracy to better than about one percent. The older value[9] of 20.5 minutes is, nevertheless, definitely too low.

In Fig. 1 is the observed momentum distribution of the positrons from C^{11}, giving an upper limit of 0.95 ± 0.03 Mev. Because of the lead backing used for our boron targets, and because of the scattering in the target well of the cloud chamber, as well as the indeterminate solid angle into which the lower energy electrons are emitted, we have not included the low energy portion of the spectrum. All targets used for measuring the C^{11} spectrum were aged for at least one minute to permit the C^{10} activity to disappear before observations were made.

The period of C^{10} was found to be 8.8 ± 0.8 sec. In Fig. 2 is shown one of the decay curves observed, and the curve obtained after the C^{11} activity was subtracted.

The momentum distribution of the positrons from C^{10} in the region above the upper limit of the C^{11} spectrum is shown in Fig. 3. From this one obtains an upper limit of 3.36 ± 0.1 Mev.[10]

That the short period is really associated with C^{10} by $B^{10}(p,n)C^{10}$ one concludes from the circumstance that all other energetically possible reactions lead to well-known products, none of which so far has been found to have an isomeric form.

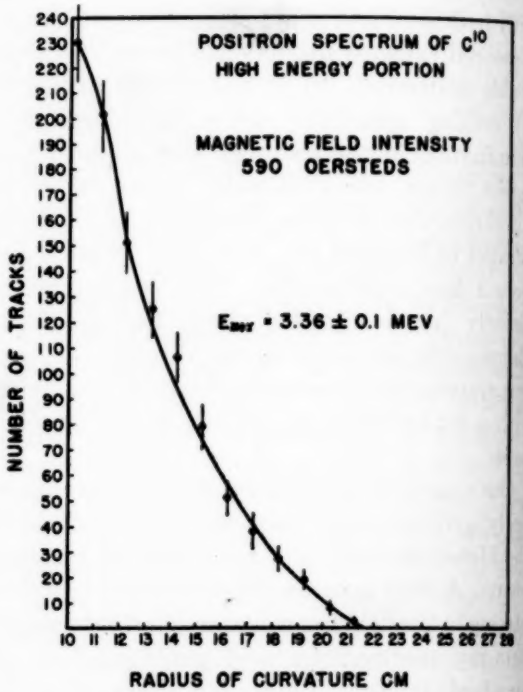

FIG. 3. Momentum distribution of the high energy end of the positron spectrum of C^{10}. Foil correction of 0.03 Mev has been added to the visually extrapolated upper limit.

[8] J. J. Livingood and G. T. Seaborg, Rev. Mod. Phys. 12, 30 (1940).
[9] M. S. Livingston and H. A. Bethe, Rev. Mod. Phys. 9, 359 (1937).

[10] The error placed on the upper limit neglects the possibility of recoil Si nuclei from the aluminum window. However, from a consideration of the difference in the upper limits of C^{10} and Si^{27} and the range of heavy particles, it is believed that this would not increase the value by more than 0.05 Mev.

Discussion

Beta-disintegration energies arise from mass differences between isobars, which for light elements show the influence of four terms, each of which by various means[11,12] may be isolated for study. These are as follows: (a) the mass difference between a neutron and a proton, (b) the electrostatic energy difference between a charge Ze and a charge $Z'e$ confined to the nuclear volume, (c) the effect of "spin dependent" forces, (d) the effect of the Pauli principle on the symmetry properties of the nuclei.

In the mass difference between C^{11} and B^{11} only the terms (a) and (b) are expected to appear. Using the simple formula[11,13]

$$\Delta E = 0.594(A-1)A^{-\frac{1}{3}} \text{ Mev},$$

where A is the mass number, which gives the binding energy difference for two such isobars, one computes a value of 0.91 Mev for the upper limit of the positron spectrum. The agreement with the observed limit of 0.95 ± 0.03 Mev is satisfactory especially in view of the rather detailed, though reasonable, assumptions involved in the calculation. A similar good agreement has been found[13,14] for other light isobaric pairs of this type.

C^{10} is unique in that it has the greatest excess of protons of any known nucleus. The triplet of isobars C^{10}, B^{10} and Be^{10} provides data from which one may draw quantitative conclusions regarding the terms contributing to the isobaric splitting. C^{10} and Be^{10} are believed to be homologs since one may be obtained from the other merely by exchanging the protons and neutrons. That the interaction between two neutrons is essentially the same as that between two protons except for the electrostatic force is verified by the agreement between computed and observed disintegration energies of the odd nuclei (e.g., C^{11} in this paper). Therefore, one should expect C^{10} and Be^{10} to differ in mass only by terms (a) and (b), both of which are known fairly accurately. Taking the mass of B^{10} to be 10.01578 we obtain from our measurement of the beta-radiation a mass of 10.02048 for C^{10}. One may compute[12] the Coulomb energy difference between C^{10} and Be^{10} to be 5.33 mMU, while the mass difference between two neutrons and hydrogen atoms is 1.6 mMU. Our mass of C^{10} together with these estimates for the terms (a) and (b) imply a mass of 10.01675 for Be^{10}. Pollard[15] has measured the energy of protons, presumably from the reaction $Be^9(D,p)Be^{10}$, indicating an energy release of 4.52 Mev. With 9.01482 for the mass[16] of Be^9 the value of 10.01656 is then implied for Be^{10}. The agreement between these values for Be^{10} to within less than 0.2 Mev is as good as could reasonably be expected considering that the probable error in each of the intermediate masses is about this order of magnitude. We may take this as another numerical example to illustrate to what extent two useful and simplifying assumptions of current nuclear theory are justified. These are (1) that the protons have a uniform distribution throughout a nuclear volume which is proportional to the mass number, and (2) that, except for the electrostatic force, the interaction between two protons is the same as between two neutrons.

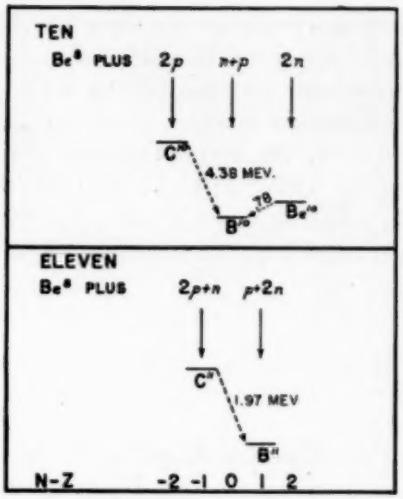

FIG. 4. Diagrammatic representation of the isobaric splittings at mass numbers ten and eleven.

[11] E. Wigner, Phys. Rev. **51**, 947 (1937).
[12] W. Barkas, Phys. Rev. **55**, 691 (1939).
[13] White, Delsasso, Fox and Creutz, Phys. Rev. **56**, 512 (1939).
[14] W. Barkas, E. C. Creutz, L. A. Delsasso, R. B. Sutton, and M. G. White, Phys. Rev. **58**, 383 (1940).
[15] E. Pollard, Phys. Rev. **57**, 241 (1940).
[16] Allison, Skaggs and Smith, Phys. Rev. **57**, 550 (1940).

One may also evaluate the term (c), the effect of which is apparent in nuclei containing an odd neutron and an odd proton such as B^{10}. The disintegration energy of C^{10} we observed to be 4.38 Mev. The terms (a) and (b) account, however, for only 2.01 Mev. One deduces therefore, that the extra binding energy in B^{10} due to a term of type (c) amounts to 2.37 Mev.

In Fig. 4 is shown graphically the relative masses of the isobars at mass numbers 10 and 11.

The half-life and beta-ray energy found for C^{10} may be interpreted[11] to mean that transitions between the even-even and odd-odd isobars are of the "allowed" type. In some other cases (e.g., for Na^{22} and P^{30}) this does not, however, seem to be true.

OCTOBER 1, 1940 PHYSICAL REVIEW VOLUME 58

On the Angular Distribution of Fast Neutrons Scattered by Hydrogen, Deuterium and Helium

H. H. BARSCHALL AND M. H. KANNER
Palmer Physical Laboratory, Princeton University, Princeton, New Jersey

(Received July 8, 1940)

The angular distribution of *d–d* neutrons scattered by hydrogen, deuterium and helium was measured by observing the distribution in energy of the recoil particles in an ionization chamber. The scattering in hydrogen and deuterium was found to be essentially isotropic in the angular interval investigated. In helium, collisions with small energy transfer were more frequent than large angle scattering. The absolute differential scattering cross section of helium was measured.

I. INTRODUCTION

MEASUREMENTS of the energy of fast neutrons or the angular distribution of scattered neutrons have in the past been carried out principally in the cloud chamber. This method is the most direct and accurate; however, the evaluation of the experiments is tedious if good statistical accuracy is required.

In the present experiments an attempt is made to measure distributions both in angle and in energy in an ionization chamber by recording the energy of the recoil particles produced in the chamber. The use of an ionization chamber for energy measurements was first proposed by Baldinger, Huber and Staub.[1] These authors derived a simple formula which enables one to obtain the distribution in energy, $S(E)$, of the primary neutrons from the energy distribution $H(E)$ of the recoil particles. For the case in which the scattering is isotropic in the center of mass system and the whole range of the recoil particles is contained in the chamber they show that

$$S(E) = -\frac{1}{n \cdot \sigma(E) \cdot d} E \frac{dH}{dE}, \qquad (1)$$

where $\sigma(E)$ is the scattering cross section of the gas in the chamber, n the number of gas atoms/cm³, d the depth of the chamber. Their experiments were carried out in a chamber filled with He. After the experiments of Staub and Stephens[2] had shown that $\sigma(E)$ for He is strongly dependent on energy around 1 Mev it seemed preferable to use hydrogen for such experiments.

With hydrogen, one is confronted with the difficulty that the recoil protons from fast neutrons have very long ranges. Since the experiments have to be carried out in such a way that the range of the recoils is small compared with all dimensions of the chamber, it is necessary to use very high pressures for measurements in hydrogen in order to reduce the range. Energy measurements in an ionization chamber filled

[1] E. Baldinger, P. Huber and H. Staub, Helv. Phys. Acta 11, 245 (1938).

[2] H. Staub and W. E. Stephens, Phys. Rev. 55, 131 (1939).

with gas at high pressure are difficult because of the very high fields necessary to obtain saturation and sufficiently short collecting times. For the present experiments a special ionization chamber was constructed which makes possible the application of high fields over large volumes.

An ionization chamber can also be used for the measurement of angular distributions. If $\sum(\vartheta)$ is the cross section per unit solid angle for scattering into the angular interval between ϑ and $\vartheta+d\vartheta$ in the center of gravity system, the number scattered into this interval is proportional to $2\pi \sin\vartheta \sum(\vartheta)d\vartheta/4\pi$. From conservation of energy and momentum it follows that $\cos\vartheta=(E_{max}-2E)/E_{max}$, where E is the energy of the recoil particle in the room system and E_{max} the maximum energy the recoil particle can obtain in the room system. Therefore

$$\tfrac{1}{2}\sin\vartheta\sum(\vartheta)d\vartheta=-\tfrac{1}{2}\sum(\vartheta)d(\cos\vartheta)$$
$$=\sum(\vartheta)dE/E_{max},$$

which is proportional to $H(E)dE$, $H(E)$ being the measured energy distribution. E_{max} is related to the energy E_0 of the impinging neutron by

$$E_{max}=\frac{4M_n\cdot M_r\cdot E_0}{(M_n+M_r)^2},$$

M_n being the neutron mass and M_r the mass of the recoiling nucleus. If mono-energetic neutrons are used the distribution in energy of the recoil particles therefore gives a direct measure of the angular distribution of the scattered neutrons in the center of mass system.

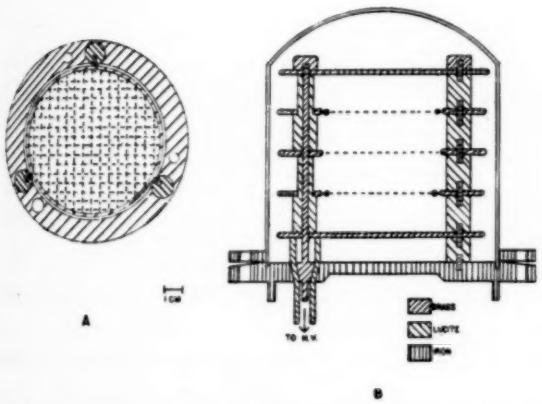

FIG. 1. A. Collecting electrode of the ionization chamber. B. Schematic diagram of the inside of the ionization chamber.

FIG. 2. Photograph of the inside of the ionization chamber.

II. EXPERIMENTAL

The $d-d$ reaction was used as a neutron source. The $d-d$ neutrons emitted at 90° with respect to the deuteron beam are mono-energetic as confirmed recently by Hudspeth and Dunlap,[3] and this fact is corroborated by our experiments. The deuterons were accelerated by the voltage supplied by the transformer-rectifier set in this laboratory. Voltages between 125 and 210 kv were used. No attempt was made to separate the different sorts of ions in the beam in order to avoid secondary neutron sources which might have been produced by the unused beams striking the tube walls. The target consisted of D_2O ice.

In order to obtain sufficiently high collecting fields in the ionization chamber a method first proposed in principle by Ortner and Stetter[4] was applied. Instead of using only two parallel plates as electrodes several are used, connected alternately to the high voltage supply and to the grid of the first stage of the amplifier. The intermediate electrodes are designed to be as transparent as possible to the charged particles. Ortner and Stetter proposed the use of thin Al foils. Electrodes covered with thin foils, however, are too microphonic if they extend over large areas. After various trials the following arrangement was found to be most satisfactory. Square mesh grids were made out of 0.25-mm fuse wire.

[3] E. Hudspeth and H. Dunlap, Phys. Rev. **57**, 971 (1940).
[4] G. Ortner and G. Stetter, Wien. Ber. **142**, 493 (1933).

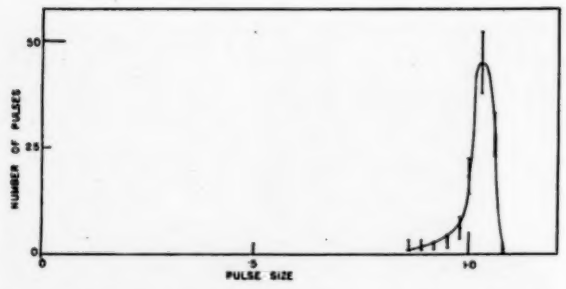

FIG. 3. Distribution in pulse size of 5.3-Mev α-particles in a H_2-Kr mixture.

The wires were six mm apart. At every intersection two perpendicular wires were fixed together by a drop of shellac. Each grid was then clamped between two brass rings. If a grid was used as a collecting electrode, the rings were fixed to Lucite insulators mounted in the guard ring which surrounded them as shown in Fig. 1A. This kind of electrode is relatively nonmicrophonic, and its transparency for perpendicular incidence was measured optically to be 92 percent.

Figure 2 shows a photograph of the inside of the chamber. A schematic diagram is given in Fig. 1B. Five electrodes were used. The first and last ones consisted of plates one mm thick; the three intermediate electrodes were grids of fuse wire. The inner diameter of the rings was 8 cm; the distance between the two end electrodes was likewise 8 cm. Three columns of insulators supported the electrodes. One of the columns contained in its center the high voltage lead. The high voltage electrodes touched this lead. The guard rings of the collecting electrodes were insulated from the high voltage lead by Lucite sleeves which slipped through holes in the guard rings. The connections to the grid of the first stage were made by a lead not shown in Fig. 1. This lead, which was surrounded by a grounded shield, passed between the side wall of the chamber and the electrodes. The walls and the top of the chamber were made of 1.2-mm iron. The whole chamber was suspended by springs from a square frame. The first amplifier tube was contained in a compartment behind the chamber. The collecting voltage was supplied by a 10,000-volt transformer-rectifier circuit with three RC filter stages. For most of the experiments a collecting voltage of 7500 volts was used, producing 3750 volts/cm over a depth of 8 cm.

The ionization pulses were amplified by a 7-stage amplifier with strong inverse feedback and were recorded by means of a torsion type oscillograph[5] on recording paper. The linearity and calibration of the outfit were tested with the aid of artificial pulses of variable size. The pulse generator was described by us previously.[6] A full calibration was photographed at both ends of each record and pulses of one size were recorded at intervals during each run. Both amplifier and oscillograph were found to be linear.

Experiments were carried out in the following three gas mixtures: 5 atmos. Kr+4 atmos. H_2, 5 atmos. Kr+4 atmos. D_2, 7 atmos. He. Krypton is added in order to reduce the range of the recoil protons and deuterons. The maximum range of the H recoils from 25-Mev neutrons was 1.2 cm, that of the D and He recoils smaller.

In order to check the performance of the instrument a very thin source of Po was put into the chamber and fixed to the inside of the top collecting plate. This source emitted 5.3-Mev α-particles in all directions. A study of the α-particle ionization pulses enables one to find out whether the pulse size depends in any way on the direction of the ionization column with respect to the collecting field.

The energy distribution of the Po α-particles was measured in the Kr$-H_2$ mixture and in He. The number energy curves for the two series of experiments are shown in Fig. 3 and Fig. 4. It can be seen from the curves that the peak is sharper in He than in the Kr$-H_2$ mixture. This

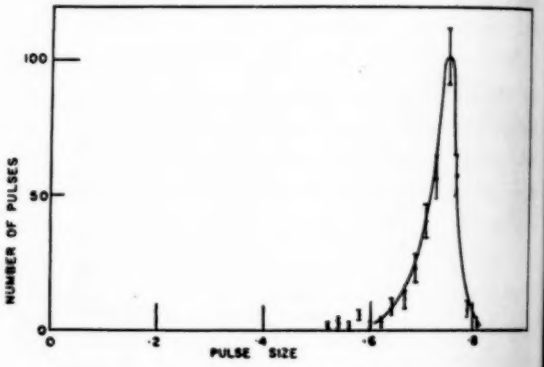

FIG. 4. Distribution in pulse size of 5.3-Mev α-particles in helium.

[5] J. R. Dunning, Rev. Sci. Inst. 5, 387 (1934).
[6] M. H. Kanner and H. H. Barschall, Phys. Rev. 57, 372 (1940).

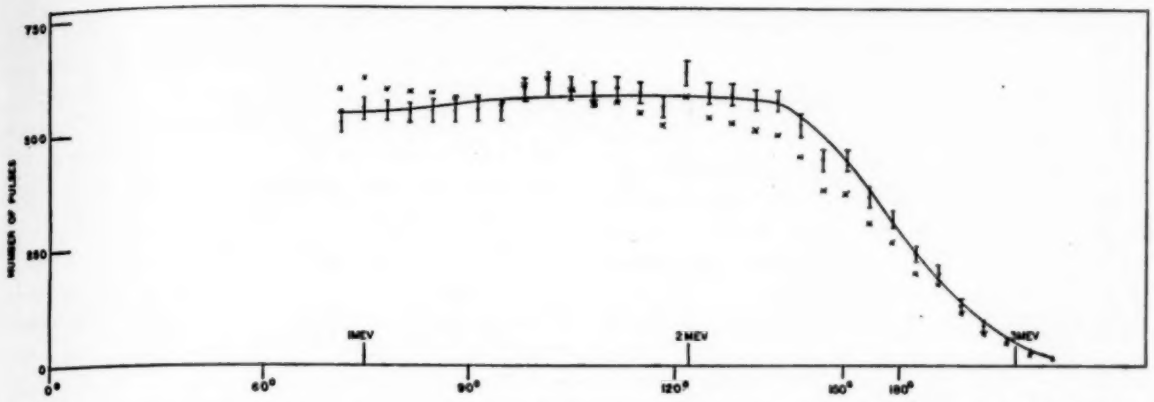

FIG. 5. Distribution in energy of recoil protons. Crosses indicate measured points, bars points corrected for wall effect.

is attributable to the fact that in spite of the high collecting field the collection of the ions in 5 atmos. of Kr is so slow that it is difficult to transmit the pulses through the amplifier without deforming them slightly. In order to obtain good wave forms at the output of the amplifier it had been necessary to increase all time constants to 1/50 sec. or longer. Another drawback to the use of Kr at high pressure is the fact that single fast electrons traversing the large collecting volume produce enough ionization in the chamber to make pulses of appreciable size. This set a lower limit on all energy measurements in Kr, as the pulses produced by electrons could not be distinguished from those produced by low energy recoils. The γ-ray background in the laboratory was sufficient to produce a number of pulses made by electrons comparable with that due to recoils. In evaluating the records care was taken to measure only those pulses which were clearly separated from each other.

The effect of recoil protons from the insulators was tested by taking a run in Kr alone. The number of pulses other than those due to electrons was found to be quite negligible compared to the number of recoils observed with H_2 added.

III. RESULTS

The number energy curve for the $Kr-H_2$ mixture is shown in Fig. 5. The measurement was made at 90° with respect to the deuteron beam (neutron energy 2.53 Mev) at a distance of 45 cm from the target. The crosses represent the measured number of recoils per energy interval at the indicated energies. The scattering angle in the center of mass system is also indicated on the axis of abscissae. The measured numbers were corrected for various edge effects which affect mostly the long range particles and make their pulses appear smaller. Recoils entering the effective volume after starting beyond the edges of the collecting electrodes were also corrected for. For these corrections the range was assumed to be proportional to the $\frac{3}{2}$ power of the energy and as a first approximation the angular distribution was assumed to be isotropic. The corrected points with their statistical errors are plotted in the figure. The large width of the break at the high energy end is probably mostly due to the fact that the transmission through the amplifier is not entirely frequency independent for the very slow pulses. The curve appears essentially flat except for a slight decrease toward lower energies. This decrease appears, however, only after the application of the rather uncertain edge corrections and is not entirely outside the experimental uncertainty which exists in addition to the statistical uncertainty. It is estimated that variations of the cross section as a function of angle could be detected unambiguously only if they were larger than 10 percent and varied slowly with angle.

Figure 6 shows the analogous plot for the case in which the H_2 was replaced by D_2.[7] In this case no deviation from the isotropic scattering law could be detected in the range of angles under investigation. As the deuterium recoils have a

[7] We wish to express our gratitude to Mr. T. Mariner for a mass-spectrographic analysis of the deuterium which had been used in these experiments. The deuterium was found to contain only 2 percent light hydrogen.

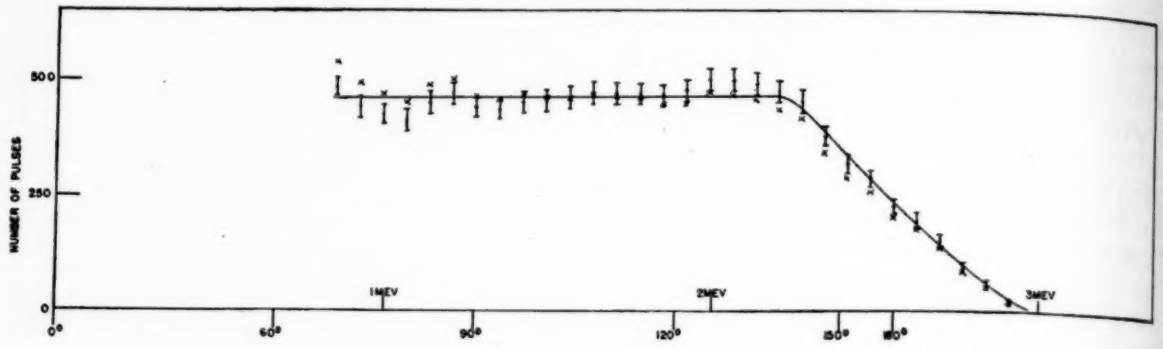

FIG. 6. Distribution in energy of recoil deuterons.

smaller range than the protons, the wall correction is less important.

It follows from Eq. (1) that if 1-Mev neutrons were present[8] the distribution curve would show a break at the corresponding energy of recoil. The height of the rise at this break would be five times greater than that which would be produced by an equal number of 2.5-Mev neutrons as in formula (1) E is smaller by a factor of 2.5 at 1 Mev and $\sigma(E)$ larger by a factor of about 2. The distribution curves in H and D thus seem to indicate that a low energy neutron group is not present with an intensity of more than 3 percent of the main group in agreement with the results of Hudspeth and Dunlap.

Further measurements were made in He. These measurements can be expected to be more accurate than the previous ones as the collecting times are much shorter and no disturbances are produced by fast electrons. The distribution curve obtained is shown in the lower part of Fig. 7. No correction for the edge effect was applied to the measured points as this correction could be calculated conveniently only for an approximately isotropic distribution. The correction would have been small for the He recoils since in the worst case at least 12 ranges are contained in the chamber compared to 7 ranges in the case of hydrogen.

The fact that the distribution curve is almost flat in the high energy region and then rises raised the suspicion that the rise might be due to inelastically scattered neutrons having the energy corresponding to the resonance level in He^5, especially since recent experiments of Staub and Tatel[9] have shown that the resonance reaches up to neutron energies of 1.5 Mev. Neutrons might have been scattered inelastically (1) by various parts of the apparatus in such a way that they would not go directly from the target to the chamber, (2) in the target chamber, (3) in the walls of the ionization chamber.

To test these possibilities the following check experiments were carried out: (1) A cylindrical block of paraffin of diameter somewhat larger than that of the chamber was placed between the target and the chamber in order to absorb neutrons coming directly from the target and give a measure of the number of neutrons which came indirectly. The measurement was made under conditions otherwise exactly the same as those for the previous measurement. The distribution curve showed that the proportion of neutrons which did not come directly from the target was less than 10 percent and that of these neutrons less than half had suffered an energy loss before entering the chamber. (2) To exclude the possibility of inelastic scattering in the liquid air used for cooling the target some experiments were carried out with an air-cooled target of heavy paraffin. No change in the distribution curve could be observed with this arrangement. (3) Neutrons which might have been scattered inelastically in the walls or the iron base plate of the chamber in the absence of the paraffin shield would not have been observed when the paraffin was interposed. The chamber was accordingly surrounded with 20 kg of iron, this being more than five times the total mass of the chamber. The iron consisted of two blocks which had a

[8] T. W. Bonner, Nature **143**, 681 (1939).

[9] H. Staub and H. Tatel, Phys. Rev. **57**, 936 (1940).

cross section of about 70 cm². One of them was placed next to the chamber wall on each side, and about 1 cm from it. Within the rather large statistical uncertainty of this experiment (10 percent) no change in the distribution curve could be noticed when the scatterer was introduced. In a further experiment most of the direct neutrons from the target were absorbed by a paraffin cone which was placed in front of the chamber. The recoil distribution thus found was compared with the one obtained when two 5-kg iron scatterers were placed next to the chamber in such a way that the direct neutrons could strike the iron. The additional recoils observed following the introduction of the iron scatterer amounted to less than 10 percent of the number which would have been observed if the direct neutron beam had been allowed to fall on the chamber. As the scatterer had $2\frac{1}{2}$ times the mass of the chamber and subtended about the same solid angle at the center of the collecting volume as the base plate of the chamber, it follows that the effect of the neutrons scattered by the chamber and measured in He was of the order of 5 percent.

If the rise of the distribution curve at low energies (Fig. 7) were due to neutrons of an energy corresponding to the resonance level in He^5, one would expect its position on a number-energy plot to be independent of the neutron energy. For this reason the chamber was also placed below the target where the neutrons have an energy of 3.1 Mev when 210-kv deuterons are used. The distribution curve found using 3.1-Mev neutrons is shown in the upper part of Fig. 7. A definite shift of the rise towards higher energies occurs. In the two parts of Fig. 7 different energy scales, but the same angle scale, were used. It appears that the rise occurs roughly at the same scattering angle in both cases.

All these experiments lead one to the conclusion that the observed distribution is actually due at least in large part to an anisotropy in the neutron-helium sacttering. It is interesting that Baldinger, Huber and Staub[1] found a distribution curve very similar to ours (compare the circles in Fig. 7), although in their case there were probably more slow neutrons present than in ours.

IV. The Absolute Scattering Cross Section of Helium

In view of a possible comparison with theory of the present results on the angular distribution of the scattered neutrons, it seemed desirable to measure the absolute differential scattering cross section, which is defined as the scattering cross section per unit interval of recoil energy.

Both the neutron and the proton yield of the $d-d$ reaction at 90° with respect to the beam are known[10] and the ratio of these yields is known to be independent of the deuteron energy.[11] The number of neutrons incident on the chamber was determined by counting the number of protons from the reaction $d(d, p)H^3$ emitted into a known solid angle, using a second ionization chamber. The number of recoils whose energy lies in the region in which the distribution curve (Fig. 7) is flat (i.e., for $\vartheta > 110°$) was compared with the

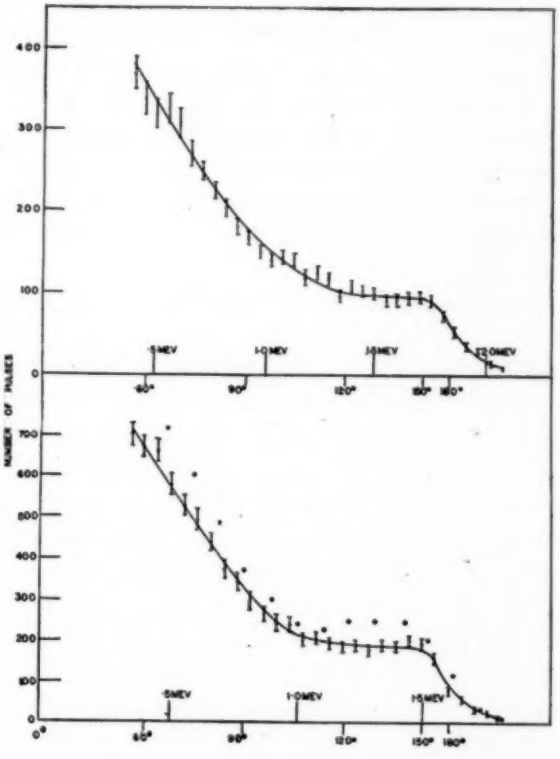

FIG. 7. Distribution in energy of recoil α-particles. Lower curve: distribution due to 2.5-Mev neutrons. Upper curve: distribution due to 3.1-Mev neutrons.

[10] R. Ladenburg and M. H. Kanner, Phys. Rev. **52**, 911 (1937).
[11] R. B. Roberts, Phys. Rev. **51**, 810 (1937).

number of neutrons of 2.5-Mev energy incident on the chamber. This number was calculated from the number of protons counted in the same time interval and from the geometry of the apparatus. As the number of He atoms in the effective chamber volume is known the cross section can be computed.

In the energy interval between 1.1- and 1.6-Mev recoil energy the differential cross section was found to be 9.3×10^{-26} cm² per 100-kv recoil energy or

$$E_{\max}\, dQ(E)/dE = 16\times9.3\times10^{-26} = 1.5\times10^{-24}\ \text{cm}^2.$$

This number is corrected for scattered neutrons which do not come directly from the target. The main uncertainty of this result is due to the uncertainty in the value of the absolute neutron yield of the $d-d$ reaction which is estimated to be ±20 percent. The area under the curve for the differential cross section from the highest recoil energies down to the lowest measured values (~0.35 Mev) is 1.9×10^{-24} cm², which is therefore a lower limit to the total cross section for neutrons of 2.5-Mev energy. A more reasonable lower limit of 3.2×10^{-24} cm² is found by extrapolating the curve in Fig. 7 horizontally to zero energy.

Staub and Stephens[2] found $\times1.41\pm0.18$ as the ratio of the scattering cross sections of He and H for 2.5-Mev neutrons which gives about 3.1×10^{-24} cm² for the absolute value of the He cross section. This result was obtained under the assumption of isotropic scattering, and it should probably be compared with our value for the differential cross section for backward scattering of the neutrons. This discrepancy may be partly due to the fact that in their case only a fraction of the highest energy recoils had their whole range in the chamber. More recent cloud-chamber measurements of Staub[12] which will be published in the near future agree essentially with our value for the helium scattering cross section.

[12] Private communication from Dr. H. Staub.

V. Discussion

The angular distribution of the neutron-proton scattering has been measured by many observers[13] with rather contradictory results. The most reliable measurements are probably those by Dee and Gilbert. These authors find an essentially isotropic distribution in angle over the interval corresponding to our energy measurements. After applying a correction for scattered neutrons Dee and Gilbert find a small deviation from isotropy in the same sense as shown by our corrected values. C. W. Lampson *et al.* and S. Kikuchi *et al.* found a deviation from isotropy in the same direction.

No other experiments on the angular distribution of the neutron-deuteron or neutron-helium scattering have been made.

The fact that no deviation from isotropy could be detected in deuterium in the angular region investigated was unexpected. Measurements of Tuve, Heydenburg and Hafstad[14] showed a very large deviation from Rutherford scattering in the proton-deuteron scattering. A similar deviation from isotropy might have been expected for the scattering of 2.5-Mev neutrons.

The theoretical implications of the scattering of neutrons in helium will be discussed in a separate paper.[15]

VI. Acknowledgments

We wish to express our gratitude to Professor Rudolf Ladenburg for his interest and encouragement and to Professors Louis A. Turner and J. A. Wheeler for much helpful advice.

We are indebted to Dr. I. Brody of the Egyesult Izzo R. T., Hungary, for the gift of 60 liters of krypton.

[13] P. I. Dee and C. W. Gilbert, Proc. Roy. Soc. **A163**, 265 (1937); T. W. Bonner, Phys. Rev. **52**, 685 (1937); F. N. D. Kurie, Phys. Rev. **44**, 463 (1933); L. Meitner and K. Philipp, Zeits. f. Physik **87**, 484 (1934); P. Auger and G. Monod-Herzen, Comptes rendus **196**, 1102 (1933); W. D. Harkins, M. Kamen, H. W. Newson and D. M. Gans, Phys. Rev. **47**, 511 (1935); P. G. Kruger, W. E. Shoupp and F. W. Stallmann, Phys. Rev. **52**, 678 (1937); C. W. Lampson, D. W. Mueller and H. A. Barton, Phys. Rev. **51**, 1021 (1937); S. Kikuchi, H. Aoki and T. Wakatuki, Proc. Phys.-Math. Soc. Japan **21**, 410 (1939).

[14] M. A. Tuve, N. P. Heydenburg and L. R. Hafstad, Phys. Rev. **50**, 806 (1936).

[15] J. A. Wheeler and H. H. Barschall, to be published soon.

Nuclear Isotope Shift in the Spectrum of ZnH

S. MROZOWSKI*
Institute of Theoretical Physics, Joseph Pilsudski University, Warsaw, Poland
(Received July 9, 1940)

The structure of the lines in the (0,0) band of the band system $^2\Pi_i \rightarrow {}^2\Sigma$ of zinc hydride has been studied by means of a Fabry-Perot etalon. The spectrum was excited in a hollow cathode tube. A structure caused by the isotopic constitution of zinc was observed for the lines near the head of the branch $^0P_{12}$. The measured shifts are larger than those calculated by the usual formulas for the vibrational and rotational isotope effects, thus showing the presence of an additional shift at least partly of nuclear origin, amounting to about 0.007 cm^{-1} for the consecutive isotopes of zinc of even mass. This case is quite similar to that of the nuclear shifts in HgH, the chief differences being that they are about 10 times smaller in absolute value and in the opposite direction.

A NUCLEAR isotope effect was found by the author some years ago in the spectra of HgH and HgD and an explanation of its dependence on the vibrational, and possibly also rotational, energy of the molecule has been given by Bohr.[1,2] Recently analogous shifts were found in the spectra of HgH^+ and HgD^+.[3] The author[2] has previously given some explanation of why nuclear isotope shifts have not been heretofore observed in spectra of other molecules. Nevertheless the molecule of HgH cannot in principle represent a unique case in this respect. Therefore it seemed important to find this effect in the spectrum of another molecule, and thus to show its generality and at the same time to furnish a new contribution to the problem of nuclear isotope shifts in band spectra and their correlation with the effects in the respective atomic spectra.

The recently discovered spectra of the hydrides of thallium and lead would be very promising in this respect, but unfortunately they can be excited only in presence of a high pressure of hydrogen, thus making impossible their study with instruments of very high resolving power, because of pressure broadening. Therefore an attempt has been made to investigate the spectrum of zinc hydride, although it was clear from the beginning that the nuclear isotope shift in this case should be much smaller than in mercury hydride and that exceptional sharpness of the lines would be required. The experiments originated from an observation made during investigations of the spectra of Be and B. The hollow cathode of the discharge tube (see detailed description of this tube in a recent paper[3]) in these latest experiments was made of brass. When even a very small amount of hydrogen was present in the tube a strong spectrum of ZnH($^2\Pi \rightarrow {}^2\Sigma$) was observed in the visible and near ultraviolet. By increasing the pressure of hydrogen to the point where the Hα line became almost as intense as the red He line,[4] the intensity of these bands was further increased. In this discharge the ultraviolet bands of ZnH^+ are also emitted, although considerably weaker. The bands (0,1), (0,2), (1,3), (2,4), (3,5), (0,3) and (1,4) of the $^1\Sigma^* \rightarrow {}^1\Sigma$ system of the ion were found. Because of lack of time only the long wave-length bands of ZnH were analyzed with high resolving power, and the measurements were limited to some lines in the (0,0) band of the $^2\Pi_i \rightarrow {}^2\Sigma$ system near 4300A. This band is the most suitable for detection of a nuclear isotope shift. Stenvinkel[5] has shown that in the spectrum of ZnH the separations of components corresponding to different isotopes of Zn follow the formulas for the normal mass isotope shift almost exactly, the differences not exceeding the limits of error, estimated at about ± 0.02 cm^{-1}. The nuclear isotope shift is then probably still smaller and in order to obtain clear evidence of the existence of such a small shift a band with the smallest

* Now at the Radiation Laboratory, Department of Physics, University of California.
[1] S. Mrozowski, Zeits. f. Physik **95**, 524 (1935).
[2] S. Mrozowski, Zeits. f. Physik **99**, 236 (1936).
[3] S. Mrozowski, Phys. Rev. **58**, 332 (1940).
[4] Compare G. M. Almy and R. B. Horsfall, Phys. Rev. **51**, 491 (1937).
[5] G. Stenvinkel, *Das Bandenspektrum des Zinkhydrides* (Stockholm 1936), p. 96.

possible separation of the isotopic components has to be chosen, so that the effect looked for constitutes not too small a part of the total isotope splitting.

The spectrographic apparatus was the same as that described in a former paper,[3] with the sole difference that instead of the quartz optical system a very fast glass system was used in the spectrograph. It gave a dispersion of about 7A/mm in the neighborhood of 4300A. For high resolving power the Fabry-Perot etalon with plates covered with Hochheim alloy and with a separation of 27.2 mm was used. The exposures lasted about a half an hour with a discharge current of 0.3 amp. Although the hollow cathode was cooled only by running water, the lines appeared to be quite sharp, having a half-width of about 0.035 cm^{-1}. The band investigated has a relatively complicated structure—lines belonging to several branches lie close together, giving rise to considerable overlapping. Only the lines of the long wave-length branch ${}^0P_{12}$ are entirely clear, because they fall outside of the strong band head and only the lines of low quantum number have appreciable intensity. The maximum of the intensity distribution occurs between ${}^0P_{12}(4\frac{1}{2})$ and ${}^0P_{12}(5\frac{1}{2})$ and the intensity decreases sufficiently before reaching the long wave-length edge of this branch so that the higher lines beyond the turning point do not interfere. Therefore the structure of lines lying quite close to the head of the branch could be investigated. These lines show a complex structure, which is certainly due to the isotopic constitution of zinc. The observed structure corresponds exactly to the expected distribution shown in Fig. 1. The separation of the components of the isotopes 64 and 66 was impossible to measure, because there is no minimum of intensity between them. The separation of the components 64 and 68 was measured for two lines, ${}^0P_{12}(10\frac{1}{2})$ and ${}^0P_{12}(9\frac{1}{2})$, giving 0.066 and 0.058 cm^{-1}. Traces of structure were also detected in the line ${}^0P_{12}(8\frac{1}{2})$, but no reliable measurements could be made. The normal isotope effect was computed from the data given by Stenvinkel.[5] From the band constants the position of the zero line of the band system was found to be 23099.0 cm^{-1} and taking the value $\rho_{64,66}-1=0{,}000226$ from the mass-spectrographic data the mass isotope shifts

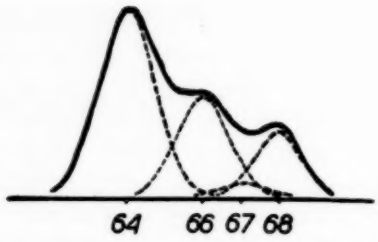

FIG. 1. Structure of lines from ZnH.

between components of consecutive even isotopes of zinc were found to be 0.0255 cm^{-1} and 0.0225 cm^{-1} for these lines. The two corresponding experimental values 0.033 cm^{-1} and 0.029 cm^{-1} are larger, showing without question the presence of a nuclear isotope shift of about 0.007 cm^{-1}. The smallness of these nuclear shifts is in excellent agreement with Stenvinkel's measurements.[6]

The smallness of this nuclear shift, as well as the smallness and relatively low precision of the measured splittings, might cast some doubt upon the reality of the effect found. Fortunately one can check this result in a different way by observing the width of the consecutive band lines. The rotational part of the isotope effect produces a linear change of isotope splitting with frequency. The sign and magnitude of the vibrational effect for this band are such that the total isotope effect changes sign in the region of the ${}^0P_{12}$ branch. Thus a minimum of the width is produced at a point where the total isotope effect vanishes (exact overlapping of all isotope components). It was easy to see by inspection that the minimum width falls between ${}^0P_{12}(3\frac{1}{2})$ and ${}^0P_{12}(4\frac{1}{2})$, rather closer to the former. From this one can calculate the nuclear shift, because at the minimum it is exactly compensated by the normal isotope effect. In the absence of any nuclear shift, the minimum where the rotational effect exactly compensates the vibrational effect should lie between the next pair, ${}^0P_{12}(4\frac{1}{2})$ and ${}^0P_{12}(5\frac{1}{2})$, which is certainly not the case. Thus the presence of a nuclear shift of about 0.007 cm^{-1} is independently confirmed. This convenient method of measuring the nuclear shift could not be applied to the (0,0) bands in HgH^+ and HgD^+,[3] because even for the highest rotational lines the minimum width is not reached in these bands.

The nuclear shift in ZnH is about one-tenth

of the shifts previously reported in the analogous bands of HgH and HgD (0.06 cm^{-1}). Furthermore it has the opposite sign. The correlation of this effect in the ZnH molecule with the same effect in the Zn atom is at first somewhat disturbing. Billeter[6] has shown that the resonance line of Zn $4^3P_1 \rightarrow 4^1S_0$ at 3076A is anomalously broadened, which he explained as due to an isotope shift of about 0.0185 cm^{-1} between the lines of the even isotopes. He assumed the sign of the shift to be the same as in the resonance line of Hg at 2537A. If the directions of the shifts in both Zn and Hg are the same why should they be opposite in the hydride spectra when the electron configurations in both molecules are analogous? The argument given by Billeter[6] for the signs adopted is misleading, because the sign cannot be inferred directly from the shifts observed by Schüler and Westmeyer[7] in some lines of ZnII. One must consider the shifts of *levels*. In a paper published shortly afterwards, Schüler and Westmeyer[8] showed that for ZnII, just as for CuI, the direction of the nuclear shift is opposite to that in heavier atoms like Cd and Hg, the levels of the heavier isotopes lying lower. It should be remarked that the order of the isotopic levels thus disagrees with the current theory of nuclear isotope shifts. There is every reason to expect that this same inversion holds for the levels of ZnI and that Billeter's assumption is wrong. Then it is clear that the nuclear shift found in ZnH and its correlation with the corresponding atomic spectrum present exact analogs of the effects previously found in HgH, except for reversed directions and the much smaller magnitude.

It must be emphasized, however, that for ZnH it is not certain whether the whole shift of about -0.007 cm^{-1} is to be explained as pure nuclear effect, because in this case the shift is much smaller than in HgH and the correction terms[9] to be applied to the usual isotope mass formula are much greater than for HgH. Hence a part of the effect found may represent a mass effect. Nevertheless this effect certainly cannot be large enough to explain more than half of the shift found in the spectrum of ZnH. On the other side the true nuclear isotope shift in the line 3076A of ZnI is different from the value found by Billeter.[6] For such a relatively light element a correction for the mass effect has to be applied, which in this case makes the nuclear isotope shift probably considerably smaller. (In the case of the lines in ZnII investigated by Schüler and Westmeyer,[7] the true nuclear shifts are bigger than the measured ones, but the correction is relatively very small.) The normal mass shift amounts to about 0.008 cm^{-1} and the specific shift has probably the same sign but is comparatively much smaller (compare for instance the calculations of Vinti[10] for MgI).

As to other possible cases of nuclear isotope shifts the author suggested some years ago[2] that the shift of 0.33 cm^{-1} found by Jenkins and McKellar[11] in the system origins in the spectra of $B^{10}O$ and $B^{11}O$ may have a nuclear origin. It was recently shown by Opechowski and de Vries[12] that the observed shifts in the spectrum of boron are pure mass shifts. Therefore a possible nuclear origin of the shift in BO is excluded and the whole effect must be explained as due to mass correction terms. The order of magnitude seems to be in agreement with formulas for these terms.[9] Thus no indications of the presence of a nuclear isotope shift in other spectra than the cases mentioned above—namely HgH(HgD), HgH^+-(HgD^+) and ZnH—have been found up to the present.

I wish to express my sincere thanks to Professor C. Bialobrzeski for his kind interest in this experiment. This paper was submitted in August of last year for publication in the *Acta Physica Polonica*. Subsequent events have made it impossible to proceed with the printing of this journal and the paper has therefore been rewritten in English and is presented here. I am very much indebted to Professor F. A. Jenkins for the kind help he has given me in the writing of this paper.

[6] W. Billeter, Helv. Phys. Acta **7**, 524 (1934).
[7] H. Schüler and H. Westmeyer, Zeits. f. Physik **81**, 565 (1933).
[8] H. Schüler and H. Westmeyer, Zeits. f. Physik **82**, 685 (1933).
[9] Compare J. H. Van Vleck, J. Chem. Phys. **4**, 327 (1936).
[10] J. P. Vinti, Phys. Rev. **56**, 1120 (1939).
[11] F. A. Jenkins and A. McKellar, Phys. Rev. **42**, 464 (1932).
[12] W. Opechowski and D. A. de Vries, Physica **6**, 913 (1939).

Electron Scattering in Bromine Gas*

C. H. SHAW AND T. M. SNYDER
Rowland Physical Laboratory, The Johns Hopkins University, Baltimore, Maryland
(Received July 15, 1940)

Calculations have been made on the angular dependence of electron scattering in bromine gas with the scattering phases obtained in a recent paper. For the lower energies it is essential that atomic polarization be included in the calculations of the phase defects. The results are compared with previous experimental work by Arnot.

IN a paper recently published,[1] the authors have calculated the fine structure to be expected on the high frequency side of the Br K-absorption edge in gaseous bromine. The position of the transmission band as calculated agrees well with that obtained experimentally by means of a double crystal spectrometer. The calculated intensity, on the other hand, is far too low. As a check on the values of the electron scattering phases used in the previous paper, we have calculated the dependence on angle of the elastic scattering of electrons from the bromine molecule and compared the predicted scattering with the empirical results of Arnot.[2]

THEORY AND CALCULATIONS

The intensity of electron single scattering in a monatomic gas at the angle θ from the direction of the incident beam is given by the expression[3]

$$I(\theta)=\frac{1}{4p^2}\Big\{\sum_{l=0}^{l=\infty}(2l+1)[e^{2i\delta_l}-1]P_l(\cos\theta)\Big\}^2,$$

where p is the momentum of the scattered electron, δ_l is the phase shift upon scattering of the partial electron wave of angular momentum l and $p_l(\cos\theta)$ is the lth order Legendre polynomial. If the electron momentum p is measured in "atomic units" ($p=(2E)^{\frac{1}{2}}$) the intensity $I(\theta)$ is said also to be in atomic units.

If the gas is diatomic the molecular scattering I_m is somewhat different from the atomic and is given by[4]

$$I_m(\theta)=2I_a(\theta)\left[1+\frac{\sin x}{x}\right],$$

where $x=2p\rho\sin(\theta/2)$ and ρ is the interatomic distance. In general in the angular region experimentally convenient the corrective term for the molecule is relatively unimportant and the molecular scattering is approximately twice the atomic.[5]

The problem of calculating the electron scattering as well as that of the fine structure of the x-ray absorption edge of bromine is complicated by the fact that the self-consistent field has not as yet been calculated. Two methods have been used for the determination of electron scattering phases—both admittedly only approximate in nature. The first[5] was to obtain a Hartree field for bromine by extrapolation from the known Hartree field for Rb^+. The phase defects were then computed by either the Jefferys[6] or the Born[7] approximate formula. The major criticism of this method as used is that the final field so obtained is uncorrected for the polarization of the scattering atom by the scattered electron. The errors in the resulting phases are especially large for the higher values[8] of l. The second method is to assume the Hartree field for krypton corrected for polarization[8] and extrapolate the "exact" phases for krypton to obtain those for bromine by a method given by Henneberg.[9] The major criticism of this method is that the

* This work was supported by a grant-in-aid from the American Philosophical Society.
[1] T. M. Snyder and C. H. Shaw, Phys. Rev. **57**, 881 (1940).
[2] F. L. Arnot, Proc. Roy. Soc. **A144**, 360 (1934).
[3] N. F. Mott and H. S. Massey *The Theory of Atomic Collisions* (Oxford University Press, New York, 1933), p. 24.
[4] H. S. Massey and E. C. Bullard, Proc. Camb. Phil. Soc. **29**, 511 (1933).
[5] F. L. Arnot and J. C. McLauchlan, Proc. Roy. Soc. **146**, 662 (1934).
[6] F. L. Arnot and G. O. Baines, Proc. Roy. Soc. **A151**, 651 (1934).
[7] N. F. Mott, Proc. Camb. Phil. Soc. **25**, 304 (1929).
[8] J. Holtsmark, Zeits. f. Physik **66**, 49 (1930).
[9] W. Henneberg, Zeits. f. Physik **83**, 555 (1933).

extrapolation formula assumes the Thomas-Fermi form of the atomic field. For low energies the latter method is the better and has been used in the present work.

In applying the second method to bromine the question immediately arises as to whether the atomic polarizability of bromine is the same as that of krypton. The comparison may be made by means of refractive index data. The molar refractivity may be expressed in terms of the atomic refractivity of the constituent atoms as follows:[10]

$$K=\sum_i N_i k_i,$$

where N_i is the number of atoms of type i in the molecule. But

$$k_i=\left(\frac{M}{\rho}\right)_i \frac{n_i^2-1}{n_i^2+2}\approx\frac{2}{3}\left(\frac{M}{\rho}\right)_i (n_i-1).$$

Since M/ρ is a constant for all gases, the molar refractivity is given by

$$K=\frac{2}{3}\frac{M}{\rho}\sum_i N_i(n_i-1).$$

The refractive indices of krypton and bromine have been measured in the region from 4000 to 7000A.[11] Calculation of the atomic refractivities as indicated above shows that k for bromine is about 25 percent greater than that for krypton. In view of the approximate nature of the correction for polarization, it may be concluded, then, that Holtsmark's correction for polarization[12] of krypton may be applied to bromine.

The angular distribution of electrons elastically scattered in bromine vapor has been investigated experimentally by Arnot.[2] He used electron energies of 15, 41, 80, and 121 ev. Table I lists the scattering phases used by Arnot and McLauchlan[5] and those of the present paper.[1] As discussed in a previous paragraph, the difference is especially marked for the higher order phases and is due to the fact that polarization was included in the latter work. Calculations were not completed for 80 and 121 ev because it was found for these voltages that phases higher than the sixth were required.

TABLE I. *Scattering phases.*

PHASE	ARNOT AND MCLAUCHLAN 15 V	ARNOT AND MCLAUCHLAN 41 V	SHAW AND SNYDER 15 V	SHAW AND SNYDER 41 V
δ_0	11.02	10.20	10.71	9.78
δ_1	7.75	7.23	8.13	7.47
δ_2	3.36	3.94	4.12	4.28
δ_3	0.035	0.535	0.30	0.96
δ_4	0	0.092	0.13	0.34
δ_5	0	0.024	0	0.18
δ_6	0	0	0	0.085

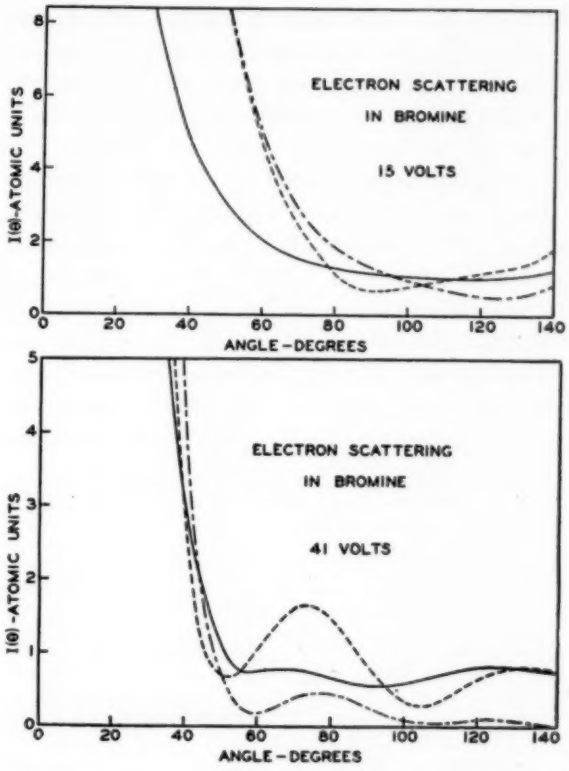

FIG. 1. ——— theory—Arnot and McLauchlan; - - - - - - - - theory—Shaw and Snyder; ——— experiment—Arnot. The scale of the experimental curve is adjustable by an arbitrary multiplying constant.

Figure 1 shows the experimental data of Arnot, the theoretical curve of Arnot and McLauchlan, and the theoretical curve of the present authors. That the agreement between experiment and theory is not closer may be due both to the approximations in the theory and to errors in the experiments. Errors in the experiments would probably be due to the effects of space charge and to low resolving power. Arnot considered the effects of the radial field produced by the electron beam[13] and came to

[10] J. H. Van Vleck, *Electric and Magnetic Susceptibilities* (Oxford University Press, 1932) p. 82.
[11] Landolt-Börnstein, *Tabellen II*, p. 961.
[12] J. Holtsmark, Zeits. f. Physik **55**, 437 (1929).
[13] F. L. Arnot, Proc. Camb. Phil. Soc. **27**, 73 (1931).

the conclusion that errors from this source were negligible for his experiments in mercury vapor. However, since the electron affinity of the halogens is large it is possible that an appreciable space charge might be built up through the formation of negative ions by electron capture.

Assuming a simplified form for the molecular field, Fisk[14] extended the quantum mechanical method of Allis and Morse[15] to the calculation of the total cross section for elastic scattering of slow electrons from diatomic molecules. He has completed calculations for nitrogen, oxygen, hydrogen and chlorine. Excellent agreement between experiment and theory was obtained for the first three gases, but wide deviations were found for chlorine, for which the total cross section for scattering (elastic and inelastic) was measured. The discrepancy was interpreted as meaning that considerable inelastic scattering was present.

It would be instructive to apply Fisk's method to bromine, for which Arnot has made measurements for *elastic* scattering. The agreement for low energies would probably not be very good in view of the strong effect of atomic polarization, which in Fisk's theory is ignored. The agreement, however, should be considerably better than that for chlorine because of the absence of inelastically scattered electrons in the experimental work.

[14] J. B. Fisk, Phys. Rev. **49**, 167 (1936); **51**, 25 (1937).
[15] W. P. Allis and P. M. Morse, Zeits. f. Physik **70**, 567 (1931).

OCTOBER 1, 1940 PHYSICAL REVIEW VOLUME 58

Scattering of Fast Electrons in Helium

J. B. HORNER KUPER
Washington Biophysical Institute, Bethesda, Maryland

AND

EDWARD TELLER
George Washington University, Washington, D. C.

(Received July 23, 1940)

Failure of the quantum mechanical theory of elastic scattering to account for experimental results of Kuper on scattering of 50- to 80-kilovolt electrons in helium has been explained by neglect of the inelastic scattering. Computation of the cross sections including inelastic as well as elastic collisions by an approximate method yields satisfactory agreement without requiring any modification of the theory.

MEASUREMENTS by Kuper[1] on the scattering of fast electrons (50 to 80 kilovolts) in rare gases were in satisfactory accord with the quantum mechanical theory for elastic scattering in the cases of argon and neon. In helium, however, the observed scattering cross sections were much larger and increased more rapidly at the smaller angles than the elastic scattering theory predicted.

In spite of the fact that the resolving power of the electrostatic energy analyzer was such as to permit passage of electrons which had lost as much as 100 electron volts it was assumed that inelastic scattering was absent for two reasons. First it was thought that at these energies the losses would be large compared to 100 electron volts, and second that if only elastic scattering was found in neon and argon the same would be true in helium. Both of these assumptions seem to be wrong. The first would be true if we were dealing with larger angles but at angles smaller than 2° the predominant energy losses will be well under 100 electron volts. This can readily be seen by considering the momentum changes involved. The second assumption neglects the fact that while the inelastic cross section (for losses not exceeding 100 ev) will vary approxi-

[1] J. B. H. Kuper, Phys. Rev. **53**, 993 (1938).

mately as the number of electrons in the outer shell, the elastic cross sections increase very roughly as the square of the effective atomic number. For example the elastic cross sections[2] for 80-kilovolt electrons near 1° are in the ratio 1 : 25 : 119 for He, Ne, and A, respectively. Thus we can see that the inelastic scattering contribution in the case of argon would scarcely affect the shape of the curve at all. In neon we could expect the inelastic scattering to become appreciable at the smallest angles and this was in fact observed.

An exact calculation of the cross sections for inelastic scattering in helium would be extremely laborious as it would be necessary to sum the contributions of the various excitations and ionization. Fortunately, the expression for the total inelastic scattering in hydrogen given by Bethe[3] and Mott and Massey[4] can readily be modified to apply to the case of helium. This involves an approximation in using excited hydrogen wave functions for helium, but this procedure has been well justified by experiments at lower energies.

The modified expression used for the total inelastic cross section is

$$I_{in}=2\cdot\frac{4m^2e^4}{\hbar^4k^4}\cdot\frac{\cos\theta}{\sin^4\theta}\left[1-\frac{1}{(1+\frac{1}{4}k^2(a_0^2/Z^2)\sin^2\theta)^4}\right],$$

I_{in} being the effective cross section for inelastic scattering through the angle θ into unit solid angle. Here m, e, and $\hbar$ have their usual meanings, k is the momentum of the incident electrons divided by $\hbar$, a_0 is the radius of the first Bohr orbit in hydrogen, and Z the effective atomic number, taken as 1.69. The factor 2 was introduced to allow for the extra electron in helium. For the energies considered here the term in brackets has a value of 0.05 at 0.3° and rises nearly to 1 at about 3°. Thus it exerts a strong influence on the cosec^4 distribution in the angular range covered by the experiments (the cosine term may be set equal to 1).

In Fig. 1 we have plotted Kuper's data on scattering of 49.5, 63.3 and 78 kilovolt electrons in helium. Also we show the elastic cross sections

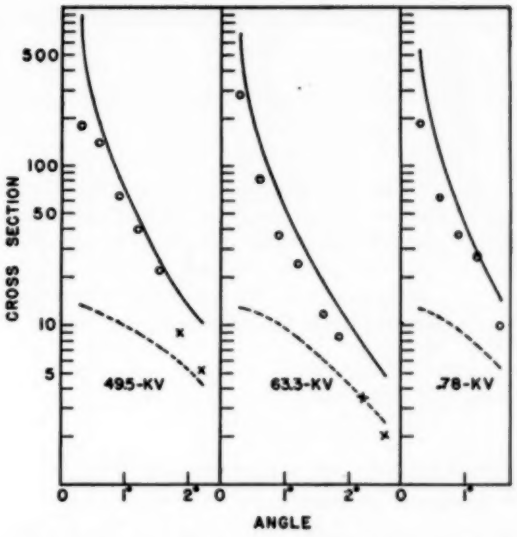

FIG. 1. Scattering of 49.5-, 63.3- and 78-kilovolt electrons in helium. Dashed curves, elastic cross sections; solid lines, total cross sections, elastic plus inelastic, in units of 10^{-18} cm^2. The experimental points were not adjusted to fit the curves but are located by the effective scattering volume of the apparatus found for neon and argon. Those points shown as crosses represent currents less than 1000 electrons per second and therefore the error may be expected to be high.

for scattering into unit solid angle from Mott and Massey[5] and the total cross sections obtained by adding to the elastic the inelastic scattering computed from the formula above. The agreement can be considered quite satisfactory, especially when it is realized that this calculation gives an upper limit to the cross sections, losses greater than about 100 electron volts being excluded by the analyzer. Also the experimental cross sections involve a determination of the effective scattering volume of the apparatus. This was obtained from the results of the measurements in neon and argon. Correction of the latter to account for the inelastic scattering would tend to raise the experimental points. No significance need be attached to the experimental points shown as crosses. In these cases the observed currents were less than 1000 electrons per second and the error is probably high.

We feel that these considerations make unnecessary the treatment suggested by Hughes[6] to account for the experiments. We wish to thank Professor J. Howard McMillen for discussion of this problem.

[2] N. F. Mott and H. S. W. Massey, *The Theory of Atomic Collisions* (Oxford, 1933), p. 120 and 124.
[3] H. A. Bethe, *Handbuch der Physik*, second edition, Vol. 24, No. 1 (1933), p. 505.
[4] N. F. Mott and H. S. W. Massey, reference 2, p. 174.
[5] N. F. Mott and H. S. W. Massey, reference 2, p. 120.
[6] A. L. Hughes, Phys. Rev. **55**, 350 (1939).

Secondary Emission from Films of Platinum on Aluminum

PAUL L. COPELAND
Department of Physics, Armour College of Engineering, Illinois Institute of Technology, Chicago, Illinois
(Received July 8, 1940)

Experimental results for secondary emission from films of platinum on aluminum indicate a direct proportionality between the primary energy (up to 800 electron volts) and the maximum depth from which the secondaries come. The depths of origin of secondaries as indicated by these studies are not out of line with those which would be expected on the basis of existing theories. The maximum depth within the target influencing the secondary emission increases more rapidly for primary energies above 800 electron volts than for those below.

INTRODUCTION

HASTINGS[1] in an interesting paper has recently discussed experiments giving rather definite information concerning the depth of origin of secondaries of various energies in films of silver on platinum. In brief his conclusions are that the secondaries of low energy originate within 15 atomic layers for primaries of 20 ev and within 30 atomic layers for primaries of 50 ev. His results for higher energy primaries are considerably less definite, although he cites evidence that for primaries of 250 ev appreciable emission comes from a depth greater than 150 atomic layers. In this paper the writer presents results for platinum films on aluminum, which, perhaps because of the great dissimilarity between platinum and aluminum, are definite even at primary energies higher than those used by Hastings.

Previously the writer has reported[2–5] some of the more pronounced features of secondary emission from complex targets. In 1934 he[2,3] presented results for secondary emission as a function of primary energy for platinum films of various thicknesses upon aluminum. These results were somewhat qualitative, since no effort was made to measure the thicknesses of the various films, but they showed that for low primary energies the secondary emission was characteristic of the superficial layer, while for primary energies of more than an electron kilovolt, and increasing with the film thickness, the secondary emission was influenced by the aluminum. Results in many ways the converse of those for platinum on aluminum were obtained from films of sodium condensed on tantalum.[4] In this case the films were measured by the microtitration of the sodium, and the results showed definitely that the thickness of the films used ranged up to 300 atomic layers. In 1937 at Montana State College the writer repeated measurements of secondary emission from films of platinum on aluminum, and these results, because they may be of interest both for comparison with those of Hastings and for consideration in connection with current theories, are presented at this time.

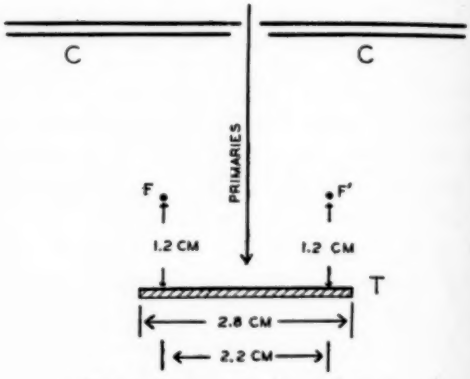

FIG. 1. Geometry of apparatus.

EXPERIMENTAL METHODS

The metal parts of the experimental tube, the essential features of which are shown schematically in Fig. 1, were sealed into a Pyrex glass envelope, and the tube was evacuated by a single stage mercury diffusion pump backed by a Cenco Hyvac. The mercury vapor was condensed in re-entrant type cold traps filled with a slush of dry ice and acetone. Two of these

[1] A. E. Hastings, Phys. Rev. **57**, 695 (1940).
[2] P. L. Copeland, Phys. Rev. **46**, 167 (1934).
[3] P. L. Copeland, Phys. Rev. **48**, 96 (1935).
[4] P. L. Copeland, Phys. Rev. **53**, 328 (1938).
[5] P. L. Copeland, Phys. Rev. **55**, 1270 (1939).

traps in series were placed between the experimental tube and the diffusion pump. Only the first trap was cooled during the first stages of the evacuation, during which the experimental tube was placed in an electric furnace and baked for several hours at temperatures around 475°C. The connecting tubing, including the second trap, was thoroughly torched during the baking process. The furnace was then removed and slush was added to the second trap. The experimental tube was left on the pumps throughout the observations, and the pressure in the tube, too low to be read on the McLeod guage, was certainly less than 10^{-6} mm Hg.

Details of the geometry at the target are shown in Fig. 1. Here T is a plate of commercial aluminum which serves as a target. Two platinum filaments, F and F', of approximately 10 mils diameter are placed in front of the target as shown. The geometry is selected so that when equal amounts of platinum are evaporated from the two filaments, a nearly uniform film is deposited on the face of the target. The diaphragms are cut so that only the secondaries emitted by the target reach the collector, C, and in this apparatus the ratio of the number of secondaries to the number of primaries is obtained for various primary energies in the usual manner.

For evaporating the platinum, the filaments are heated by passing a current through the two in parallel. Readings of the heating current and the potential difference across the filaments were made on meters accurate to one-half of one percent in the range used. For convenience the thinnest films were obtained at one evaporation rate, and the thicker films at an evaporation rate, which, from data on the vapor pressure of platinum as a function of temperature, was estimated to be 4.5 times as great as the first. The procedure, as in the previous work,[3] was to put on a film and measure the secondary emission as a function of primary energy, and then to add to the film and again measure the secondary emission. In the end the amount of platinum lost from the filaments was easily determined by weighing measured lengths of the middle sections

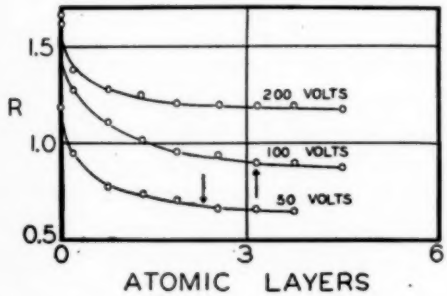

FIG. 2. Secondary emission as a function of film thickness for low primary energies.

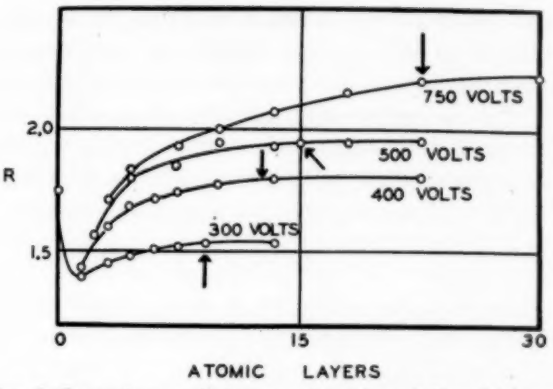

FIG. 3. Secondary emission as a function of film thickness for intermediate primary energies.

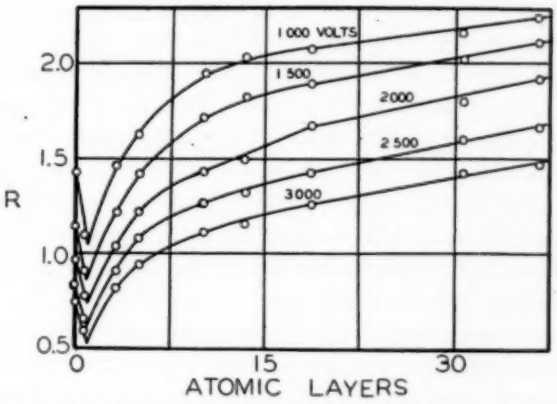

FIG. 4. Secondary emission as a function of film thickness for primaries of high energy.

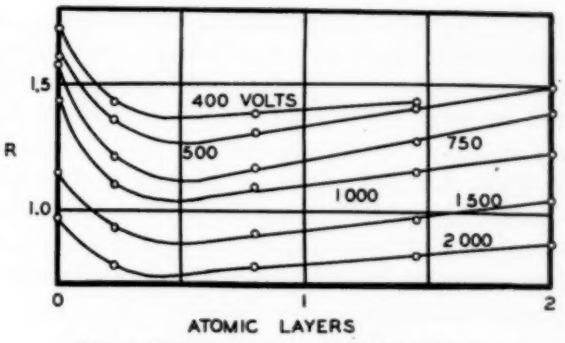

FIG. 5. Secondary emission of thin films.

on a good chemical balance. From these data and the geometry, the density of the films in micrograms per square centimeter was computed. In the accompanying graphs these data are interpreted in terms of atomic layers on the assumption that an atomic layer of platinum weighs 0.53 micrograms per square centimeter.

Results

The data are analyzed in Figs. 2, 3, 4 and 5 by plotting the secondary emission ratio, R, against the thickness of the film. For the lower primary energies such data are shown in Fig. 2. As shown here for primary energies of 50 volts, 100 volts and 200 volts, the addition of platinum causes the secondary emission to decrease continuously and to approach that characteristic of thick platinum films. For primary energies greater than 200 volts, the secondary emission at first decreases and then increases. Such data are shown in Figs. 3 and 4, where to prevent confusion in Fig. 3 those obtained for very thin films are omitted, but all of the omitted points are plotted on a larger scale in Fig. 5.

In many particulars the variations of secondary emission for platinum on aluminum are the converse of those for silver on platinum as shown by Hastings[1] as would be expected on the basis of the writer's previous work on complex targets[2,3] showing both types of behavior. In particular it is of interest to notice that, whereas for primaries of high energy Hastings shows the secondary emission increasing to a maximum at one atomic layer and then decreasing, the results in Figs. 3 and 4 show the secondary emission decreasing to a pronounced minimum and then increasing. The detailed plots of Fig. 5 are interesting in this connection, since smoothly drawn curves put the minima very close to half-coverage. This seems low, but is not unreasonable. There is evidence for believing the maximum of thermionic emission from thoriated tungsten occurs at about three-quarters of full coverage.[6]

The rise in the secondary emission for the thicker films of platinum with primaries of high energy, as shown in Figs. 3, 4, and 5, may be due in part to the relatively great scattering of primaries in platinum. If the primaries have the

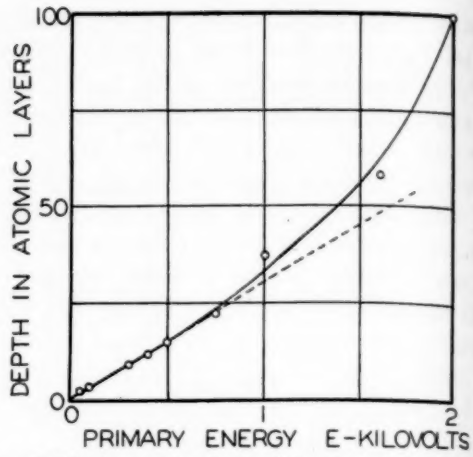

FIG. 6. Maximum depth of origin of secondaries as a function of primary energy.

low energies represented in Fig. 2, the increased scattering is ineffective in the production of more secondaries. The relatively large change in secondary emission for the thin films in all graphs would naturally be interpreted as meaning that most of the secondaries originate very near the surface. The arrows in Figs. 2 and 3 indicate the points at which the secondary emission is estimated to cease varying with film thickness. The flatness of the curve obtained at 200 ev primary energy would seem to be due to the fact that it is the borderline between the two types of curves; it probably should not be taken to indicate that secondaries arise only in the first three atomic layers. The curves in Fig. 4 fail to become flat in the region shown. Here the primary energies at which properties of the aluminum appear were determined as in previous work[3] from breaks in the plots of secondary emission against primary energy. In this work the results are definite at all primary energies, and they provide rather definite evidence that the maximum depth of origin of appreciable secondary emission is at first proportional to the primary energy as shown in Fig. 6. The reason for the departure from the proportionality at the high primary energies is probably that penetration of high energy primaries becomes proportional to the square of the energy.[7] The proportionality itself has a rather simple interpretation in the light of existing theories.

[6] W. B. Nottingham, Phys. Rev. **49**, 78 (1936).

[7] H. M. Terrill, Phys. Rev. **22**, 101 (1923); **24**, 616 (1924).

Frohlich[8] applied wave mechanics to the problem of secondary emission, and concluded that if absorption of the secondaries within the metal were neglected, the secondary emission should increase with the square root of the primary energy, while the energy of the excited secondaries would be small (about 25 ev) and approximately independent of the primary energy. Wooldridge[9] has recently shown that correcting certain errors in Frohlich's work one concludes that if primaries of energy $\hbar^2K^2/2m$ and of momentum $\hbar K$ are incident on a metal, the rate of production of secondaries is independent of the energy of the primaries and that the average energy given by the primary to the secondary is $(\hbar^2/2m)(2\pi/a)^2$ where a is the lattice spacing. For primaries of several hundred electron volts the production of secondaries accounts for practically the full loss of energy by the primaries. According to Wooldridge's picture "in a distance less than the mean free path of the secondaries, the primaries may lose so much energy that they can produce no more secondaries." This theory is capable of explaining observations of secondary emission which at low energies are almost proportional to the primary energy. This theory also indicates that the depth to which the primaries penetrate without losing the ability excite secondaries is proportional to the primary energy. Hence the proportionality between depth of origin of secondaries and primary energy would be expected.

Reliability of the Data

The proportionality of the abscissas to film thickness is more certain than the correctness of the exact numerical values of the abscissas. The individual evaporation periods were from 10 to 20 minutes and they could therefore be determined with high precision. The change in evaporation rate was made after a film of 12.3 atomic layers had been deposited. The curves show no tendency toward irregularity at this point, which fact would appear to confirm the conversion factor relating the two evaporation rates. No hot spots developed on the filaments, and at the end of the run both platinum filaments appeared to be uniform. The apparatus was designed to minimize non-uniformity of evaporation near the experimental region, and an effort was made to detect any non-uniformity that might have developed. Each of the platinum filaments was approximately 15 cm long, and only the central length of 5 cm was weighed after the evaporation of the platinum. Finally as a check on the uniformity of these 5 cm sections, a section of 2 cm length was removed from the center of each of these and these sections were carefully weighed separately on a balance of sensitivity 20 divisions per milligram with a set of weights on which the corrections indicated by a National Bureau of Standards certificate were made. This work indicated a uniform loss of platinum over the 5 cm lengths, hence confirming the assumption on which the computations of film thickness were based.

This investigation was a part of the work undertaken under a grant-in-aid by the National Research Council in 1936. The writer is glad to acknowledge his indebtedness for this assistance. The writer also takes this opportunity to express his appreciation to Dr. J. C. Turnbull, who was associated with him at the beginning of such studies, for suggestions concerning the analysis of data obtained in such experiments.

[8] H. Frohlich, Ann. d. Physik **13**, 229 (1932).
[9] D. E. Wooldridge, Phys. Rev. **56**, 562 (1939).

The Relative Secondary Electron Emission Due to He, Ne, and A Ions Bombarding a Hot Nickel Target

MONICA HEALEA AND CHARLOTTE HOUTERMANS*
Vassar College, Poughkeepsie, New York
(Received June 17, 1940)

The number of electrons emitted per positive ion from a degassed Ni target bombarded by He, Ne, and A ions was measured. For He, in an energy range from 450 to 1650 ev the emission increased from 49 to 107 percent; for Ne having energies from 900 to 1275 ev the increase was 43 to 57 percent; for A of 680 to 1480 ev from 11 to 18 percent. These results confirmed those found earlier for H_2^+ and D_2^+ ions in showing a smaller emission for the heavier ion at the same energy. Similarly, the percentage of positive ions reflected increased with the energy of the primary ions and was smaller for the heavier ions.

SECONDARY electron emission from thoroughly degassed metal targets bombarded by positive ions of low energies has been little studied. Jackson's work,[1] in which beams of Na, Rb, and Cs, ions from Kunsman sources were used to bombard a Mo target, showed for Na^+ an electron emission of about 2 percent at 1000-ev ion energy, for Rb^+ no electron emission within experimental error, and for Cs^+ a secondary emission of about 9 percent. Oliphant[2] found that the He^+ ions impinging on a Mo target the emission varied with the energy of the ions from about 8 percent to 70 percent in an energy range from 80 to 1000 ev, with two decreases in slope of the emission-energy curve as the energy increased. Healea and Chaffee[3] obtained a nearly linear increase of emission with energy when a hot nickel target was bombarded by H_2^+ ions of energy ranging from 300 to 1000 ev, and one of the present authors,[4] in a comparison of the effect of using H_2^+ and D_2^+, found a smaller emission from nickel for the D_2^+ than for H_2^+ ions of the same energy in about the same energy range as that previously used.

On the other hand, A. G. Hill, W. W. Buechner, J. S. Clark, and J. B. Fisk[5] obtained results with H_1^+, H_2^+, and He^+ ions having energies in the range from 43 to 426 kev which indicated that for particles of the same energy in this high energy range the emission was nearly proportional to the mass of the bombarding particle. Further studies have therefore been undertaken with He, Ne, and A ions in the lower energy range.

Apparatus and Procedure

The essential parts of the tube and the vacuum system were the same as previously described. A beam of ions, drawn from a discharge, was accelerated through a collimating canal and bent by an electric field to strike a target in a bulb whose platinized inner surface acted as collector for the secondary electrons and the reflected positive ions. The impinging ions were probably largely singly charged, since Oliphant who used a magnetic deflection method in conjunction with a similar tube reported his results as due to a He^+ beam. In the electrical circuit the batteries supplying the discharge and accelerating voltages were replaced by transformers, rectifiers and stabilizing devices. The discharge part of the circuit used three Westinghouse WL-706 stabilizing tubes, the accelerating part a circuit described by letter to the first of the present authors by Dr. R. W. Hickman of Harvard University and later reported in *The Review of Scientific Instruments*.[6]

The target box, containing as before a tungsten filament enclosed in a quartz tube, was kept at a bright red heat in the vacuum as near to the melting point as was considered safe for about two months. All thermionic emission of positive

* Research assistant in physics.
[1] W. J. Jackson, Phys. Rev. **30**, 473 (1927).
[2] M. L. E. Oliphant, Proc. Roy. Soc. **A127**, 373 (1930).
[3] Monica Healea and E. L. Chaffee, Phys. Rev. **49**, 925 (1936).
[4] Monica Healea, Phys. Rev. **55**, 984 (1939).
[5] Hill, Buechner, Clark, and Fisk, Phys. Rev. **55**, 463 (1939).
[6] F. V. Hunt and R. W. Hickman, Rev. Sci. Inst. **10**, 6 (1939).

ions then ceased and reproducible values of secondary emission for helium could be obtained. The final values of the emission were taken at a somewhat lower temperature. At the higher temperature, after a steady state had apparently been reached, there occurred a sudden and permanent increase of about 10 percent in the emission. This was probably caused by a change in the metal surface due to recrystallization. The temperature was lowered to reduce the chance of further change. Thereafter there was no evidence that the state of the surface was not constant during the observations on the three gases.

The difficulty previously encountered in maintaining a beam of H_2^+ and D_2^+ ions, due to the disappearance of the hydrogen, was certainly as great with helium, somewhat less in the case of argon, and much worse in the case of neon. These gases must therefore have a greater adsorbability at some surface in the vacuum system than is usually attributed to them.

Another difficulty arose in obtaining the values of the emission in the cases of neon and argon. When a new supply of gas was let in after each disappearance the emission of electrons rose sharply and then fell gradually to a minimum

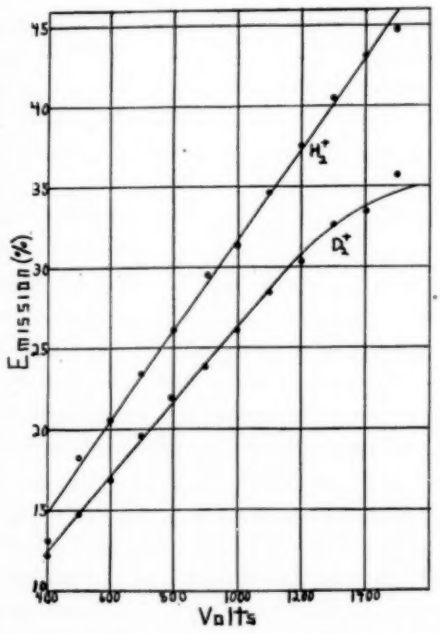

FIG. 1. Variation of the secondary electron emission with the positive ion energy expressed in volts. Values for He, Ne, and A.

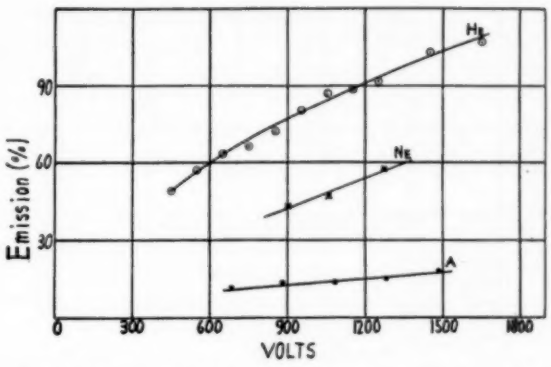

FIG. 2. Variation of the secondary electron emission with the positive ion energy expressed in volts. Values for H_2^+ and D_2^+.

value as readings were obtained at a constant ion energy. These minima could be accurately reproduced and the behavior was as if neon and argon were adsorbed even on the hot target and were knocked off by the beam until the minimum value obtained represented the emission from the metallic surface. This was surprising but it was difficult to attribute the effect to an impurity since the three gases, obtained as spectroscopically pure from the Linde Air Products Company, were let into the system in the same way and without any disturbance of the vacuum. Any foreign substance would have been present in the case of helium also. It is believed that further studies on the adsorption of noble gases on metals would be valuable.

Fewer values were obtained for neon and argon than for helium ions, partly because of the difficulty of maintaining a neon discharge, and partly because the resistance of the filament cathode of the discharge increased with use to such a marked degree that it was necessary to get a few data for these ions before the filament burned out. The conclusions to be drawn on the variation of the results with mass and energy of the ion are, however, unmistakable.

RESULTS

The curves showing the number of secondary electrons knocked out of the target per He, Ne, and A ion are shown in Fig. 1 plotted as percent against the energies of the ions expressed in electron volts. The deviations were nearly all well under 1 percent and the largest was 3 percent. In Fig. 2 are shown the curves for H_2^+

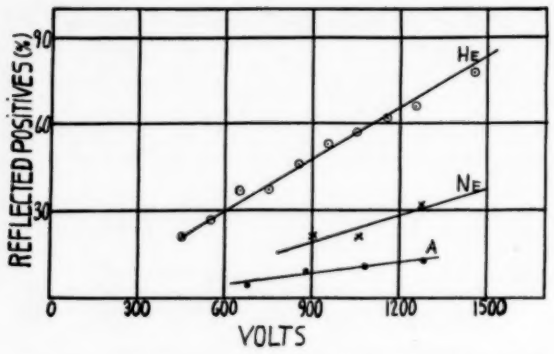

FIG. 3. Variation of the positive ion reflection with the primary positive ion energy expressed in volts. Values for He, Ne, and A.

and D_2^+ already reported in a letter to the *Physical Review*.[4] A rough test with a magnet showed that the beams in these cases consisted largely if not entirely of one kind of ion. Experience indicates that these ions are probably molecular. Clearly in all cases the emission caused by the lighter ion is greater at the same energy.

The values of the emission due to the noble gases cannot be compared with those due to the two hydrogens since different Ni targets were used in the two cases and their heat treatment was different. The choice of nickel as a target metal seems to have been an unfortunate one because of its anomalous behavior when heated. Miss Raines[7] has observed irregularities in the change of resistance of nickel with heat treatment unlike the behavior of other metals. Probably the change in emission after unusual heat treatment earlier reported[4] was due to recrystallization of the nickel and a consequent change in angle of impact of the ions on the target face. As stated above, however, no evidence was found for a change in the structure of the surface during either set of observations and the results show a comparison of the effect of different kinds of ions in each case.

When the percent emission is plotted against the velocities of the ions the helium curve lies between the one for neon and that for argon; when plotted against momentum, however, they lie in the same order as for the energy.

[7] Barbara Raines, Phys. Rev. **54**, 481 (1938).

The number of reflected positives plotted also as percent against the initial ion energy (Fig. 3) shows a similar trend, the number increasing with energy and a larger proportion of the lighter ions being reflected. The regularity of the increase in this case is to be compared with the more erratic results obtained for hydrogen[3] which were probably dependent on a varying small amount of hydrogen adsorbed on the surface.

DISCUSSION

Secondary emission curves may be compared in two respects, the shape of the curves themselves and the point at which they cut the emission axis. All of Jackson's work on the alkali ions showed a flattening of the curves similar to that due to primary electrons for which a maximum secondary emission is always found; it also showed no emission below a few hundred volts ion energy. Oliphant, on the other hand, found two changes in slope below 1000 volts and considerable emission at zero energy (extrapolated curve). The curves for the hydrogens, helium, neon, and argon show little if any departure from linearity, except that above 1000 volts both the He^+ and D_2^+ curves tend to flatten. Both the H_2^+ and D_2^+ curves when extrapolated show no emission below a certain value of the energy, but of course such an extrapolation is questionable. In this respect the results for He, Ne, and A are not at all definite. Hence no conclusions can be drawn as to the effect of the ionization energy of the ion in producing electrons.

No attempt is made to interpret the smaller emission of the heavier ions other than to say that it may be more difficult for a larger ion to penetrate the metal. Interpretation of results would probably be facilitated by using target surfaces formed by evaporation in the chamber in which measurements are made and by the use of a beam of ions of much lower energy. Further work along this line is contemplated.

The authors are indebted to Professor E. L. Chaffee of Harvard University for his continued interest in this work and to Professor Edna Carter of Vassar College for her interest and help at crucial moments.

Steady-State Diffusion Under Conditions of Generalized Source and Incident Current Distributions

E. A. SCHUCHARD AND E. A. UEHLING
Department of Physics, University of Washington, Seattle, Washington
(Received July 2, 1940)

The method of Laplace transformations is extended to the more general case of neutron diffusion in half-infinite media containing source distributions, and an exact expression for the emergent current distribution is obtained. This expression depends on the total m.f.p., on the ratio N of the capture to scattering m.f.p., and on the type of source distribution. For a uniform source distribution and with N sufficiently large, the values of the normalized current as a function of angle agree closely with those given by the Fermi law. More significant discrepancies between the results of elementary theories and the exact theory are to be found in the ratio R of detector activities corresponding to positions deep within the medium and at the surface. The exact theory gives $R=(N+1)^{\frac{1}{2}}+1$ for uniform source distributions. A recent quotation of $R=14$ for the case of thermal neutron diffusion in paraffin then implies $N=168$ instead of 196 as given by the elementary theory.

INTRODUCTION

THE diffusion of thermal neutrons in hydrogenous materials lends renewed significance to a class of problems in the theory of gases which have not hitherto had adequate treatment. In order to make application to the experimental situation of interest, one requires exact solutions of the Boltzmann conservation equation in closed form subject to boundary conditions which determine the behavior of the gas as a whole. The point of view which one adopts for the contemplation of the theoretical problem is necessarily very different from that adopted in the usual theory of gases. According to the latter one seeks solutions of the Boltzmann equation which describes the state of a gas within a differential volume element subject to arbitrarily assigned values of the gas parameters and their derivatives within this element. Such solutions are completely general, and they are in principle sufficient to determine the steady-state condition prevailing in the experimental problem of neutron diffusion. But there are two difficulties connected with such applications of the general solutions. On the one hand these solutions are obtained by perturbation methods and the resulting series converges rapidly to the exact solution only in the limiting case of small deviations from spherical symmetry, a condition which may not be even approximately fulfilled when an arbitrary assignment is made on the boundary conditions in the steady-state problem. On the other hand, one would require not only the solutions of the Boltzmann equation giving the distribution function in terms of the gas parameters and their derivatives, but also the solution of the steady-state hydrodynamical equations giving the spatial dependence of the gas parameters subject to the imposed boundary conditions.

A more direct approach would appear to be the search for solutions of the Boltzmann equation itself subject to the boundary conditions imposed on the entire gas. This point of view has been used already in the case of no external forces to give solutions of well-known problems in astrophysics, namely, the transmission of radiant energy through stellar[1,2] and planetary atmospheres.[3] The treatment has not been based explicitly on the Boltzmann equation, but this can be done by considering radiation as a gas[4] of photons.

In the problem of neutron diffusion one is interested in such questions as the distribution emergent from the surfaces of a medium when neutron currents of a particular character are incident on the surfaces and source distributions

[1] E. A. Milne, "Thermodynamics of Stars," *Handbuch der Astrophysik*, Vol. III/1 (Springer, 1930), pp. 96–183; V. A. Kostitzen, Mem. Sc. Math. **69** (1935).
[2] E. Hopf, *Problems of Radiative Equilibrium*, Cambridge Tract No. 31 (1934).
[3] L. V. King, Phil. Trans. Roy. Soc. **A212**, 375–433 (1913).
[4] G. Jaffe, Ann. d. Physik [5] **6**, 195–252 (1930).

exist within the medium. The assumption of source distributions and the property of finite absorption probabilities possessed by neutrons introduce new features into the physical situation insofar as particle diffusion is concerned; and the requirement of exact solutions in closed form demanded by the importance of the boundary effect and the slow convergence of usual series solutions introduces new features into the mathematical treatment.

The method of attack on this problem used by Halpern, Lueneburg and Clark[5] in connection with the study of the albedo coefficient is most satisfactory. According to this method the integral equation associated with the Laplace transform of the density function is studied, and solutions of this equation subject to the imposed boundary conditions are obtained before attempting to find the general solution of the Boltzmann equation. It is the object of the present paper to extend this method to the more general case of diffusion in a half-infinite medium within which there exist source distributions, to establish a certain equivalence between the problem of source distributions and that of finite incident currents, to consider questions of uniqueness of solutions, and to state more fully than has been done in the past the analyticity considerations fundamental to the rigorous and complete solution of the problem. Numerical applications are then made to the problem of thermal neutron diffusion in paraffin.

I. The Fundamental Integral Equations

§1. Boltzmann equation

In the class of problems under consideration mutual interactions are regarded as negligible and all interactions with centers of force within the medium are regarded as occurring isotropically without the exchange of energy. Such conditions represent a convenient mathematical idealization satisfactorily describing many physical situations involving the scattering, absorption and penetration of particles of one kind through a fixed uniform distribution of particles of another kind, and, in particular, the diffusion of thermal neutrons in certain hydrogenous materials. A further idealization according to which all spatial variations are one dimensional with azimuthal symmetry of all functions about this direction may be introduced for purposes of simplification without restricting essentially the validity of applications of the theory to many experimental situations. Isotropy of scattering without energy exchange has two important consequences. The first of these is that the absolute value of the velocity enters only parametrically in the equations. The second is that the total scattering into, as well as out of, a particular velocity class (defined by the differential solid angle containing the velocity vector) is proportional to a total scattering probability. Under these conditions the fundamental Boltzmann equation describing the steady-state condition in the absence of external forces is

$$v\alpha\frac{\partial f(x,\alpha)}{\partial x}=q(x,\alpha)-(P_s+P_c)f(x,\alpha)+\frac{P_s}{2}\int_{-1}^{1}f(x,\alpha)d\alpha, \quad (1)$$

where $f(x,\alpha)$ represents the number of particles per unit volume per unit solid angle at the point x having a velocity of magnitude v lying in $d\alpha$ where $\alpha=\cos\theta$ and θ is the angle between the velocity vector and the x-direction. Furthermore, P_s and P_c represent the total scattering and capture probabilities, and $q(x,\alpha)$ is the source strength representing the rate of production of v-speed particles per unit volume per unit solid angle.

§2. Integral equations in f(x, α)

Equation (1) together with certain boundary conditions defines $f(x,\alpha)$ everywhere within a single homogeneous isotropic medium. If there are several media possessing different scattering properties, an analogous equation exists for each. The properties of these equations are such that the boundary conditions may be specified in terms of arbitrary functions of α only in a particular way. The physical equivalent of such a specification is the arbitrary assignment of incident current distributions on the two outermost faces of the several media together with the requirement of continuity in the distribution function, but not its derivative, in passing from one medium to the next.

[5] O. Halpern, R. Lueneburg and O. Clark, Phys. Rev. 53, 173–83 (1938).

For a single homogeneous isotropic medium lying between the planes $x=0$ and $x=a$, one may specify consequently

$$f(0,\alpha)=f_0(\alpha), \quad \alpha>0; \qquad f(a,\alpha)=f_a(\alpha), \quad \alpha<0, \tag{2a}$$

where $f_0(\alpha)$ and $f_a(\alpha)$ are arbitrary functions defined in the restricted range of α and piece continuously in x onto the distributions within the medium. Equation (1) may now be integrated to give two integral equations in $f(x,\alpha)$ instead of a single integro-differential equation. Introducing the concept of mean free paths defined by

$$l_s=v/P_s, \quad l_c=v/P_c, \quad 1/l=1/l_s+1/l_c$$

and using the integrating factor $e^{x/l\alpha}/\alpha v$, one obtains

$$f(x,\alpha)=f_0(\alpha)e^{-x/l\alpha}+\int_0^x \frac{dx'}{\alpha}\left[\frac{F(x')}{4\pi l_s}+\frac{q(x')}{v}\right]e^{(x'-x)/l\alpha}, \quad \alpha>0, \quad 0\leqslant x\leqslant a; \tag{2b}$$

$$f(x,\alpha)=f_a(\alpha)e^{(a-x)/l\alpha}-\int_x^a \frac{dx'}{\alpha}\left[\frac{F(x')}{4\pi l_s}+\frac{q(x')}{v}\right]e^{(x'-x)/l\alpha}, \quad \alpha<0, \quad 0\leqslant x\leqslant a \tag{2c}$$

where

$$F(x)=2\pi\int_{-1}^{1} d\alpha f(x,\alpha) \tag{2d}$$

is the total density of particles at x.

These equations have a simple physical interpretation in terms of kinetic theory concepts. Thus, for example, the first part of the integral represents the density contribution to the distribution function at a specified x plane due to free flight trajectories (straight lines for no external forces) from a plane at x' where the density is $F(x')$. The contribution from a layer of thickness dx' is made up of the product of four factors: (a) the number of collisions per second $vF(x')dx'/l\alpha$ in the "ray volume element" dx'/α; (b) the probability $1/4\pi$ of scattering into unit solid angle about α under isotropic conditions; (c) the probability l/l_s that the collision is a scattering act and not one of capture; and (d) the probability $\exp[-|(x'-x)/l\alpha|]$ that the particle will travel the ray distance $|(x'-x)/\alpha|$ without further collision. The product of these factors actually yields the current density per unit solid angle about α at x, and division by v must be made to obtain the corresponding distribution function. A similar interpretation in terms of the contribution due to incident currents and source distributions can be made for the other terms of the equations.

§3. Integral equation in F(x)

A general method of solving the simultaneous integral equations in $f(x,\alpha)$ is to solve first the single integral equation in $F(x)$ obtained by performing the integration of Eq. (2d) on the functions f defined by Eqs. (2b) and (2c). This integral equation may be put into the form

$$F(x)=g(x)+\frac{l}{2l_s}\int_0^a dx'K(|x'-x|)F(x'), \quad 0\leqslant x\leqslant a, \quad 0\leqslant\frac{l}{l_s}\leqslant 1, \tag{3a}$$

where all distances are measured in units of the total m.f.p. l. The inhomogeneous term is a continuous function for all problems of physical interest, and is given in terms of incident current distributions and isotropic source distributions by the equation

$$g(x)=2\pi\left[\int_0^1 d\alpha f_0(\alpha)e^{-x/\alpha}+\int_{-1}^0 d\alpha f_a(\alpha)e^{(a-x)/\alpha}+\frac{l}{v}\int_0^a dx'K(|x'-x|)q(x')\right]. \tag{3b}$$

The symmetric kernel of the integral equation is the logarithmic integral function defined by

$$K(s)=\int_0^1 d\alpha e^{-s/\alpha}\alpha^{-1}, \quad s>0. \tag{3c}$$

Because of the properties of K, the general solution of Eq. (3a) may be obtained in the form of an

infinite series (the Neumann iteration solution)[6] by the method of successive approximations. One can show that no other bounded continuous solution exists.[7] However, for half-infinite medium problems ($a \gg 1$, a measured in units of l) and a small capture probability ($l/l_s \sim 1$), which is the case of interest for example in the diffusion of thermal neutrons in extended hydrogenous materials, convergence of the series is slow and a solution in closed form is desirable. Such a solution may be obtained by the method of Laplace transformations.

§4. Integral equation in f(0, z)

The form of the emission current expression for the case of isotropic sources ($q(x, \alpha) = q(x)$) and half-infinite medium conditions ($a = \infty$), which is given by Eq. (2c) when x is set equal to zero, suggests the use of the Laplace transformation of the density function. The following Laplace transformation is obtained by analytic continuation of (2c) into the complex plane

$$-zf(0, z) = \int_0^\infty dx' e^{x'/lz} \left[\frac{F(x')}{4\pi l_s} + \frac{q(x')}{v} \right], \quad R(z) < 0. \tag{4a}$$

The integral defines a regular function for $R(z) < 0$ as long as $F(x)$ and $q(x)$ are absolutely integrable over any finite interval and the above integral exists.[8] If, furthermore, $F(x)$ and $q(x)$ are continuous, the transformation (4a) has a unique inversion of the form[9]

$$\frac{F(x)}{4\pi l_s} + \frac{q(x)}{v} = \lim_{t_2 \to \infty} \frac{1}{2\pi i} \int_{t_1 - it_2}^{t_1 + it_2} dt \frac{e^{xt}}{lt} f(0, -1/lt), \quad t_1 > 0, \quad 0 < x < \infty. \tag{4b}$$

It is now evident that the problem can be solved in closed form if a closed analytic expression for $f(0, z)$ with $R(z) < 0$ can be found. The integral equation which $f(0, z)$ must satisfy in the general case of isotropic sources and axially symmetric incident currents on the face of the half-infinite medium can be obtained in a manner analogous to that for the case of incident current distributions alone.[5] One obtains

$$p(z, \sigma) f(0, z) - I(z) = \sigma \int_{-1}^{0} d\alpha \frac{\alpha f(0, \alpha)}{\alpha - z}, \quad R(z) < 0 \quad \text{and} \quad z \neq (-1, 0), \tag{4c}$$

where

$$p(z, \sigma) = 1 + \sigma z \int_{-1}^{1} d\alpha/(\alpha - z), \quad \sigma = l/2l_s, \tag{4d}$$

$$I(z) = \sigma \int_0^1 d\alpha \frac{\alpha f_0(\alpha)}{\alpha - z} - \int_0^\infty dx e^{x/lz} q(x)/vz, \quad R(z) < 0. \tag{4e}$$

II. Function Theory Treatment for Half-Infinite Medium Problems

§5. Regularity conditions

The integral equation (4c) and its analytic continuation have the particular significance of giving the analytic behavior of $f(0, z)$ everywhere in the complex z plane where it is not already known, i.e., in the right half-plane. For, assuming $f(0, \alpha)$, $-1 \leq \alpha \leq 0$, piecewise continuous, the right-hand side of (4c) or

$$\sigma \int_{-1}^{0} d\alpha \frac{\alpha f(0, \alpha)}{\alpha - z} = \sigma M(z) \tag{5a}$$

represents a regular function of z off the path

[6] E. Whittaker and G. Watson, *Modern Analysis* (Cambridge University Press, 3rd edition, 1920), § 11.4. The logarithmic infinity at the zero argument of the kernel function causes no difficulty since $\frac{1}{2}\int_0^a dx' K(|x' - x|) \leq 1$, $a \leq \infty$, and therefore the convergence of the iterative series may be demonstrated easily for either $l/l_s < 1$ or $a < \infty$. The limit case of $l/l_s = 1$, $a = \infty$ has been settled by E. Hopf, reference 2, Theo. VII, pp. 38–40.

[7] Cf. ahead in §8 and references 20, 21.

[8] G. Doetsch, *Theorie und Anwendung der Laplace Transformation* (Springer, 1937), pp. 40–3.

[9] Reference 8, p. 105, Theo. 2.

of integration.[10] Hence, the behavior of $p(z, \sigma)$ and of the given inhomogeneous term $I(z)$ (assumed capable of analytic continuation into the right half-plane) will impose certain analyticity requirements on $f(0, z)$ in order that the left-hand side, known regular for $R(z)<0$ and $z\neq(-1,0)$ by the validity of Eq. (4c), continue to be regular for $R(z)>0$ by the unique analytic continuation called for by $M(z)$. More important, it will appear that satisfaction by a function of these regularity conditions is not only necessary but *sufficient* that this function be a solution of the integral Eq. (4c). Briefly, the sufficiency establishment may be carried out along the following lines,[11] with the essential regularity conditions appearing in the process.

The regularity and first order vanishing at infinity of $M(z)$ gives zero as the value of the contour integral[12]

$$\frac{1}{2\pi i}\oint_L ds\frac{\sigma M(s)}{s-z}=0, \qquad \begin{matrix}L \text{ containing line}\\ (-1,0) \text{ and point}\\ z\neq(-1,0),\end{matrix} \tag{5b}$$

where L is a closed ordinary[13] contour which may touch the line $(-1,0)$ at the origin.[14] From Eq. (4c) and its analytic continuation one may restate (5b) as

$$\frac{1}{2\pi i}\oint_L ds\frac{p(s, \sigma)f(0, s)-I(s)}{s-z}=0 \tag{5c}$$

with the ordinary contour L arbitrary except for the restrictions mentioned in connection with (5b). Therefore, by taking the point z to be anywhere in the complex plane except the interval $(-1,0)$, one sees from Eq. (5c) that a proposed solution $f_1(0, z)$ must be such that the expression

> $p(z, \sigma)f_1(0, z)-I(z)$ is made regular for any $z\neq(-1,0)$ and is continuous into the origin for all approaches not including the negative axis. (A)

Under such conditions one may write by Cauchy's theorems:

$$\frac{1}{2\pi i}\oint_L ds\frac{p(s, \sigma)f_1(0, s)-I(s)}{s-z}=p(z, \sigma)f_1(0, z)$$
$$-I(z)+\frac{1}{2\pi i}\oint_{L'} ds\frac{p(s, \sigma)f_1(0, s)-I(s)}{s-z}, \tag{5d}$$

where L' is an ordinary contour enclosing only the line segment $(-1,0)$ which it touches at the origin while otherwise remaining in the left half-plane (the integration sense is the same as on L). Now if

> $f_1(0, z)$ and $I(z)$ are taken regular in the left half-plane and continuous into the origin from $R(z)<0$ approaches, (B)

the introduction of p's definition (4d) into the L' integral gives

$$\frac{1}{2\pi i}\oint_{L'} ds\left(1+\sigma s\int_{-1}^{1}\frac{d\alpha}{\alpha-s}\right)\frac{f_1(0, s)}{s-z}$$
$$=\frac{\sigma}{2\pi i}\oint_{L'} ds\frac{sf_1(0, s)}{s-z}\int_{-1}^{1}\frac{d\alpha}{\alpha-s}$$
$$=-\sigma\int_{-1}^{0} d\alpha\frac{\alpha f_1(0, \alpha)}{\alpha-z}, \tag{5e}$$

where the last expression follows formally by interchanging the order of integration and applying the residue rule, and can be justified in detail for the ordinary contours employed here by usual limit arguments. Finally, the left-hand side of Eq. (5d) will have zero as its value if

> $z[p(z, \sigma)f_1(0, z)-I(z)]$ is made regular at the infinite point. (C)

Thus the regularity conditions (A, B, C) insure through Eqs. (5d, e) that $f_1(0, z)$ actually is a solution of the integral equation (4c).

§6. Analyticity properties

In order to use the regularity conditions in constructing a solution, the analytical nature and continuation of the inhomogeneous term $I(z)$ must be given over the entire complex plane. For zero incident currents, inspection of a table of Laplace transformations shows that the simplest form for $I(z)$ is obtained by special-

[10] E. J. Townsend, *Functions of a Complex Variable* (Holt, 1915), p. 80, Theo. III.

[11] This treatment was suggested by the related one of reference 5 for the special case of incident currents of δ-function type.

[12] Reference 10, p. 273, Theo. X.

[13] Reference 10, p. 47.

[14] Reference 10, p. 71, Theo. II; only continuity with the surrounding regular values is required on the integration path for the validity of Cauchy's theorem.

izing the source emission rate to be a constant or an exponentially decaying function, namely:

$$q(x)=qe^{-mx},\quad q=\text{const.}\gtrless 0,\quad m\gtrless 0,\quad x\gtrless 0, \tag{6a}$$

when, with $R(z)<0$,

$$I(z)=-\int_0^\infty dx e^{zl/l_2}q(x)/vz=\frac{q/vm}{1/ml-z}. \tag{6b}$$

From the integrated form it is apparent that such a source term has a unique analytic continuation over the entire complex z plane with a simple pole on the positive real axis at $1/ml$.

The function $p(z,\sigma)$ must be examined now in detail. From its definition given by (4d), it may be expressed as

$$p(z,\sigma)=1+\sigma z\ln\frac{z-1}{z+1}\begin{cases}\text{principal value of ln,}\\ \text{branch cut } (-1,1).\end{cases} \tag{6c}$$

The definition (4d) shows that p is a regular function, $z\neq(-1,1)$, with the limit value $1-2\sigma$ at infinity; also, that $p(z,\sigma)=p(-z,\sigma)$. Equation (6c) shows that p has the limit value 1 at the origin, has branch points which are logarithmic singularities at $z=\pm1$, and has just two simple zeros[15] at $z=\pm s_0$ where s_0 is the positive real root of the condition for which p vanishes:

$$1=\sigma s_0\ln\frac{s_0+1}{s_0-1}=2\sigma\left(1+\frac{1}{3s_0^2}+\frac{1}{5s_0^4}+\cdots\right),\qquad 0<\sigma\leqslant\tfrac{1}{2}. \tag{6d}$$

In order that $p(z,\sigma)f_1(0,z)$ be regular on (0,1), in particular single-valued, as required by the regularity condition (A), one is forced to conclude that p can be expressed as a product of two functions one of which is regular for z on the strip (0,1) so that the other function may be taken as a reciprocal factor in f_1 and hence disappear in the product $p(z,\sigma)f_1(0,z)$. At the same time, condition (B) makes the reciprocal factor in f_1 have no zero in the left half-plane. This regularity and nonzero value required of one factor for $R(z)<0$ is met by the following product decomposition of p through the aid of Cauchy's integral formula on ln p:

$$\ln p(z,\sigma)=\frac{-2iz}{2\pi i}\oint_{N'+N''}\frac{\ln p(it,\sigma)}{t-iz}\frac{dt}{t-(-iz)},\quad -iz \text{ inside contour } N'+N'' \tag{6e}$$
$$\equiv\ln p_1(z,\sigma)+\ln p_2(z,\sigma),$$

where the closed contour $N'+N''$ of integration encloses no singularities of $\ln[p(it,\sigma)]/(t-iz)$ and is considered to be composed of two parts N' and N'' uniting only at the origin (positive-real side) and $+\infty$ with, say, N' being the part that starts from the origin and passes to the infinite point beneath the point $-iz$ in the complex t-plane, and where the N' portion of the integral is to be associated with ln $p_1(z,\sigma)$, the N'' with ln $p_2(z,\sigma)$. By taking $R(z)<0$, the N' path may be deformed continuously to coincide with the positive-real axis giving for ln p_1:

$$\ln p_1(z,\sigma)=\frac{-z}{\pi}\int_0^\infty dt\frac{\ln p(it,\sigma)}{z^2+t^2},\quad \frac{\pi}{2}<\arg z<\frac{3\pi}{2}\quad (R(z)<0),\quad 0\leqslant\sigma\leqslant\tfrac{1}{2}.^{16} \tag{6f}$$

With $R(z)<0$, analogously

$$\ln p_2(z,\sigma)=\frac{z}{\pi}\int_0^\infty dt\frac{\ln p(it,\sigma)}{z^2+t^2}=\ln p_1(-z,\sigma)=\frac{1}{\pi}\int_0^\infty du\frac{\ln p(izu,\sigma)}{1+u^2},\quad -\frac{\pi}{2}<\arg z<\frac{\pi}{2},\quad 0\leqslant\sigma\leqslant\tfrac{1}{2}. \tag{6g}$$

The last integral form in (6g) is uniformly convergent, $0\leq z\leq\infty$, for $\sigma<\frac{1}{2}$ by the dominance in absolute value of $-\ln(1-2\sigma)\int_0^\infty du/(1+u^2)\pi=-\ln(1-2\sigma)^{\frac{1}{2}}$, so that $z=0$ and $z=\infty$ may be inserted inside the integral sign[17] to evaluate ln $p_2(0,\sigma)=0$ and ln $p_2(\infty,\sigma)=\ln(1-2\sigma)^{\frac{1}{2}}$. The uniform con-

[15] Cf. E. T. Copson, *Theory of Functions of a Complex Variable* (Oxford University Press, 1935), p. 119, for the "principle of the argument" by which it can be shown that no other zeros of p exist.

[16] This is essentially the same result for $p_1(z,\sigma)$ as obtained in reference 5 where, however, the validity for $\sigma=\frac{1}{2}$ was not demonstrated.

[17] E. Wilson, *Advanced Calculus* (Ginn, 1912), p. 369.

tinuity continues to exist for $\sigma=\frac{1}{2}$ and z finite, $R(z)>0$, since the integrand vanishes sufficiently strongly at infinity. In fact, the integral represents an analytic function in z whose derivatives of all orders may be formed by differentiation under the integral sign,[18] $R(z)>0$. This last property is useful in establishing the rate of p_2's decrease along the positive real-axis evident in Eq. (6g), in particular, that p_2 has a vertical tangent of logarithmic order at the origin. By the definitions of $p_1(z, \sigma)$ and $p_2(z, \sigma)$ through the N' and N'' contour integrals of (6e) and all analytical continuations possible by continuous deformations of the paths of integration N' and N'', it follows that p_1 and p_2 are regular functions of z over the whole plane except that p_1 contains p's branch cut singularities (0,1) and p's zero in the right half-plane while p_2 shows these same properties of p in the left half-plane ($p_1(z, \sigma) = p_2(-z, \sigma)$ and $p_1(z, \sigma)p_2(z, \sigma)=p(z, \sigma)$).

§7. Solution for exponentially-distributed sources

The complete satisfaction of the regularity conditions is now readily verified for the inhomogeneous term (6b) by the following function:

$$f(0, z)=\frac{q/vm}{1/ml-z}\,\frac{1}{p_1(z, \sigma)p_2(1/ml, \sigma)}, \quad \sigma<\tfrac{1}{2} \quad \text{or} \quad m>0, \tag{7a}$$

which therefore constitutes the solution of the integral equation (4c) for exponentially-distributed sources. When z is negative-real, Eq. (7a) gives a positive definite function, as is, indeed, necessary for physical meaning. When $\sigma=\frac{1}{2}$ and $m=0$, one can show that $ql\sqrt{3z}/vp_1(z, \frac{1}{2})$ satisfies the regularity conditions because $p_2(z, \frac{1}{2})$ behaves like $1/\sqrt{3z}$ around the infinite point;[19] however, this is a non-physical solution, being negative when z is in $(-1,0)$ with $q>0$, and is a consequence of the fact that the homogeneous integral equation arising from (4c) has solutions when $\sigma=\frac{1}{2}$. The latter are found from the corresponding regularity conditions obtained by setting $I(z)=0$ in statements (A, C). A one-signed solution for $\sigma=\frac{1}{2}$ is evidently:

$$f_h(0, z)=C/p_1(z, \tfrac{1}{2}), \quad C=\text{const.} \tag{7b}$$

§8. Uniqueness considerations

The uniqueness of the solution (7a) and the significance of (7b) must now be determined. A related point is the verification that these solutions of the complex-variable integral are actually the ones coming from the Boltzmann equation with given boundary conditions, or from the integral equations (2b and c) for the half-infinite medium case. These questions can be answered through the uniqueness of the Laplace transformation and its inversion, and the uniqueness of the solutions for the number density integral equation (3a). The existence of a solution for the number density equation has already been indicated. Its uniqueness among continuous bounded solutions when either $l/l_s<1$ or $a<\infty$ follows out of the zero solution of the corresponding homogeneous integral equation arising from (3a) for $g(x)\equiv 0$.[20] The same uniqueness exists in the limit case, too, unless unbounded solutions at infinity are allowed. Then a one-signed solution exists which is unique except for a multiplicative constant and which represents the limit solution of a problem (free of sources) in which the medium slab thickness becomes indefinitely large while the sole incident current at the far face becomes likewise indefinitely large. These last two statements are inferred from the work of E. Hopf[21] on the equivalent problem (pure scattering, half-infinite medium) in astrophysical radiation theory. Such number density uniqueness means that there is essentially only one associated $f(0, z)$ coming from the integral equations in f and therefore satisfying the relations (4a, b). The question is then whether the solutions (7a, b) are

[18] Reference 15, pp. 110–1, the simultaneous integrand continuity in z and u is assured by that of the product zu and by the regularity of $\ln p(izu)$ here.

[19] Reference 5, Eqs. (34), (55) and (58).

[20] Cf. K. Schwarzschild, Berlin Sitz., 1914, Part 2, pp. 1191–2, who gives a simple method applicable here.

[21] E. Hopf, Zeits. f. Physik **46**, 374 (1927–8); **49**, 155 (1928); also, reference 2, p. 37 (Lemma 2).

capable of representation in the form (4a), i.e., that the $F(x)$ function they define by (4b) is inversely related to them by (4a). This representation is indeed possible for functions of the type called for by the regularity conditions and the inhomogeneous terms involved.[22] Hence the uniqueness of the solutions of the complex-variable integral equation (4c) which are regular in the left half-plane with a finite limit value at the origin and positive-realness on the negative-real axis is just that of the corresponding number density solutions obtained from the integral Eq. (3a). Furthermore, these $f(0, z)$ functions necessarily satisfy the Boltzmann equation and boundary conditions since they have the required representation character. The significance and essential uniqueness of the solution (7b) is evident from the corresponding one-signed number density solution for $\sigma=\frac{1}{2}$, $a=\infty$ and its interpretation as the limit of a finite medium problem (by which the arbitrary constant C can be considered determined). When z lies in the interval $(-1,0)$, a suitable transformation of form displays the equivalence of the solution (7b) and that obtained by E. Hopf for starlight emission[23] by means of somewhat different analytical arguments.

§9. Incident current equivalence

For the case of no interior sources within the medium but with incident currents on the finite face, considered in detail by Halpern, Lueneburg and Clark,[5] the same form of inhomogeneous term as (6b) arises when the incident distribution (axially-symmetric) is restricted to a single direction, i.e.,

$$f_0(\alpha)=f\delta(\alpha-\alpha_0), \quad f=\text{const.}\geqslant 0, \qquad 0<\alpha\leqslant 1, \quad 0<\alpha_0=\text{const.}\leqslant 1. \tag{9a}$$

Then

$$I(z)=\sigma\int_0^1 d\alpha\frac{\alpha f_0(\alpha)}{\alpha-z}=\frac{f\sigma\alpha_0}{\alpha_0-z} \tag{9b}$$

for which the solution can be obtained from Eq. (7a) by the parameter association:

$$1/ml=\alpha_0 \quad \text{and} \quad q=f\sigma v/l. \tag{9c}$$

The restriction of $\alpha_0\leq 1$ is interesting as it is one evidence of the lack of complete equivalence of an incident current "beam" to an exponentially-decaying interior source distribution of arbitrary decay constant m. A beam of particles incident on a half-infinite medium decays in primary strength as $e^{-r/l}$ where $r=x/\alpha_0$ is the "ray" distance into the medium from the finite face and l is the total m.f.p. in the medium. Likewise, the number of particles left behind in any element dr is proportional to $e^{-z/l\alpha_0}$. Because of the isotropic no-energy-exchange character of the scattering assumed here, this decay of the direct beam as it enters the medium acts like a source distribution of exponentially decaying form e^{-mz} with $m\geq 1/l$ $(m=1/l\alpha_0,\ \alpha_0\leq 1)$. For such a type of source distribution the equivalence is complete insofar as the emission current from the medium and the interior distribution $f(x, \alpha)$ with $\alpha\neq\alpha_0$. The form and limitations of the equivalence are evidently determined by the type of medium scattering-capture character.

§10. Analytic continuation for general distributions

The solution (7a) for $f(0, z)$ is an analytic function in $1/ml$ (considered as a complex variable) when $1/ml$ is excluded from the point z, the points of the line $(-1,0)$, and the zero of p in the left half-plane. As far as the emission distribution (4a) or the inversion of the Laplace transformation in (4b) is concerned, it is only necessary to have $R(z)<0$ in $f(0, z)$. Hence, the analyticity in $1/ml$ in (7a) exists for the whole right half-plane including the imaginary axis (but only continuity at the origin); and therefore, a unique analytic continuation of the solution from positive-real $1/ml$ values to those with pure imaginary ones can be made. Since the complex-variable integral equation (4c) is linear,

[22] Reference 8, p. 126–8, Theo. 2–3.
[23] Reference 2, pp. 31, 77, 105.

TABLE I. *Numerical values for* $\ln 1/p_2(z, N)=\ln 1/p_1(-z, N)$.

N	$z=0$	1/8	1/4	1/2	3/4	7/8	98/100	1	∞
∞	0	0.2629	0.4358	0.6980	0.901	0.9887	1.0558	1.0674	∞
150	0		0.4004	0.6297	0.7998	0.8715		0.9395	$\ln(151)^{\frac{1}{2}}$

there exists a superposition principle of individual solutions corresponding to particular inhomogeneous terms, which superposition is unique provided the homogeneous integral equation has no solutions—as certainly is the case for $\sigma<\frac{1}{2}$ or bounded solutions. Thus, by adding solutions corresponding to $m=in$ and $m=-in$ (n=positive integer), the solution corresponding to a cosine source distribution will be obtained; and analogously, for sine distributions. Therefore, the solution for any source distribution representable by a finite Fourier series can be written down in principle. Superposition of the incident current solutions then takes care of the more general case.

III. Applications to Thermal Neutron Diffusion

§11. Emission from paraffin

Thermal neutrons from natural radioactive sources are normally obtained from the Fermi standard paraffin cylinder.[24] A Rn-Be capsule inside the cylinder gives off high speed neutrons which are quickly degraded by collisions with the many protons in the paraffin molecule into the thermal energy region. Once the neutron's energy is below the lowest vibrational level of the C−H bond (0.1 ev[25]), collision effects are with the CH_2 group as a whole insofar as conservation laws are concerned. Lower energies make still more of the paraffin molecule ($\sim C_{22}H_{46}$) the effective mass group with which the neutrons interact. Because of the short range of interaction, only the s type of scattering is of importance for slow neutrons. The mutual interactions of the neutrons can be neglected for the low concentrations available in the laboratory; and the diffraction effects from the space lattice appear to be small. Hence one is led to consider the scattering of thermal neutrons in paraffin to be approximately of the type considered in the preceding theory for which exact solutions are now available when the mean free paths and source distribution are given. The experimental m.f.p. for thermal neutrons in paraffin is 0.3 cm, with scattering occurring about 150 times as often as complete capture. In first approximation it is usual to assume that the production of thermal neutrons is uniform over the hydrogenous material in the final steady state.

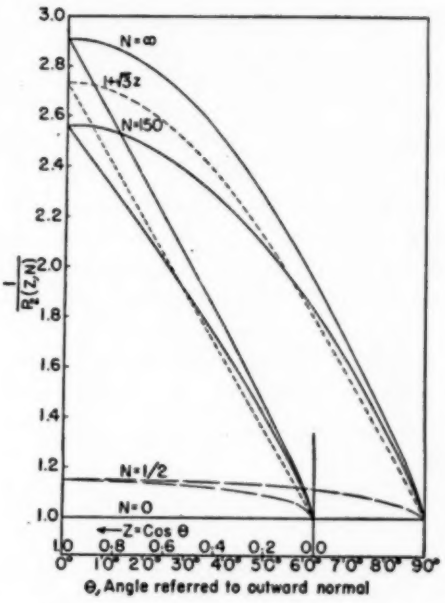

Fig. 1. Emergent number distribution-in-angle for uniform sources.

[24] E. Amaldi and E. Fermi, Phys. Rev. **50**, 901 (1936).
[25] H. A. Bethe, Rev. Mod. Phys. **9**, 126 (1937).

Table II. *Normalized current density emission values.*

θ or $\cos^{-1}\alpha$	$\frac{\alpha p_3(1,150)}{p_2(\alpha,150)}$	$\frac{\alpha p_2(1,\infty)}{p_1(\alpha,\infty)}$	$\frac{\alpha+\sqrt{3}\alpha^2}{1+\sqrt{3}}$	$\frac{\alpha+3\alpha^2/2}{1+3/2}$	$\frac{\alpha p_3(1,150)}{0.896 p_2(\alpha,150)}\left(1-\frac{0.209}{1+\alpha}\right)$
0°	1.	1.	1.	1.	1.
10°	0.978	0.976	0.976	0.976	0.977
20°	0.911	0.905	0.904	0.906	0.907
30°	0.805	0.794	0.793	0.797	0.798
40°	0.671	0.656	0.653	0.659	0.661
50°	0.522	0.501	0.498	0.506	0.509
60°	0.367	0.345	0.342	0.350	0.353
70°	0.219	0.202	0.200	0.207	0.207
80°	0.0925	0.0832	0.0827	0.0876	0.0847
90°	0	0	0	0	0

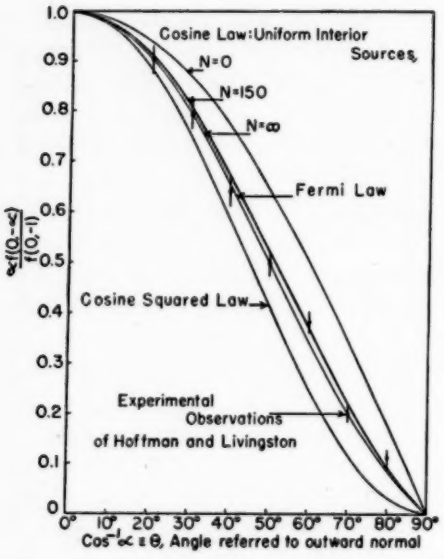

FIG. 2. Normalized emission current distribution-in-angle for thermal neutrons in paraffin.

Concerning the nature of the thermal neutron emission from the paraffin block, Fermi proposed the current density distribution (per unit zonal angle) $\cos\theta(1+\sqrt{3}\cos\theta)$, where θ is the zonal angle referred to the *outward* normal of the emitting face. Fermi[26] and Bethe[27] in deriving this relation neglect the small capture effects, introduce the classical diffusion coefficient, assume isotropic scattering, and consider no distributed interior sources in the block (idealized into a half-infinite medium) but merely assume the number density to vary linearly near the boundary. These many assumptions are not completely compatible. Therefore, it is of interest to obtain the emergent number distribution-in-angle on the basis of the present theory which incorporates source and capture effects directly, makes no use of a diffusion coefficient, and has an exact solution.

The emission distribution is given by Eq. (7a) when z lies in the interval $(-1,0)$ or $z=-\cos\theta$. Only the case of a uniform source distribution ($m=0$) will be considered in detail. Since $p_1(z,\sigma)$, or $p_2(-z,\sigma)$, appears to constitute a new transcendental function, numerical evaluation of the definite integral definition was necessary to obtain the results given in Table I for various values of the ratio N of capture to scattering mean free path, or the inverse ratio of the cross sections σ_c, σ_s; i.e.,

$$N=l_c/l_s=\sigma_s/\sigma_c=2\sigma/(1-2\sigma). \tag{10}$$

The notation $p_2(z,N)$ has been introduced for $p_2(z,\sigma)$, where σ and N are related as in (10). To effect the evaluation, the infinite integral of Eq. (6g) was transformed to the following proper one by introducing the new variable $\arctan(1/zu)$ and then integrating partially the fractional part of the resulting integrand:

$$\ln\frac{p_2(z,N)}{(1+z)^{\frac{1}{2}}}=\frac{-1}{\pi}\int_0^{\pi/2}d\theta\frac{\cot\theta+N\theta}{N+1-N\theta\cot\theta}\arctan(z\tan\theta),\quad R(z)<0. \tag{11}$$

The curves of $1/p_2(z,N)$ as a function of z and of θ are shown in Fig. 1.

These curves can be interpreted as being proportional to the emission distribution from the half-infinite medium. The pure scattering case of $N=\infty$ has meaning only in a limiting sense, since the factor of proportionality $1/p_2(\infty,N)=(N+1)^{\frac{1}{2}}$ becomes infinite, unless the interpretation is made on the basis of the homogeneous equation solution (7b) due to an "infinitely-strong" current incident on the "infinitely-far off" face. The exact solutions have a marked dependence on N; and the Fermi relation $1+\sqrt{(3)}z$ is but a rough approximation to the case $N=150$, having a slope more nearly corresponding to $N=\infty$. If the distributions had been reduced to the same value at normal emission, $z=1$, then the Fermi relation and the $N=\infty$ case would agree for not too large angles—which is not surprising considering the homogeneous equation interpretation of the $N=\infty$ case and the generally-corresponding character of the assumptions underlying the Fermi relation.

Passing to the quantity which can be observed directly in experiments, namely, the current density distribution normalized with respect to the normal emission value, one obtains the curves of Fig. 2 together with the

[26] E. Fermi, Ricerca Scient. 7, 13 (1936).
[27] Reference 25, pp. 132–3.

experimental observations of Livingston and Hoffmann[28] on thermal neutron emission from the standard paraffin cylinder. Any value of N from infinity down to 150 in the exact solution appears compatible with the experimental results. The simple cosine law corresponding to pure capture is definitely outside of the experimental data, as also is the cosine-squared law drawn in for comparison. To the scale used, the Fermi law and the $N=\infty$ case are indistinguishable, while the discrepancy with the $N=150$ case has been reduced over that present in the number distribution-in-angle because of the normalization process and the addition of the $\cos\theta$ factor. It may be noted that the relation $\cos\theta(1+\frac{3}{2}\cos\theta)/(1+\frac{3}{2})$ gives a curve intermediate between $N=\infty$ and $N=150$ with, therefore, a better approximation to the exact solution for $N=150$ than the Fermi law.[29] However, the differences for N greater than 150 are hardly large enough to be emphasized in comparison with the indicated statistical uncertainty of the experimental observations. The numerical data are summarized in Table II (the last column will be referred to in the next section).

§12. Ratio of capture to scattering mean free path

The comparison with experiments just made indicates that the lower limit to be expected for N is approximately 150. However, it is to be observed that the deduction is based on the hypothesis of a uniform production of thermal neutrons, whereas it is probably more reasonable to expect the production rate to fall off near the emitting face. To obtain some idea of the effect of such a falling-off, the solution for a source distribution like $1-e^{-mz}$, $m=1/l$, was obtained by superposition (the smallest m value possible with the extent of the calculations given in Table I was used). The resulting current distribution lies roughly halfway between the $N=150$ and the $N=\infty$ uniform source cases, as shown by the last column of Table II. Thus N can possibly take smaller values than 150. The source distribution or the emission current must be known more precisely to fix N in this way.

Another method for the determination of N appears in the cross section expression. Combining two different experimental values for the scattering cross section[30,31] with the capture cross section measured for water[32] (a direct measurement for paraffin is not known), one obtains for N the two values, 169 ± 8 percent and 195 ± 8 percent, indicating that N actually lies between 150 and 200.

The Fermi "albedo" formula[33] gives an expression for evaluating N as

$$N=R^2, \tag{12a}$$

where R is the ratio of the activity of a thin detector placed deep in the interior of the paraffin to that at the surface of the paraffin. The exact solution for uniform sources furnishes a somewhat modified formula:

$$N=R^2-2R. \tag{12b}$$

If one uses a recent quotation[34] of $R=14$ he

[28] J. G. Hoffman and M. S. Livingston, Phys. Rev. **53**, 1020L (1938).

[29] The current law $\cos\theta[1+(3/2)\cos\theta]$ can be obtained by a modified treatment based on the assumptions underlying the Fermi law.

[30] J. G. Hoffman and M. S. Livingston, Phys. Rev. **53**, 929A (1938).

[31] H. Carroll and J. R. Dunning, Phys. Rev. **54**, 541L (1938); H. B. Hanstein, Phys. Rev. **57**, 1045L (1940).

[32] A. H. Spees, W. F. Colby and S. Goudsmit, Phys. Rev. **53**, 326A (1938).

[33] Reference 24, p. 910, Eqs. (10) and (11).

[34] J. H. Manley, H. H. Goldsmith and J. Schwinger, Phys. Rev. **55**, 44 (1939).

TABLE III. *Transmission ratios for absorption coefficient measurements.*

Kx	Eq. (14) with Exact Solution $N=150$	$\frac{K_1(Kx)+(3/2)K_2(Kx)}{1+3/4}$	$\frac{K_1(Kx)+\sqrt{3}K_2(Kx)}{1+\sqrt{3}/2}$	Eq. (14) with Exact Solution $N=\infty$
0	1.	1.	1.	1.
0.2	0.620	0.629	0.634	0.634
0.4	0.435	0.443	0.448	0.447
0.6	0.316	0.322	0.326	0.325
0.8	0.234	0.238	0.242	0.241
1.0	0.175	0.179	0.181	0.181
1.4	0.101	0.103	0.105	0.105
2.0	0.046	0.047	0.048	0.048

obtains $N=168$. The expression (12b) involves the usual assumption that a thin detector's activity is proportional to the number density at its location and that N is constant over the thermal speed band. The expression comes from

$$R=\frac{F(\infty)}{F(0)}=\frac{f(0,-\infty)-ql/v}{f(0,0)-ql/v}=(N+1)^{\frac{1}{2}}+1, \quad (12c)$$

where the second equality comes from the Laplace transformation (4a), and the third, from the use of the solution (7a) for the f's with $m=0$.[35]

§13. Thermal neutron absorption coefficients

With the character of the thermal neutron emission from the standard paraffin block known, the experiments with plane parallel layers of absorbers and detectors exposed to the emission can be interpreted. Scatterers, however, may introduce complications due to the disturbances of the boundary condition by the back scattering. A class of experiments for which the emergent number density distribution (and not current density) enters more directly into the interpretation of the results is represented by absorption coefficient measurements for different materials with thermal neutrons. Varying thicknesses of the absorber material are placed between the paraffin face and the detector; and the resulting reduction in the activity of the latter depends essentially upon the particle numbers allotted by the paraffin block to the different oblique directions through the absorber, as the following analysis shows:

Let K and x denote the absorption coefficient and thickness of the pure absorber, and k and t the same quantities for the detector. Then the number absorbed per second per unit area by the detector in the v-speed class will be:

$$a(v, Kx)=\int_0^1 d\alpha v\alpha f(0,\alpha)e^{-Kx/\alpha}(1-e^{-kt/\alpha})$$
$$\doteq vkt\int_0^1 d\alpha f(0,\alpha)e^{-Kx/\alpha}, \quad (13a)$$

where $v\alpha f(0,\alpha)$ represents the emission current density (α=direction cosine referred to outward normal from the paraffin block), $e^{-Kx/\alpha}$ represents the fraction emerging from the absorber plate, and $1-e^{-kt/\alpha}$ represents the chance of capture by the detector plate, all edge effects due to finite area of extent being neglected. The last integral in (13a), valid for an infinitely-thin detector, is just the number density $F(x)$ of v-speed neutrons at the location of the detector. From this one sees that proportionality between absorption rate and number density will always exist for a very thin detector producing no appreciable disturbance at the place of insertion. The activity of the detector for a given speed class should bear a definite relation to the absorption rate, and in the final steady state should be proportional to it; i.e.,

$$A(v, Kx)=C(v)\alpha(v, Kx)\doteq C(v)vktF(x), \quad (13b)$$

where $C(v)$ is a proportionality coefficient.

The transmission ratios become

$$A(v, Kx)/A(v, 0)$$
$$\doteq\int_0^1 d\alpha f(0,\alpha)e^{-Kx/\alpha}\Big/\int_0^1 d\alpha f(0,\alpha), \quad (14)$$

giving the reduction in detector activity due to the interposition of an absorber of thickness x in terms of its absorption coefficient K and the source's characteristic number density distribution $f(0,\alpha)$. Amaldi and Fermi[36] have given plots of Eq. (14) for the cases: (a) f constant, giving the first associated logarithmic integral $K_1(Kx)$,[37] and (b) the Fermi relation $1+\sqrt{3}\alpha$, giving $[K_1(Kx)+\sqrt{3}K_2(Kx)]/(1+\sqrt{3}/2)$.

For the exact solution obtained in this paper

[35] In connection with the albedo it should be mentioned that the approximation $\sigma=\frac{1}{3}$ used by Halpern, Lueneburg and Clark in their numerical formula for albedo with incident currents on a half-infinite medium is quite serious if N is actually of the order of 150. This is easily seen in the case of a normally-incident current when the numerical factor $2.91(N=\infty)$ in Eq. (66a) should be changed to approximately $2.56(N=150)$, and the corresponding N value inferred from Amaldi's and Fermi's measurements lowered from 261 to approximately 203—the exact value requiring further calculations of the $p_2(1, N)$ function. The case of uniform incident currents has been discussed explicitly by W. de Groot and K. F. Niessen, Physica 7, 199 (1940).

[36] Reference 24, p. 902, Fig. 2.

[37] The associated logarithmic integrals are defined as: $K_n(s)=\int_0^1 d\alpha e^{-s/\alpha}\alpha^{n-1}$, $n=0, 1, 2, \cdots$ with the logarithmic integral being the zeroth member. V. A. Kostitzen, Institut des Math. de Moscous (1926), p. 15, gives a tabulation of the first five associated logarithmic integrals.

in the case of $N=150$ and uniform sources, the second column of Table III gives the results of an approximate calculation for the transmission ratios. The calculation has been made by averaging an upper and lower linear approximation to the curve shown in Fig. 1 (z-scale) for $N=150$. It is evident from Table III that $f=1+(\frac{3}{2})\alpha$ is again a better approximation to the $N=150$ case than the Fermi relation, and that the $N=\infty$ case follows closely the Fermi-Amaldi transmission ratios. Further possible applications of the exact solutions, such as in nuclear level widths,[34] will not be considered at this time.

OCTOBER 1, 1940 PHYSICAL REVIEW VOLUME 58

Temperature Dependence of the Work Function of Tungsten from Measurement of Contact Potentials by the Kelvin Method*

JAMES G. POTTER**
Sloane Physics Laboratory, Yale University, New Haven, Connecticut and Ryerson Physical Laboratory, University of Chicago, Chicago, Illinois

(Received March 13, 1940)

The Kelvin method for the determination of contact potentials is adapted for measurements between filaments in vacuum. Measurements between a heated and a cool tungsten filament indicate an increase in the work function of tungsten, with temperature, of 6.3×10^{-5} volt per degree centigrade. This effect is distinguished from changes in work function arising from variations, with temperature, in contaminating layers on the tungsten, which tend to obscure the true temperature coefficient even under the best vacuum conditions. The observed true temperature coefficient appears to be comparatively independent of the existing degree of surface contamination. This suggests that the temperature effect must reside primarily in the thermodynamic potential of the electrons inside the metal and not in the potential barrier at the surface. The coefficient obtained resolves the discrepancy between the experimental value of A in the Richardson equation and the theoretical factor of 120 without the introduction of a reflection coefficient.

AN increase in the electronic work function of tungsten, with temperature, of approximately 6×10^{-5} volt per degree centigrade was estimated by Waterman and Potter[1] in 1936 from data they obtained from measurements of contact potentials employing the Kelvin method. This positive temperature coefficient of the work function was in definite disagreement with a negative coefficient of approximately 4×10^{-4} volt per degree reported for pure tungsten, earlier in the same year by D. B. Langmuir.[2] His calculations were made from shifts of thermionic curves attributed to changes in contact potential between a collector and an emitter. Although Langmuir expressed the opinion that the negative coefficient might be an effect resulting from imperfect vacuum conditions, this coefficient did agree well with some deductions of Nottingham.[3]

As pointed out by Becker and Brattain,[4] if the work function, w, is of the form, $w=w_0+\alpha T$, α being the temperature coefficient and T the absolute temperature in °K, then when w appears in the exponent of the Richardson equation, the effect of the second term in w is to multiply the theoretical thermionic current by the factor, $e^{-\alpha/k}$, where k is Boltzmann's constant. After the value of 6×10^{-5} volt per degree had been reported for α in the case of tungsten,[1] it was noticed that this value made the factor, $e^{-\alpha/k}$,

* Part of a dissertation presented to the Faculty of the Graduate School at Yale University in candidacy for the degree of Doctor of Philosophy.

** Now at South Dakota State School of Mines, Rapid City, South Dakota.

[1] A. T. Waterman and J. G. Potter, Phys. Rev. **51**, A63 (1937).

[2] D. B. Langmuir, Phys. Rev. **49**, 428 (1936).

[3] W. B. Nottingham, Phys. Rev. **49**, 78 (1936).

[4] J. A. Becker and W. H. Brattain, Phys. Rev. **45**, 694 (1934).

practically equal to $\frac{1}{2}$. If, as is likely, the reflection coefficient at the surface of pure tungsten is almost negligible for thermionic electrons, this factor accounts for the discrepancy between Dushman's constant factor, 120, in the Richardson equation and the accepted experimental factor of $A=60$ for tungsten. In view of the ability of the positive coefficient to explain this discrepancy notwithstanding its disagreement with the coefficient of Langmuir and Nottingham, improved techniques have been employed in a new independent determination.

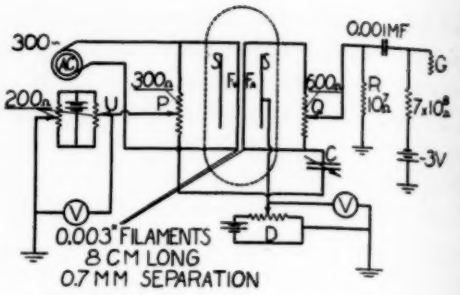

FIG. 1. Circuit for the measurement of contact potentials between filaments in vacuum by the Kelvin method. The amplifier is not shown beyond the grid of the first tube.

METHOD

The Kelvin method has again been used because it affords practically instantaneous determinations of contact potentials, allowing distinction between rapid and gradual changes of work function. In the Kelvin method the two bodies differing in work function form a condenser, which tends to become charged to their contact difference of potential, equal in magnitude to the difference in the work functions of the two bodies. When the contact potential is compensated by an applied potential, a change in capacity between the two bodies is accompanied by no electrical change.

In 1932 Zisman[5] devised a system for measuring the contact potential between two parallel plates, whereby he varied their capacity at an audiofrequency, by causing one plate to vibrate on the end of a flexible reed. The other plate was coupled to an audiofrequency vacuum-tube amplifier. An applied potential in series with a high resistance between the plates was adjusted until no signal appeared in the amplifier. At this point the applied potential had the value of the contact potential difference between the plates.

In the present investigation this method is modified to admit the measurement of contact potentials in vacuum under conditions in which the metals can be treated to yield the accepted values of the thermionic constants. Three-mil tungsten filaments approximately 8 cm in length replace the parallel plates of the above method. During measurements, one of the filaments is simultaneously heated to any desired temperature and vibrated by passing an alternating current through it in the presence of an applied magnetic field.

The electrical arrangement is indicated in Fig. 1. The two filaments, suspended parallel in one horizontal plane with a separation of 0.7 mm, appear at F_V and F_A. Above and below the filaments, outside the vacuum tube, are supported electromagnets, not shown in the figure, which maintain a steady magnetic field perpendicular to the plane of the filaments. By adjusting the strength of this field and the frequency of the current delivered to the filament, F_V, by the generator, AC, F_V may be set into resonant vibration in its fundamental mode, in a horizontal plane at any temperature above 300°K, with an amplitude such that it barely avoids striking F_A at its mid point. F_A is connected to ground at the midpoint, Q, of a shunt through a high resistance, R, and is coupled through a condenser to a two-stage inductance-coupled audiofrequency amplifier with earphones at the output. For clarity, the amplifier beyond the grid, G, of the first tube is omitted from the figure.

In order that the alternating voltage applied to F_V will produce no disturbance in the amplifier, the midpoint of this filament must be maintained at a steady potential. The midpoint may be described as that point on the two sides of which $\int Idrdc$ is the same, where Idr represents the potential drop at any instant along an element of the vibrating filament, and dc is the capacity between that element and the other filament.

When measuring the contact potential between the two filaments, the midpoint of the vibrating filament is picked up by trial at the point, P, on the slide wire in parallel with the filament, and its potential relative to ground is adjusted on the

[5] W. A. Zisman, Rev. Sci. Inst. **3**, 367 (1932).

potential divider arrangement at U until there is no signal in the amplifier. With this adjustment, the net electric flux between the two filaments is zero throughout the cycle of vibration. The applied potential, which is read directly on the voltmeter, V, connected between P and ground, is then equal to the contact potential between the vibrated filament at any chosen temperature and the filament at room temperature, connected to the amplifier. If the applied potential which will eliminate the signal when the filament is at a different chosen temperature is then found, the difference in the two potentials is equal to the change in work function of the vibrating filament resulting from its change in temperature.

Obviously, the electrical midpoint of the filament should coincide with the geometrical center of symmetry throughout each vibration. Compensation for any accidental slight departure from symmetry in the construction of the tube is effected with the small auxiliary capacity, designated by C in Fig. 1, between the leads to the filaments at one end outside the tube. In the event of an incorrect setting for the auxiliary capacity, C, or for the point of contact, P, of the vibrating filament, a disturbance from the alternating potential applied to the filament enters into interference effects with the disturbance arising as a result of the change of capacity between the filaments during vibration when the contact potential between the two filaments is not exactly compensated. A reversal of the applied magnetic field, however, reverses the phase of the vibration, and hence, of the latter disturbance, without affecting the former. As would be expected, when the vibrated filament is picked up at a point remote from its true electrical midpoint, a different value of potential has to be applied to the filament to suppress the signal in the amplifier with each of the two orientations of the magnetic field. As the true midpoint is approached, the two values of apparent contact potential converge on the true value. Accordingly, reversing the magnetic field serves as the critical test while adjusting for symmetry.

Although the tube and circuits are fully shielded in copper while measurements are being made, the shield inside the tube, designated by S in Fig. 1, is desirable. If there is an appreciable field arising from contact potential, or applied potential, between the filaments and their environment, any movement of the vibrating filament will, in general, result in an immediate change in the potential of the filament connected to the amplifier, since the latter is insulated except for the high resistance to ground. This effect may require that a potential very different from the true contact potential between the filaments be applied to the vibrating filament in order to prevent a signal in the amplifier. In any accurate measurements of absolute values of contact potentials by the Kelvin method it is essential that external fields be eliminated by surrounding the specimens with an electrostatic shield to which is applied a potential equal to the contact difference of potential between the shield and the specimen connected to the potential detector, in the present case, the filament, F_A. This fact has been ignored by many users of the Kelvin method, and instances may be cited in which shields involved in comparatively large changes of capacity with the moving element have been grounded instead of being held at the correct potentials. According to measurements made in the present investigation, this leads to absolute values for contact potentials in considerable error. The shield may be set at the correct potential for measurements at all temperatures of the vibrating filament by adjusting it until the contact potential between the filaments measures zero when both filaments are practically cold and contaminated to the same degree. The potential of the shield may also be set from a knowledge of its work function and that of the filament connected to the amplifier, but contamination effects limit the accuracy of this latter method. When, as in the present project, attention is restricted to changes in work function involving only differences in contact potentials, the value of the potential of the shield is not important since it affects the absolute magnitude of all the contact potential measurements by the same additive amount.

Equipment and Experimentation

In the design of the vacuum tube for the filaments and shield, primary consideration must be given to the maintenance of symmetry. For high sensitivity, the capacity between the elements of the circuits connected to the two

filaments is kept as low as possible in order that the change of capacity during vibration may be a large fraction of the total capacity. The tension on the filament which is vibrated has to be maintained with considerable precision, the most practicable value turning out to be about seventeen grams. This gives the filament a natural fundamental frequency of vibration of approximately 300 cycles per second. Such a tension, however, is impossible when the filament is heated to a high temperature for the purpose of outgassing.

The foregoing considerations lead to radical departures from conventional vacuum-tube design. The horizontal filaments and concentric cylindrical shield are supported by a glass rod framework, suspended from the ends of the tube. The portions of the filaments between which the capacity is altered by vibration are confined between small horizontal quartz rollers. In passing over the rollers, the filaments rest in peripheral grooves ground to maintain their proper spacing. The rollers allow the filaments to expand with temperature without changing the length of the segments between which the capacity is varied. A short distance beyond the rollers, the ends of the filaments are led off in opposite directions to the sides of the tube through capillaries. One capillary for each filament, but at opposite ends, is fastened rigidly to the frame. The second capillary for each filament, which is allowed to swing freely below the rollers, has fastened to it a weight that maintains the tension in the filament. The capillaries, which fit the filaments snugly, anchor them to the frame and weights with the introduction of a minimum amount of capacity which does not vary during the vibration. Beyond the capillaries the ends of the filaments are connected to tungsten leads sealed into the sides of the tube. The fact, that the vibrated segment of the filament is held fixed at its ends by the quartz rollers, minimizes error in measurement from end effects.

While a filament is heated to a high temperature during outgassing, a partial support is introduced under the weight used to maintain the tension in the filament during vibration. The support is attached to a lever carrying a counterweight on the opposite side of a bearing, the bearing being somewhat above the center of gravity of the weight and counterweight so that, as the filament elongates, the lifting moment of the counterweight increases. The support is withdrawn when the filament is to be vibrated, the counterweight being propped up by a cam. Both the cam and the support are moved into position by levers carrying iron armatures which are pulled by magnets manipulated outside of the tube. To minimize the problem of outgassing, the armatures and counterweights are encased in glass. The levers, also of glass, are operated on sleeve bearings of glass.

With a view to detecting possible effects from imperfect shielding, two different designs of shield have been tried inside the tube. The shield is a hollow cylinder, approximately 4 cm in diameter, surrounding the portion of the filaments between the quartz rollers. The cylinder is partially closed at its ends, holes being left for the passage of the filaments. In one design, the shield was of glass, which was given a coating of evaporated silver after a satisfactory vacuum had been obtained. Small shadow casters prevented the deposition of silver from the molten source onto the quartz rollers. In the other design, the shield was fashioned from a sheet of tantalum. This shield was outgassed at a yellow heat by electron bombardment from the filaments employed in the contact potential measurements. No difference was discerned in the results obtained with these two types of shield.

Three-mil tungsten wire from a number of sources has been tried for the filaments. All of the specimens of wire have been found to develop inhomogeneities and regions of brittleness after any program of heating in vacuum, for the purpose of outgassing. When brittleness occurs at locations subjected to considerable mechanical disturbance, the filaments fail before data can be taken. Three sets of filaments have permitted the taking of data, while after fourteen other successful attempts to assemble and evacuate the tube, filament failures prevented the taking of data. The most satisfactory wire has been that prepared especially for the work through the courtesy of Dr. W. L. Enfield and Mr. W. P. Zabel of the Nela Park Laboratory of the General Electric Company. According to Mr. Zabel, this wire is prepared by oxidizing the black drawn "218 wire" in air, for roughly $\frac{3}{4}$ of a second at a

temperature of 800°C and then annealing and cleaning it in wet hydrogen for 1½ seconds at 2000°C.

Filament temperatures throughout the investigation were determined from filament currents with the aid of the tables prepared by Langmuir and Taylor[6] and Langmuir and Jones.[7]

In the course of the investigation two kinds of pumps have been employed: a two-stage mercury diffusion pump and a three-stage diffusion pump operating with organic fluids, essentially of the design devised by Hickman.[8] Following a preliminary dehydration of the entire vacuum system by the application of heat while the forepump is in operation, a bake for about 48 hours at a temperature between 475° and 500°C is given the main tube as well as an ionization gauge and an adjacent trap. Refrigerant is maintained on a second trap, next to the diffusion pump, which is in operation during the baking. Near the middle, and again, at the end of the period of baking, all metal parts are heated by conduction or electron bombardment. The filaments are heated for a total period of about 10 hours at a temperature of 2400°K, for a period of two hours at 2600°K, and for a brief interval at 2900°K, refrigerant being applied to the trap closer to the tube before the heating schedule is completed. This procedure results in a pressure ranging between 1.4×10^{-8} and 7×10^{-9} mm of mercury, which obtains as long as the pumps are in operation throughout the duration of the experiment. The lower figure for the pressure has been realized only with the organic fluid diffusion pump, but it has been achieved under optimum conditions with each of three commercial types of organic pumping fluid when the traps are refrigerated with dry ice. It is believed that this lower figure does not understate the pressure since it is determined with an ionization gauge which has been calibrated by several groups of investigators from pressures existing when a mercury diffusion pump is used. The high probability of ionization of the organic molecules of the pumping fluid compared to that of mercury would tend to make the pressures read high in the present instance.

The employment of liquid nitrogen, instead of dry ice as a refrigerant with the organic pumping fluid, results in no measurable change in the magnitude of the pressure indicated by the ionization gauge, but it does eliminate some small component of the residual vapor which profoundly alters the contamination effects of the vapor on the filaments. Measurements of contact potential, when using the colder refrigerant, can be interpreted on the basis that the contaminating layer which forms on the filaments, after they have been flashed at a high temperature and then allowed to cool, results in a gradual increase in the work function of the filaments. A steady state is attained after about a day, when the work function appears to have been increased by several tenths of a volt. When a mixture of dry ice and acetone replaces the liquid nitrogen on the trap, the behavior of the contact potential suggests that the work function increases to a maximum value in a few hours following a flashing of the filaments and then gradually decreases for a number of days before the contamination has reached an equilibrium condition. Thus, experimentally, the removal of contaminating agents by moderate heating of a filament may either increase or decrease its contact potential depending upon the stage of its contamination.

More significant than the change with contamination, there is a second superimposed change in contact potential whose direction and magnitude is always uniquely determined by the change in temperature of the filament. Whereas the change attributed to contamination transpires comparatively slowly, especially following a reduction in temperature of the filament, this second change in contact potential immediately accompanies a variation in the temperature of the filament. This change is interpreted as a modification with temperature, in the metal itself, and thus gives a measure of the temperature coefficient of the work function of tungsten, α.

Although the variation in work function attending the driving off or return of contamination when the temperature is altered is, in general, larger than the change in work function determining α, the latter can often be clearly differentiated from the former by making a rapid

[6] I. Langmuir and J. B. Taylor, Phys. Rev. **50**, 68 (1936).
[7] I. Langmuir and L. A. Jones, Gen. Elec. Bull. 419 (Sept. 1927).
[8] K. Hickman, Synthetic Organic Chemicals **9**, 1 (1935).

TABLE I. *Changes in contact potential from contamination effects and effects characteristic of tungsten, following changes in temperature. T, temperature in °K; S, seconds since last alteration of temperature; V, contact potential of heated filament in volts. Changes determining temperature coefficient of tungsten are in italics.*

					A						
T	300	935	935	300	300	300	300	300	300	935	300
S		30	180	35	50	65	90	100	300	30	40
V	0	−0.26	*−0.26*	*−0.30*	−0.30	−0.26	−0.18	−0.16	−0.16	*−0.26*	*−0.30*
					B						
T	300	935	935	935	935	300	300	300	300	300	
S		30	55	80	300	25	55	135	150	600	
V	*−0.26*	*−0.22*	−0.24	−0.26	*−0.26*	*−0.30*	−0.30	−0.26	−0.26	−0.26	
					C						
T	935	935	300	300	300	300	300	300	300		
S		120	30	120	225	300	380	435			
V	0.76	*0.76*	*0.72*	0.72	0.70	0.66	0.62	0.56	0.56		
					D						
T	935	300	300	300	300						
S		20	60	180	360						
V	*0.46*	*0.42*	0.42	0.42	0.36						
					E						
T	935	300	300	300	300						
S		17	40	60	135						
V	*−0.32*	*−0.36*	−0.32	−0.26	−0.26						

series of determinations of contact potentials with an accurate record of the time of each determination. Some representative sets of determinations, from which the distinction between the two types of change may be appreciated, are presented in Table I. They are all selected to cover the same temperature interval, but different stages of filament contamination. Each row designated by *T* lists the successive temperatures, in °K, of the vibrating filament. *V* is the potential in volts applied to this filament to obtain a minimum signal in the amplifier, that is, the contact potential between the vibrating filament and the stationary filament which is at room temperature. The instant at which the contact potential is measured is indicated by *S*, the number representing the time interval in seconds which has elapsed since the temperature of the filament was last altered. For example, the set of data under *A* was taken when the contamination was at a stage to indicate a decrease of work function with increase of temperature. The first entry, made after both filaments had been left unheated to accumulate equal amounts of contamination for several hours following their flashing at 2900°K, indicated that the apparatus was in adjustment to register zero contact potential when the vibrated filament was at 300°K, practically the temperature of the other filament. As shown in the table, when the temperature of the vibrated filament was subsequently raised to 935°K, a measurement completed 30 seconds later revealed a contact potential of −0.26 volt, which persisted until the filament was cooled 180 seconds after it had been heated.

Comparison with subsequent data will show that the reduction in work function signified by the foregoing change in contact potential should be attributed primarily to the driving off of contamination from the filament by the application of heat. A measurement of −0.30 volt, made 35 seconds after the filament had cooled, disclosed that the cooling had reduced the work function 0.04 volt. Although a reading 15 seconds later detected no change in the contact potential, an observation 65 seconds after the filament had cooled showed that a new trend toward a higher quasi-stable value of work function was in progress. The above 0.04-volt transition in work function, which is in italics in the table and is repeated identically in a second temperature cycle recorded in italics at the end of the first set of data, was reproducible indefinitely on the occasion from which the above sample of data was taken. The fact that this transition always seemed to accompany, and go to com-

pletion with, the cooling of the filament whereas the subsequent reversal in the trend of the work function always began gradually after the filament had cooled, indicated that the former was a genuine temperature effect in the metal itself while the latter was the effect of a redeposition of contaminating layers on the surface.

Although, as would be expected, the changes in work function attributed to the driving off of contamination from the filament, when its temperature was raised, were, in general, more rapid than the changes attributed to the return of contaminants to the cool filament, there were occasions when the first mentioned changes were slow enough to be followed. The set of data under *B* in Table I is an example. This sample of data is taken from an occasion when the contaminations of the filaments resulted in a comparatively stable contact potential of −0.26 volt with both filaments at room temperature. Here the stage of contamination was such that its alterations with temperature gave rise, comparatively slowly, to variations in work function which exactly nullified the immediate changes with temperature in the work function of the metal itself. The transitions recorded in italics, which are instances of the true temperature effect, are obviously of a different nature from the slow changes in the opposite direction which follow them.

The set of data under *C* reports a stage where the modifications of work function from contamination effects are in the same direction as the modifications from the behavior of the metal itself but are still less rapid than in the preceding examples. On this occasion the contaminations gave rise to a comparatively stable contact potential of 0.56 volt when both filaments were at room temperature. A similar situation is reported under *D* with somewhat lower absolute values of contact potentials.

The foregoing examples are typical of data taken from the equipment over practically the same temperature interval in more than one hundred different instances. It is significant that, regardless of the stage of contamination, the same 0.04-volt change in contact potential consistently appears immediately with the 635-degree change in temperature whenever it is not masked by the always irregular contamination effects. Moreover, this contact potential change seems to be independent of the absolute magnitudes of the contact potentials, which are governed by the contamination history of each filament and vary widely in the course of time.

Although it would be desirable to have data on a filament absolutely free of contamination, the foregoing fact reduces the importance of such data. After the contamination effects were understood, attempts were made to obtain data on the true temperature effect on the work function of a filament immediately after it was heated to a high temperature, but the rapidity of the contamination changes, which always occurred immediately following such a heating, defeated all attempts until filament failure terminated the investigation. Data obtained with a minimum of delay, after the filaments were outgassed, are recorded under *E* in Table I. On this occasion observations were commenced twenty minutes after the filaments had been cooled from a temperature of 2900°K. Although the initial measurement, made with both filaments cold, showed zero contact potential, the contact potentials shifted rapidly and erratically on heating, and it was not until twenty minutes later that they showed any stability at moderate temperatures and the recorded data were obtained.

Most of the data have been taken with the shield inside the tube grounded. Since the work function of tantalum differs from that of tungsten by only a few hundredths of a volt, grounding should give the proper potential to the tantalum shield, to within the accuracy sought. When the two filaments and shield had been recently outgassed and the subsequent treatment of the two filaments was identical, the contact potential was always found, appropriately, to read zero with the tantalum shield directly grounded. With contamination on both the shield and the filament connected to the amplifier, the potential to be applied to the shield to give correct absolute values of the contact potentials between the filaments becomes problematical. However, since differences in contact potentials, and not absolute values, are of interest in the present investigation, the potential setting of the shield becomes unimportant. As would be expected, data show that the effect of changing the potential on the shield is simply to shift the apparent absolute magnitude of the contact potentials, the apparent

TABLE II. *Temperature coefficient of work function of tungsten for various observed temperature intervals.*

T_1	935	588	675	695	937	932	935	1025	1120	1260
T_2	300	387	303	308	387	587	802	308	398	308
V_1	0.36	0.474	0.280	0.344	1.040	0.60	0.496	1.16	1.064	−0.32
V_2	0.32	0.460	0.256	0.320	1.006	0.58	0.486	1.10	1.004	−0.40
$\alpha \times 10^5$	6.3	7.0	6.4	6.2	6.2	5.8	7.5	8.5	8.3	8.4

shift in contact potential being approximately one-tenth the change in potential on the shield and in the same direction. The immediate change in contact potential accompanying a variation in temperature is found to be independent of the potential on the shield. Thus, the data show one occasion when a potential of −3 volts applied to the shield reduced the apparent contact potential of the vibrated filament to zero with the filament at a temperature of 300°K. With an increase in its temperature to 935°, the contact potential of the filament became 0.04 volt.

Although the most intensive study of contact potentials with the equipment was conducted over the temperature interval just quoted, scattered measurements were made over other temperature intervals. Some representative data on these temperature intervals are included in Table II, where, in each column, V_1 and V_2 are the contact potentials, in volts, observed immediately before and after the temperature of the filament is changed from T_1 to T_2 and α is the change of work function, in volts per degree centigrade, computed from the data in the column. The first column gives, for comparison, typical data on the interval discussed heretofore in more detail.

It will be noted that the data involving temperatures above 935°K do not give values of α in agreement with those for the lower temperatures. The data, in general, indicate a higher temperature coefficient but lack reproducibility. This may be accounted for, in part, by the fact that for the higher filament temperatures the signal in the amplifier becomes less quiet when the contact potential is balanced, possibly resulting in reduced sensitivity. However, the reversal in phase of the signal arising from imperfectly balanced contact potential, when the applied compensating potential, on being increased or decreased, passes through the correct compensating value, results in a change of quality of the signal from which the correct compensating value can be quite accurately identified. The irregularity of the data at the higher temperatures may probably be attributed primarily to the formation, by thermionic emission, of an electron sheath around the heated filament. The results of Langmuir[8] for temperatures above 1000°K have been criticized on this basis.[9]

Even though the results for the higher temperatures are not considered, an evaluation of the accuracy of the data below 935°K is not simple. Since, with the difficulties of the experimental work, it was not feasible to obtain systematic data over subintervals in the temperature range from 935° to 300°K, any calculation on precision from the data obtained for these subintervals would be quite artificial. Although considerable data were obtained, which are not presented in Table II, they are not extensive enough to give a fair sample of the accuracy of measurement nor to merit statistical treatment, and with single observations over a given temperature interval there is always some uncertainty as to whether contamination effects have been completely differentiated from the true temperature dependence of the work function of the metal itself. Accordingly, it seems advisable to regard these data only as a check and to base the final evaluation of the temperature coefficient entirely on the data obtained from the temperature interval, 935° to 300°K.

While the 0.04-volt change in contact potential always observed with this temperature interval appears to be only a rough approximation and the exact figure belonging in the next decimal place is admittedly not known, it becomes fairly evident from the history of the observations that this potential change cannot differ greatly from 0.04 volt. In the first place, prior to the date when it had been learned how to distinguish between the true temperature effect and contamination effects and before any attempt was made to express

[9] A. L. Reimann, Proc. Roy. Soc. **163**, 499 (1937).

filament heating currents in terms of temperatures, the 0.04-volt interval may be found in the data a large number of times accompanying temperature intervals which deviated, on the average, only negligibly from the above interval. After the interval was identified with the change in the work function of the metal itself, serious attempts were made to detect some slight departure from the number 0.04. Tests with the equipment showed that contact potentials could be located reproducibly to the nearest 0.005 volt; however, with this sensitivity there was obtained practically no evidence of a departure from 0.04 volt. Whereas with this sensitivity a sizable error could be consistently made in numerous observations as a result of prejudice, there is no reason to believe that the consistency of the result in the more than one hundred observations over this interval should not reduce the probability of error somewhat.

It seems reasonable, therefore, to conclude that a temperature coefficient for the work function of tungsten may be established from the results for this interval to within a probable error of ten percent. It is significant that the deviation measure of the coefficients calculable from the data taken from subdivisions of this temperature interval falls well within this ten percent limit. Accordingly, using the value in Table II, it may be stated that in the temperature range from 300° to 935°K, with a probable error of not over ten percent, the work function of tungsten increases approximately linearly with temperature at the rate of 6.3×10^{-5} volt per degree centigrade.

Discussion of Results

The examples of data in Table I indicate the magnitude of the error in determinations of the temperature coefficient of the work function which may arise from contamination effects. The observed modifications of the work function by contaminants are of the order of magnitude encountered by investigators of other electronic phenomena under the best vacuum conditions obtainable with contemporary techniques.[10,11] They stress the desirability of a method, such as the present one, which can follow rapid changes in surface conditions. The wide divergence in the several values of the temperature coefficient of the work function of tungsten which have been noticed by other observers[2,9,12–14] may have its explanation in confusion resulting from a predominance of the contamination effect instead of the true temperature effect.

Attention has already been directed to the most surprising aspect of the results; namely, the apparent independence of the true temperature coefficient of the work function on the existing stage of contamination on the filament. This is in agreement with the findings of Reimann[9] published shortly after the preliminary announcement of results on the present investigation. Using thoriated tungsten over a wide range of states of activation, Reimann found a temperature coefficient of the work function which was independent of the state of activation. Reimann's method of measurement was similar to that of Langmuir.[2] The value of the positive temperature coefficient obtained, 7.5×10^{-5} volt per degree, is in fair agreement with the value, 6.3×10^{-5} volt per degree, determined in the present investigation.

The results of both investigations suggest that the temperature effect in the work function does not reside primarily in the surface potential barrier of the metal, which varies with activation and contamination, but in the energy distribution of the electrons inside the metal. If the opposite were the case, it would be difficult to understand how a change with temperature in the surface would be independent of the contamination. Interpreted in the terms of the Sommerfeld theory of metals, in which the work function is expressed in the form, $W_a - W_i$, where W_a is the amount of work which an electron at rest must do to escape from the surface and W_i is the Fermi "characteristic energy" of the electrons in the metal, the above experimental evidence implies that the temperature effect in W_i predominates over that in W_a.

The existing state of the theory of potential barriers admits of no decisive theoretical predictions on the effect of temperature on W_a.[4] On the other hand, the order of magnitude of W_i

[10] L. J. Haworth, Phys. Rev. **48**, 88 (1935).
[11] P. A. Anderson, Phys. Rev. **54**, 753 (1938); **57**, 122 (1940).
[12] F. Kuhn, Ann. d. Physik **5**, 15, 825 (1932).
[13] W. B. Nottingham, Phys. Rev. **46**, 339 (1934).
[14] A. King, Phys. Rev. **53**, 570 (1938).

may be computed on the simple Sommerfeld theory. Considering the effect of thermal expansion on the density of tungsten, which enters into the computation, W_i may be computed to decrease with increase of temperature by about 10^{-4} volt per degree. This would account for an increase of the same magnitude in the work function. The agreement of this figure with the experimental values for the temperature coefficient of the entire work function provides further evidence that the temperature effect in W_a is small compared to that in W_i.

It is of interest to note that the temperature coefficient for the work function of tungsten reported here is of the order of magnitude of the coefficients deduced by less direct methods for other pure metals by other investigators in several instances. Much of the data, including the preliminary result of the present investigation,[1] has been summarized and interpreted in terms of temperature coefficients in a paper by Cashman.[15] The similarity in magnitude of the coefficients for the different metals can be taken as additional support for the theory that the temperature dependence occurs primarily in W_i, since it would be expected to vary little here from one metal to another.

As shown by Cashman in the case of the coefficients for the other metals, the inclusion of a term involving the coefficient resulting from this investigation, when the work function for tungsten is introduced in Richardson's expression for thermionic emission current, completely resolves the long recognized discrepancy between the Dushman theoretical emission factor, 120, and the experimental emission factor, commonly designated by A. The effect of the temperature coefficient, 6.3×10^{-5} volt per °K, is to multiply 120 by a factor which results in the quantity, 58 amp. cm^{-2} $°K^{-2}$. This is in agreement with the accepted experimental value of A for tungsten to within the accuracy of the data.

This agreement admits no appreciable reflection coefficient in the thermionic emission for pure tungsten. Although polycrystalline tungsten has been the subject of the present investigation, if the deduction may be relied upon that the temperature coefficient resides primarily in W_i and not in W_a, the results should apply to single tungsten crystals and be independent of the face considered.

An interesting aspect of the contact potential measurements, which have been presented here, is the information they provide on the magnitude of a theoretical reversible heating effect in the surface of the tungsten when charge is added to, or subtracted, from it. As deduced independently by Lorentz and Kelvin and developed recently by Bridgman,[16] the addition of unit positive charge to the surface of a metal must, whenever the operation is isothermal, be accompanied by an addition of heat equal to TdV/dT, where T is the absolute temperature and the derivative is the contact potential between two specimens of the metal differing in temperature by one degree. The derivative obtained in the present investigation indicates a "surface heat of charging"[17] for tungsten at 300°K of 1.5×10^{-12} calorie per electrostatic unit of charge. Although direct measurements of surface heat of charging seem impracticable with present techniques, Bridgman[18] suggests that values calculated from contact potential measurements may have significance in theories of the electronic structure of metals, providing for different binding forces on electrons on the surface from those existing in the interior of the metals.

The author wishes to acknowledge his great indebtedness to Professor A. T. Waterman, of Yale University, who initiated the project reported here and provided invaluable counsel throughout its execution. He is furthermore particularly indebted to Mr. F. P. Noble for his resourceful and untiring assistance in the design and construction of the glassware. Appreciation is also tendered the faculty of the University of Chicago for the privilege of using the facilities of the physical laboratory for the conclusion of the experimental work.

[15] R. J. Cashman, Phys. Rev. **52**, 512 (1937).

[16] P. W. Bridgman, *Thermodynamics of Electrical Phenomena in Metals* (Macmillan, 1934), p. 90.

[17] L. Tonks and I. Langmuir, Phys. Rev. **29**, 524 (1927).

[18] P. W. Bridgman, reference 16, p. 73.

Theoretical Magnetic Susceptibilities of Metallic Lithium and Sodium

J. B. SAMPSON AND FREDERICK SEITZ
Randal Morgan Physics Laboratory, University of Pennsylvania, Philadelphia, Pennsylvania
(Received July 17, 1940)

The magnetic susceptibilities of metallic lithium and sodium are computed by using the best available theoretical information. Bardeen's effective masses and exchange and correlation terms are included. This procedure appreciably affects the theoretical paramagnetism for free electrons, giving results considerably different from those obtained from Pauli's equation with the assumption that the electrons are perfectly free and that exchange and correlation terms may be neglected. The final computed susceptibility for sodium is close to the observed value, but that for lithium is about twice the highest experimental one. The possible sources of error are investigated and it is concluded that the presence of a quartic term in the expansion of the one-electron energy parameter in terms of a power series in the electron wave number would be sufficient to account for the deviation. The level density curves obtained from x-ray emission curves are discussed and it is concluded that all details of these curves cannot be explained on the basis of the simple picture ordinarily used.

1. INTRODUCTION

THE purpose of this paper is to apply our present knowledge of the electronic structure of metallic lithium and sodium to a computation of their magnetic susceptibilities. It is convenient to regard the computation from the standpoint of the following four stages of approximation:

1. Paramagnetism of valence electron, neglecting the influence of exchange and correlation energy.
2. Paramagnetism of valence electrons including exchange and correlation effects.
3. Inclusion of diamagnetism of valence electron on the basis of the Landau-Peierls-Wilson theory.
4. Inclusion of ion-core diamagnetism.

The first approximation corresponds to the original Pauli[1] theory of paramagnetism, in which the change in energy arising from the interaction of spin and magnetic field is considered on the basis of the simple band picture. In this approximation, the volume susceptibility is

$$\chi = 2\beta^2 g_s / V, \tag{1}$$

where β is the Bohr magneton, g_s is the density of electronic levels of one spin at the top of the filled region, and V is the volume of the specimen. This term is practically temperature independent.

[1] W. Pauli, Zeits. f. Physik **41**, 81 (1927).

The next approximation is that in which the spin-aligning exchange forces and opposing correlation forces are taken into account. The qualitative importance of exchange for the susceptibilities of metals was first pointed out by Bloch[2] in connection with his discussion of free electron ferromagnetism, whereas the importance of correlation was pointed out by Wigner.[3] These terms cannot be treated independently of the Pauli term, as we shall see in Section 3. We shall also see that they have a very great influence on the susceptibility of lithium.

The valence electron diamagnetism was first treated by Landau,[4] who showed that for perfectly free electrons the diamagnetic term is

$$-4\pi m\beta^2 h^{-2}(N/3\pi V)^{\frac{1}{3}} \tag{2}$$

where N is the total number of atoms and V the volume of the crystal. The theory was subsequently extended by Peierls[5] and by Wilson[6] for the case in which the one-electron wave functions have the form

$$\psi_{\mathbf{k}}(r) = \chi_{\mathbf{k}}(\mathbf{r}) \exp\left[2\pi i \mathbf{k}\cdot\mathbf{r}\right], \tag{3}$$

in which $\mathbf{k}$ is the electronic wave number vector and $\chi_{\mathbf{k}}$ has the same periodicity as the lattice. In this approximation there are the following three

[2] F. Bloch, Zeits. f. Physik **61**, 545 (1929).
[3] E. Wigner, Phys. Rev. **46**, 1002 (1934).
[4] L. Landau, Zeits. f. Physik **64**, 629 (1930).
[5] R. Peierls, Zeits. f. Physik **80**, 763 (1933).
[6] A. H. Wilson, *The Theory of Metals* (Cambridge University Press, 1936), p. 108.

essentially diamagnetic contributions to the susceptibility:

1. The expression

$$\chi_1=\frac{e^2}{24\pi^2h^2c^2}\int\frac{df}{d\epsilon}\left[\frac{\partial^2\epsilon(\mathbf{k})}{\partial k_x^2}\frac{\partial^2\epsilon(\mathbf{k})}{\partial k_y^2}-\left(\frac{\partial^2\epsilon(\mathbf{k})}{\partial k_x\partial k_y}\right)^2\right]d\tau(\mathbf{k}), \quad (4)$$

in which

$$f=\frac{1}{\exp\left[\{\epsilon(\mathbf{k})-\epsilon'\}/kT\right]+1}$$

and $\epsilon(\mathbf{k})$ is the energy of the electron having wave number $\mathbf{k}$. ϵ' is a constant. It is assumed in this expression and the following one that the field is in the z direction. Expression (4) reduces to Landau's result (2) when $\epsilon(\mathbf{k})=h^2\mathbf{k}^2/2m$. It may be easily seen that the integrand in (4) is proportional to the Gaussian curvature in $\mathbf{k}$ space of the energy contour associated with the boundary of the filled region.[7] Regions where this curvature is positive add a diamagnetic contribution to the susceptibility, whereas regions of negative curvature add a paramagnetic contribution.

2.

$$\chi_2=-\frac{e^2}{\pi^2mc^2}\int\frac{1}{\exp\left[\{\epsilon(\mathbf{k})-\epsilon'\}/kT\right]+1}d\tau(\mathbf{k})\times\int\left\{\left|\frac{\partial\chi_k}{\partial k_x}\right|^2+\left|\frac{\partial\chi_k}{\partial k_y}\right|^2\right\}d\tau(\mathbf{r}), \quad (5)$$

in which the first integral extends over the spatial coordinates of the electrons and the second extends over all occupied values of $\mathbf{k}$. This quantity is zero for perfectly free electrons and is equal to the atomic diamagnetic susceptibility when the atoms are widely separated. Thus it effectively provides a measure of the amount by which the electrons are "bound."

3. A third term, having no simple analog, which is zero both for perfectly free electrons and perfectly bound electrons and is estimated to be small in intermediate cases.

In previous computations of the susceptibility, the exchange and correlation terms have not been explicitly included, and, in addition, it has usually been assumed that the electrons are perfectly free. We shall include the effects of exchange and correlation as well as may be done at the present time, and shall also employ the approximation in which $\epsilon(\mathbf{k})$ has the form

$$\epsilon(\mathbf{k})=h^2\mathbf{k}^2/2m^*, \quad (6)$$

where m^* is the theoretically determined effective mass, which varies from metal to metal.

2. The Free Electron Paramagnetism Neglecting Exchange and Correlation

By using Eq. (6), Pauli's Eq. (1) may be placed in either of the forms

$$\chi=\tfrac{3}{2}n\beta^2/\epsilon(k_0)=3nm^*\beta^2/h^2k_0^2,$$

where k_0 is the value of k at the top of the filled region, and n is the number of electrons per unit volume. This term is practically temperature independent as far as we are concerned.

The value of m^*/m is almost exactly unity for sodium, whereas that for lithium is considerably larger. The most reliable values in these two cases have been determined by Bardeen[8] and are 0.93 and 1.53, respectively. One[9] of us obtained the somewhat smaller value 1.35 in the second case, using a less reliable method.

The values of the volume susceptibilities obtained when Bardeen's values of the effective mass are substituted into Pauli's equation are given in Table I. It should be noted that in this approximation the susceptibility is proportional to the effective electron mass.

3. Inclusion of Exchange and Correlation Terms

The effect of exchange and correlation terms is, in essence, to change the effective electron mass as the electrons are redistributed among the energy levels under the influence of the magnetic field. For this reason, these terms and the Pauli term must be discussed simultaneously.

Let us assume that the metal possesses n electrons per unit volume and that in a given

[7] Transforming to spherical coordinates in k space, the integral may be written as

$$\int_0^\infty\frac{\partial f}{\partial\epsilon}\frac{1}{3k}\frac{d\epsilon}{dk}\left(2\frac{d^2\epsilon}{dk^2}+\frac{1}{k}\frac{d\epsilon}{dk}\right)4\pi k^2dk,$$

when ϵ is a function of the absolute value k alone.

[8] J. Bardeen, J. Chem. Phys. **6**, 367 (1938).

[9] F. Seitz, Phys. Rev. **47**, 400 (1935).

TABLE I. *The volume susceptibilities given by Pauli's equation. (The values are expressed in c.g.s. units times 10^{-6}.)*

m^*/m	χ, CALCULATED
Li 1.53	1.22
Na 0.93	0.59

state of magnetization $\frac{1}{2}n-p$ of the electrons occupy the lowest levels of the band associated with one spin and $\frac{1}{2}n+p$ occupy the lowest levels of the band corresponding to opposite spin. If $\epsilon(r)$ is the energy of the state occupied by the rth electron, counting from bottom of the band, in the approximation in which exchange and correlation are neglected (Hartree approximation), the energy in the presence of a field and for the same approximation is

$$E(p,H)=\sum_{r=1}^{\frac{1}{2}n-p}\left[\epsilon(r)+\frac{eh}{4\pi mc}H\right]+\sum_{r=1}^{\frac{1}{2}n+p}\left[\epsilon(r)-\frac{eh}{4\pi mc}H\right]. \quad (7)$$

Pauli's equation may be derived from this by computing the value $p'(H)$ for which this is a minimum, by determining the magnetic moment per unit volume M from the relation

$$M(p'(H))=2p'(H)eH/4\pi mc$$

and by using the equation

$$\chi=\partial M(H)/\partial H. \quad (8)$$

We shall carry through the equivalent procedure after adding exchange and correlation terms.

The exchange energy is a result of interaction between electrons of parallel spin and its average is

$$-0.458e^2/r_s, \quad (9)$$

when p is zero, where r_s is related to n by the equation

$$(4\pi/3)r_s^3=1/n. \quad (10)$$

When p is not zero, the average value for the electrons in the band containing $\frac{1}{2}n+p$ electrons is

$$-0.458xe^2/r_s, \quad (11)$$

where

$$x=[(n+2p)/n]^{\frac{1}{3}};$$

and the average value in the other band is

$$-0.458ye^2/r_s, \quad (12)$$

where

$$y=[(n-2p)/n]^{\frac{1}{3}}.$$

Thus the total exchange energy is

$$-0.458e^2(x^4+y^4)n/2r_s. \quad (13)$$

The correlation energy is principally dependent upon the number of electrons having opposite spins. Its average value when p is zero is

$$-e^2f(r_s)=-0.288e^2/(r_s+5.1a_h) \quad (14)$$

where a_h is the Bohr radius. When p is not zero, the total value is

$$-e^2[(\tfrac{1}{2}n+p)f(r_s/y)+(\tfrac{1}{2}n-p)f(r_s/x)]. \quad (15)$$

Adding Eqs. (7), (13), and (15), and minimizing the result with the assumption that p/n is small, we find

$$p=n\beta H/4\alpha, \quad (16)$$

where

$$\alpha=\frac{n}{4}\left(\frac{d\epsilon}{dr}\right)_{r=\frac{1}{2}n}-\frac{2}{9}\frac{0.458e^2}{r_s}-\frac{5}{9}f'(r_s)r_se^2-\frac{1}{18}f''(r_s)r_s^2e^2. \quad (17)$$

Using Eq. (8), we obtain

$$\chi=n\beta^2/2\alpha. \quad (18)$$

It is easy to see that the exchange term tends to decrease α and hence increase the susceptibility. The first correlation term, containing f', is positive, and hence increases α, whereas the second has opposite sign. Since the second is usually no more than one-tenth of the first in absolute magnitude, the net effect of the correlation term is opposite to that of the exchange term.

The contributions to α are listed in Table II along with the susceptibility computed from Eq. (18). It may be seen that α is reduced by a factor of nearly three in the case of lithium as a result of the influence of exchange and correlation terms. The reduction is not as large for sodium, but is still appreciable. The susceptibilities obtained with and without the correction terms are compared in Table V.

It may be mentioned at this point that the susceptibility determined in the present approximation, and also in the final one, is very sensitive to the value of the effective mass because of the close competition between the first term in α and the other two. Thus a decrease in m^* of the order of ten percent decreases the susceptibility by about twenty-five percent in the case of lithium and about fifteen percent in the case of sodium.

4. The Free Electron Diamagnetism

The only appreciable contribution to the susceptibility from the three free electron diamagnetic terms is that arising from Eq. (4). The values obtained from this by using Eq. (6), that is, by neglecting any influence of exchange and correlation on the Gaussian curvature, are given in Table III. We shall discuss the influence of exchange below.

The second term was computed for lithium, by using the wave functions derived by one of us,[9] and was found to be less than 0.02×10^{-6}. The value for sodium should be even smaller, of course, so the term is practically negligible in both cases.

The third term, which also vanishes for perfectly free electrons is of the same order of magnitude as the second, and hence is also negligible.

The question of the extent to which the occupied levels of these metals satisfy the equation

$$\epsilon(\mathbf{k})=h^2\mathbf{k}^2/2m^* \tag{19}$$

will be discussed in more detail in Section 5.

Finally, we must consider the effect of exchange and correlation upon the free-electron diamagnetism. Bardeen has pointed out that at the absolute zero of temperature the slope of $\epsilon(\mathbf{k})$ is infinite at the top of the filled region in the approximation including exchange. An examination of the function[10] giving exchange as a function of k at absolute zero of temperature, namely

$$-Ck_0\left(1-\frac{k_0^2-k^2}{2k_0k}\log\left|\frac{k_0-k}{k_0+k}\right|\right), \tag{20}$$

where $C=2e^2$, and k_0 is the value of k at the top of the filled region, shows that the mean value of the second derivative is also infinite (negatively) thereby indicating that the Gaussian curvature is infinite. In order to investigate this point further, we carried through an extensive solution of Bardeen's integral equation[11] for $\epsilon(k)$ for perfectly free electrons, namely,

$$\epsilon(k)=\frac{h^2k^2}{2m}+C\int\frac{1}{\exp\left[\{\epsilon(k')-\epsilon'\}/kT\right]+1}\frac{k'}{k}\times\log\left|\frac{k'-k}{k'+k}\right|dk', \tag{21}$$

where ϵ' is a constant. This was solved to an approximation in which the form of $\epsilon(k)$ near the top of the filled region is given by

$$\epsilon(k)=\epsilon(k_0)+a(k-k_0)+b(k-k_0)^2, \tag{22}$$

where a and b are constants. The solution was obtained by substituting (22) into the integral term, expanding the Fermi-Dirac distribution function to quadratic terms in $(k'-k_0)$, by integrating the result, and then determining implicit equations for a and b by differentiation. The resulting equations are

$$\begin{aligned}a&=\frac{h^2k_0}{m}+C\log\frac{k_0a}{kT},\\ b&=\frac{h^2}{m}-\frac{C}{k_0}\log\frac{Ck_0}{kT}+\frac{3}{2}\frac{C}{k_0}+C\frac{b}{a}.\end{aligned} \tag{23}$$

The solution of these for the vicinity of room

Table II. *Contributions to α (Eq. (17)), and the volume susceptibility computed from Eq. (18). (The values of terms in α are expressed in ev.)*

	$\frac{1}{2}n(d\epsilon/dr)_{r=\frac{1}{2}s}$ $=\frac{1}{2}\epsilon(k_0)$	Exchange	Correlation	Total	$\chi\cdot10^6$(c.g.s.)
Li	1.02	−0.86	0.19	0.35	3.54
Na	1.12	−0.70	0.19	0.61	1.11

Table III. *The free electron diamagnetism obtained from the first term of the Peierls-Wilson theory (neglecting effects of exchange and correlation terms).*

	m^*/m	$\chi\cdot10^6$ (c.g.s.)
Li	1.53	−0.17
Na	0.93	−0.23

[10] J. Bardeen, Phys. Rev. **49**, 656 (1936).
[11] E. P. Wigner, Trans. Faraday Soc. **34**, 678 (1938); J. Bardeen, Phys. Rev. **50**, 1098 (1936).

TABLE IV. *The diamagnetic contribution to the magnetic susceptibility from the ion-core terms (after Van Vleck).*

	$\chi \cdot 10^6$
Li	−0.05
Na	−0.18

temperature shows that b is negative, so that, in this approximation, an electron near the top of the filled region behaves like an electron having positive charge. The absolute magnitude of the effective electron mass derived from b varies between 2.5 and 3.0 times the actual mass for lithium and sodium. These results do not agree with experiment, for if they did the Hall coefficient would be positive (opposite to that of bismuth), whereas the observed coefficients are negative. Since the influence of correlations on the density of levels of the entire solid is opposite to that of exchange, it seems likely that the sign of the effective mass is changed back to a positive value when correlations are included.

The Gaussian curvature at the top of the filled region computed from (22) is very close to zero, being only a few tenths the value for perfectly free electrons. If our supposition concerning the influence of correlations is correct, this result would also be altered in a final approximation, presumably in such a direction as to make the Gaussian curvature larger and positive. For this reason, we have employed the free electron diamagnetic terms given in Table III in the final result. Fortunately, the free electron diamagnetism is small near room temperature in any case, so that it seems unlikely that an error in order of magnitude is introduced into the computed susceptibility by this procedure.

It is easy to see from Eqs. (22) and (23) that the reciprocal of the effective electron mass and the integrand of Eq. (4) become negatively infinite as $\log (kT/Ck_0)$ when T approaches zero. It does not seem reasonable to suppose that the influence of correlations will exactly compensate for this. As a result, we may expect a rather mild singularity in the electrical and magnetic properties of the monovalent metals near absolute zero. In particular, the susceptibility should remain paramagnetic and become logarithmically infinite if the influence of exchange is predominant. The variation in conductivity is more difficult to predict, for the mean free path as well as the effective mass and density of states enters into this quantity, and we may expect all three factors to be influenced by exchange. De Haas, Casimir, and van den Berg[12] have found that the resistivity of gold rises with decreasing temperature in the immediate vicinity of absolute zero. It certainly would be unsafe to attempt to identify this anomaly with the influence of exchange at the present time, but the possibility should not be overlooked.

5. The Ion-Core Terms

The ion-core terms are small in both lithium and sodium. The values taken from Van Vleck's book[13] are given in Table IV.

6. Summary

The various terms entering the total susceptibility are summarized in Table V and their resultant is compared with the available experimental results.

It may be seen that the agreement between the theoretical values for sodium and the closely correlated experimental ones is as good as may be reasonably expected. This supports the already well-founded belief that the electrons in sodium

TABLE V. *The contributions to the volume susceptibility of lithium and sodium. (The theoretical values are taken from previous tables; all results are expressed in terms of* 10^{-6} *times the c.g.s. unit).*

	Spin Paramag.	Free Electron Diamag.	Ion-Core Diamag.	Total	Experimental Values
Li	3.54	−0.17	−0.05	3.32	0.27 to 1.6[14] 2.0[15] 1.4[16]
Na	1.11	−0.23	−0.18	0.70	0.51[14] 0.59[17] 0.59[18] 0.63[19]

[12] W. J. de Haas, H. B. G. Casimir and G. J. van den Berg, Physica **5**, 225 (1938).
[13] J. H. Van Vleck, *The Theory of Electric and Magnetic Susceptibilities* (Oxford University Press, 1932), p. 359.
[14] K. Honda, Ann. d. Physik **32**, 1027 (1910); M. Owen, *ibid.* **37**, 657 (1912).
[15] F. Bitter, Phys. Rev. **36**, 978 (1930).
[16] S. R. Rao and S. Sriraman, Proc. Ind. Acad. Sci. **5A**, 343 (1937).
[17] W. Sucksmith, Phil. Mag. **2**, 21 (1926).
[18] J. C. McLennan, R. Ruedy and E. Cohen, Proc. Roy. Soc. **116**, 468 (1927).
[19] C. Lane, Phil. Mag. **8**, 354 (1929).

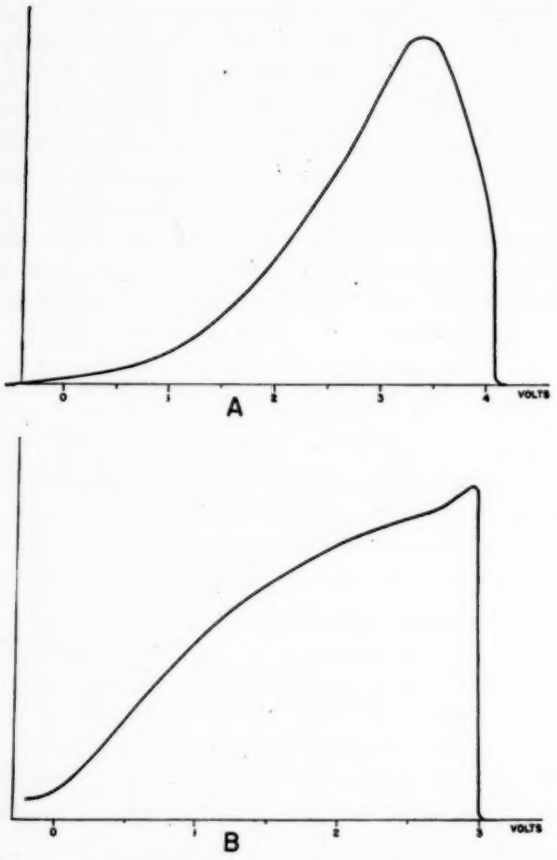

FIG. 1. The relative densities of conduction levels in lithium and sodium as determined from x-ray emission spectra (after Skinner). Curve A is for lithium and is determined from the K spectrum, whereas curve B is for sodium and is determined from the L spectrum.

behave as though they were almost perfectly free. The situation is not nearly so good in lithium, however. In the first place, the experimental values are much less certain, ranging from 0.27×10^{-6} to 2.0×10^{-6}. The most recently determined values[20] are those of Bitter[15] and of Rao and Sriraman,[16] which are, respectively, 2.0×10^{-6} and 1.4×10^{-6}, and presumably are the most reliable. The theoretical value of 3.32×10^{-6} is definitely larger than either of these, a fact indicating that the free electron model favors paramagnetism more than it should.

In this connection, it is interesting to raise the question of the extent to which the occupied levels of these metals satisfy the equation

$$\epsilon(k)=h^2k^2/2m^*.$$

[20] C. Starr has kindly communicated to us his as yet unpublished result for the observed volume susceptibility of lithium which is 1.9×10^{-6} c.g.s.

The x-ray emission spectra of lithium and sodium, obtained by O'Bryan and Skinner[21] (Fig. 1) seem to imply that there is a fundamental difference in the behavior of the levels at the top of the filled regions in these two metals. The curve for lithium seems to decrease smoothly from a maximum before dropping abruptly, whereas the curve for sodium does not exhibit the same behavior. If it is assumed that the effect is genuine, as is probably beyond question, there would seem to be three explanations:

1. The difference is intimately connected with the fact that the emission curve for lithium corresponds to K transitions, whereas that for sodium corresponds to L transitions. In the elementary theory developed by Jones, Mott and Skinner,[22] the only difference arising from this source would be that the sodium curve should vary as the three-halves power of the energy before dropping abruptly, whereas the lithium curve should vary as the square root of the energy. It is possible, however, that the emission problem is much more complicated than is assumed in the simple theory. In this event, measurement of the K-emission spectrum for sodium should serve a very useful purpose in giving us a chance to compare curves of the same emission type

2. The difference is connected with a difference in the influence of the zone boundaries in the two cases. This possibility cannot be discarded from consideration because the top of the filled region is very near the zone boundary in the (110) direction in the monovalent body-centered metals. All work on sodium indicates that the electrons in this metal are very nearly perfectly free, so that an influence of the zone boundary would seem more likely in the case of lithium. A somewhat superficial investigation of this problem has led us to conclude that a dip of the type observed in lithium could arise in this way only if the filled region extended beyond the zone boundary in the (110) direction. According to unpublished work of Herring and Huntington,[23]

[21] See H. W. B. Skinner, *Reports in Progress in Physics* (Cambridge University Press, 1939), Vol. 5, p. 257.

[22] H. Jones, N. F. Mott and H. W. B. Skinner, Phys. Rev. **45**, 370 (1934).

[23] We are indebted to Dr. Herring and Mr. Huntington for discussions of their work.

this is extremely unlikely and should not be taken as a serious possibility at present.

3. Bardeen[11] has pointed out that the absolute value of exchange energy decreases very rapidly near the top of the filled region, and gives rise to a decrease in the density of levels in this region. In fact, the density of levels would be zero at the top of this region for an ideal gas at the absolute zero of temperature. The problem of electron-electron correlations has not been solved with sufficient completeness to say accurately to what extent this minimum would be influenced by their effects. With the use of Wigner's expression (14) for the average correlation energy, it is possible to compute the change in correlation energy of the system of free electrons when an electron is added to or subtracted from the top of the filled region. This computation shows that in absolute value the change in correlation energy is only slightly greater than half the average value, thereby indicating that the function corresponding to the absolute change of correlation energy when an electron of arbitrary wave number is subtracted from the distribution also drops rapidly near the top of the filled region. Hence correlation does not tend to compensate for the effect of variation in exchange but augments it instead. If, however, we assume that the resultant effect of the variations in exchange and correlation energy for electrons near the top of the filled region is sufficient to explain the decrease in density for lithium, it is difficult to understand why a similar dip does not occur in sodium.

On the whole then, it seems that the problem of the x-ray determined densities does not have a simple solution in terms of the present knowledge of the behavior of levels in the alkali metals.

Although, for the reasons discussed in paragraph 2 above, the influence of the zone boundary in lithium probably is not sufficient to account for a minimum in electron density at the top of the filled region, it is not negligible as far as the susceptibility is concerned. The factors appear to be the following:

1. There should be a slight tendency for the $\epsilon(\mathbf{k})$ curves to bend over in the (110) direction. As far as the diamagnetic terms are concerned, this should decrease the integral (4) since the change in Gaussian curvature (cf. Section 1) would be negative. Moreover, the Pauli paramagnetism should also be increased, for the density of levels is increased. Thus the net effect of the bending in the (110) direction should be an increase in paramagnetism.

2. The $\epsilon(\mathbf{k})$ curve for lithium lies beneath the free electron parabola for small values of k, but should eventually approach this curve for sufficiently large values of $\mathbf{k}$. From the standpoint of Eq. (19), this means that the more accurate $\epsilon(\mathbf{k})$ curve should contain quartic and higher even-powered terms in $\mathbf{k}$ of essentially positive sign. We shall refer to these as quartic terms in the following discussion. Evidently the influence of quartic terms is a diamagnetic one, for they increase the Gaussian curvature at the edge of the filled region, thus increasing (4), and decrease the density of levels, thereby decreasing the spin paramagnetism.

It appears that the most likely source of error in treating lithium is the neglect of the quartic terms in the $\epsilon(\mathbf{k})$ curve. Not only will they operate to reduce the susceptibility, but preliminary calculations by Herring indicate that they will affect the value of $\epsilon(k_0)$ by an amount comparable with that required to obtain closer agreement between the computed and observed susceptibilities. Fortunately a relatively small increase in the contribution to α (Eq. (17)) arising from the Pauli term is required to lower the susceptibility by the proper amount, for this term is almost exactly balanced by the exchange and correlation terms (see Section 3).

We are indebted to Professor J. H. Van Vleck for extensive criticism of this work.

Interpretation of Ferromagnetic Colloid Patterns on Ferromagnetic Crystal Surfaces

W. C. ELMORE
Department of Physics, Swarthmore College, Swarthmore, Pennsylvania
(Received August 8, 1940)

It is shown that the bodily motion of particles rather than a magneto-optic effect is chiefly responsible for field-induced changes in ferromagnetic colloid patterns on ferromagnetic crystal surfaces. A simple relation between colloid concentration and magnetic field intensity near the crystal surface is deduced from the Boltzmann distribution law. Several implications of this relation are discussed, including the role played by magnetic interaction of the particles. The formation of elongated chains of particles in a colloid placed in a magnetic field is shown to be unlikely provided that the particles are sufficiently small in size.

IN a recent note[1] L. W. McKeehan has suggested that a magneto-optic effect, similar to the action of a magnetic field on the optical transparency of a magnetite suspension, may play a role in determining the apparent distribution of ferromagnetic colloid in patterns on polished silicon-iron crystals.[2] According to Heaps[3] suspended particles of magnetite form elongated groups under the action of an applied magnetic field, making the suspension more transparent parallel to the field and less transparent perpendicular to it. McKeehan points out that this phenomenon rather than the bodily motion of colloid particles can be used to explain the shifting of pattern lines observed when an applied normal field is reversed. Before citing experimental evidence which does not support this view, it is pertinent to mention some qualitative results of the magneto-optic experiment performed with ferromagnetic colloids which have been used for magnetic structure studies.

The ferromagnetic colloids show changes in transparency parallel and perpendicular to an applied magnetic field opposite to those shown by a coarse ferromagnetic suspension. Majorana[4] has reported that certain nonferromagnetic colloids of $Fe(OH)_3$ show a similar anomalous effect in a very intense field. In the present case changes in transparency tend to saturate at a few hundred oersteds, and they are greater with siderac-dextrin colloid prepared by a colloid mill[5] than with magnetite-soap colloid prepared by chemical means.[6] The anomalous effect lacks a simple explanation, but its existence somewhat modifies the suggested magneto-optical explanation of field-induced pattern changes.

Several observations have been made which support the view that the pattern changes produced by reversing an applied normal field are caused by the bodily motion of colloid particles rather than by the magneto-optic effect. Under high magnification (1500×) with vertical illumination it is possible to identify individual particles in a pattern by virtue of the Tyndall effect. The particles appear to be buzzing around in Brownian motion and a swarm of them can be seen to move from one region to another when the stray field is modified by an applied field. Their motion can be seen even more clearly with dark-field illumination as furnished by the Leitz Ultrapak, for with this illuminator the particle swarms appear light against a dark background. Even at low magnification the field-induced motion of unresolved colloid swarms can often be inferred from the visible motion of a few relatively large particles which may be present. It is evident that the magneto-optic effect can at most play a minor role in governing the appearance of patterns.

The problem of the distribution of colloid particles on the surface of a ferromagnetic crystal can be approached from the point of view of statistical mechanics. The following analysis applies when mutual action between particles

[1] L. W. McKeehan, Phys. Rev. **57**, 1177 (1940).
[2] L. W. McKeehan and W. C. Elmore, Phys. Rev. **46**, 226 (1934).
[3] C. W. Heaps, Phys. Rev. **57**, 528 (1940); see, also, W. C. Elmore, Phys. Rev. **57**, 842 (1940).
[4] Q. Majorana, Acc. Lincei, Rendiconti [6a] **29**, 11 (1939).
[5] W. C. Elmore, Phys. Rev. **51**, 982 (1937).
[6] W. C. Elmore, Phys. Rev. **54**, 309 (1938).

can be neglected, i.e., when the particles behave as an ideal gas. The effect of magnetic interaction will be mentioned later.

Let $\mathbf{H}(x, y, z)$ represent the magnetic field above the plane surface of a ferromagnetic crystal, the normal to the surface coinciding with the z axis. It is most convenient to consider the crystal as being a thin slab or disk having a demagnetization factor 4π so that an applied normal field $\mathbf{H}_0$ of moderate intensity will not appreciably magnetize the crystal, but will simply add vectorially to its stray field. Since the latter field is negligible except near the surface of the crystal, $\mathbf{H}(x, y, z)=\mathbf{H}_0$ for values of $z \gg d$, where d is the separation of pattern lines. Now consider the crystal to be covered by a ferromagnetic colloid containing, at a distance from its surface, n_0 particles per unit volume, each particle having a permanent magnetic moment μ. According to the Boltzmann distribution law, the number of particles in a volume dV lying with their axes in the solid angle $d\omega$ is given by

$$d^2N = Ce^{\mu H \cos\theta/kT} d\omega dV$$

$$= 2\pi C e^{a\cos\theta} \sin\theta d\theta dV, \quad (1)$$

where $a=a(x, y, z)=\mu H/kT$, θ is the angle between $\boldsymbol{\mu}$ and $\mathbf{H}$, C is a constant and kT has its usual meaning. At equilibrium the concentration of particles n, at a point where the intensity of the field is H, is given by

$$n=\frac{dN}{dV}=2\pi C\int_0^{\pi} e^{a\cos\theta}\sin\theta d\theta = 4\pi C \sinh a/a$$

$$= n_0(a_0/\sinh a_0)(\sinh a/a), \quad (2)$$

where the constant C has been evaluated from the condition that when $H=H_0(a=a_0)$, $n=n_0$.

To illustrate the application of Eq. (2) let us consider a crystal whose stray field is derivable from the potential $V=H_s(d/\pi)e^{(-\pi z)/d}\cos(\pi y/d)$. The intensity of this field is independent of y and has the value H_s at the crystal surface. Let us suppose, for example, that $H_s=500$ oersteds. If we take $\mu=5\times10^{-16}$ as a reasonable value for the magnetic moment of the particles,[7] it follows that $a=6.1$ at the crystal surface, and from Eq. (2), $n \doteqdot 30n_0$. If now there be superposed a uniform normal field of 80 oersteds directed away from the surface, the field intensity at lines on the surface given by $y=0, 2d, 4d, \cdots$ will be 580, whereas at lines given by $y=d, 3d, 5d, \cdots$ it will be only 520. The corresponding values of a will be, respectively, 7.1 and 5.1, and those of n, $80n_0$ and $15n_0$. The position of these maximum and minimum concentrations of colloid will be interchanged if the field direction is reversed. In the preceding calculation $a_0 \doteqdot 1$ so that in Eq. (2) $a_0/\sinh a_0 \doteqdot 1$. With more intense fields this approximation cannot be made, for instance, if $H_0=250$, the two sets of lines will have the concentrations $150n_0$ and n_0, respectively. This suggests that it may be possible in certain cases to estimate the intensity of the stray field by finding the applied normal field which just removes the colloid from one set of pattern lines. The maximum normal stray field will then have twice this value. Now the no-field distribution of colloid produced by the simple periodic field under discussion shows no pattern lines. Either a slight magnetic particle interaction,[8] or the magneto-optic effect could result in the appearance of a double set of lines. The analysis predicts, in agreement with observation, that the total amount of colloid drawn to the surface is greater when there is an applied field present. On removing the field more than an equilibrium amount of colloid is gathered near the surface so that the no-field pattern is considerably more dense than it otherwise would be.

It is possible to take into account magnetic interaction of colloid particles by assuming that each particle is subject to, in addition to the external field, (1) the Lorentz field $(4\pi/3)I$, and (2) a demagnetizing field due to volume and surface distributions of magnetic poles in the colloid. By means of Langevin's equation, $I=n\mu(\coth a-1/a)$, which has been shown to hold approximately for ferromagnetic colloids;[7] and Eq. (2), which relates colloid concentration to field intensity, the increase in concentration resulting from mutual action of the particles can be estimated. The increase is found to be small and ordinarily can be neglected provided that

[7] W. C. Elmore, Phys. Rev. **54**, 1092 (1938).

[8] In reference 5 where particle interaction is mentioned a mistake in sign resulted in an incorrect drawing (Fig. 3) showing the distribution of particle dipoles above the surface of a crystal. The layer of dipoles should be inverted and shifted sideways a distance d.

sufficiently fine colloids are used. A rough estimate of particle diameter required for the formation of magnetically linked chains of particles can be made by equating kT to the maximum mutual magnetic energy of a pair of particles in contact. If it is assumed that the particles are spheres of diameter D, and that each particle is a single ferromagnetic domain having an intensity of magnetization I, then $kT=\mu^2/D^3=(\pi^2/36)I^2D^3$. By taking $I=450$ for magnetite and $kT=4.1\times10^{-14}$ it follows that for chain formation $D\geq40$ mμ, to be compared with an estimated mean particle diameter of 17 mμ for colloidal magnetite.[7] Now the calculated value (40 mμ) is undoubtedly low on several counts: (1) the intensity of magnetization is considerably less than 450;[7] (2) the protective colloid (soap) increases the distance of closest approach between two particles; and (3) repulsive forces of electrical origin exist among the particles. Hence we may conclude that chain formation should be expected with suspensions, but not with colloids whose particle size is, for instance, 100 mμ or less.

OCTOBER 1, 1940 PHYSICAL REVIEW VOLUME 58

A Method for Obtaining Powders of Uniform Sodium Chloride Crystals in Various Size Ranges, and the Effect of Size upon the Intensity of X-Ray Reflection

FITZ-HUGH MARSHALL
University of Chicago, Chicago, Illinois
(Received August 1, 1940)

I. A technique is presented for precipitating powders of sodium chloride crystals, uniform in size and cubical in shape, in various size ranges from 1 to 70 microns, above which the range could be extended by screening. The crystals are prepared by precipitation with absolute ethyl alcohol from a saturated solution of sodium chloride in water, but varying excess quantities of water are added to either of the solutions before combining them. Control of size range, and of crystal uniformity within a size range, is accomplished by careful attention to certain primary variables in the precipitation process, each of which produces marked changes in the character of the powder obtained. These are discussed, and a simplified procedure is presented for producing any desired size. II. This technique was developed to make possible a study of the variation of intensity of x-ray lines reflected from such size-graded powders. The 200-reflection of Cu $K\alpha$ radiation has been investigated, and a curve is shown for the variation of intensity with crystal size. The intensity decreases slightly with increase of crystal size, according to a curve which indicates that the crystals are imperfect but are more perfect than large single crystals.

I. A Method for Obtaining Powders of Uniform Sodium Chloride Crystals in Various Size Ranges

Introduction

FINE crystalline powders, rather than single large crystals, have been used in many quantitative measurements on the intensity of x-ray reflections. Comparison of results with theory has invariably involved the assumption that the individual crystals are so small, 10^{-5} cm or less, as to offer negligible x-ray absorption. Most investigators have been greatly concerned with the degree of subdivision of their powders, and a few have ground powders successively finer until intensity determinations leveled off to constant values;[1] but on the whole, there has been no attempt at a systematic study of reflection from powders of crystals larger than allowed by simple theory. It seemed desirable, therefore, to develop a reproducible technique for making uniform crystals of various sizes and to investigate their x-ray reflections. Sodium chloride was selected for study.

Sodium chloride powders have generally been prepared either by prolonged grinding or by precipitation. Grinding produces such an irregular debris of all sizes and shapes of particles

[1] R. J. Havighurst, Phys. Rev. 28, 882 (1926).

that no precise assignment of particle size can be made, while precipitation results in comparatively uniform crystals. This paper describes the controls and variables involved in the method of precipitation with absolute ethyl alcohol from saturated sodium chloride solution in water, with varying excesses of water added to either of the solutions before combining them.

Variables controlling the precipitation process

In the present study it was found that control of size range, and of crystal uniformity within a size range, may be accomplished by careful attention to six primary variables discussed below, each of which produces marked changes in the character of the powder obtained. Since there are more variables than necessary, the problem is to find conditions under which all except one or two level off in their effects and offer no critical source of inconsistency in results.

(*1*) *Relative proportions of alcohol and salt solution.*—As would be expected, the size of crystals decreases with increase of the proportion of alcohol used, due to increased speed of precipitation. For obtaining the smallest crystals, proportions as high as 100 parts of alcohol to 1 part of salt solution were used. But for all other sizes, it was convenient to use approximately equal quantities of alcohol and salt solution.

(*2*) *Excess of water added to the salt solution.*—As increasing excesses of water are added to the originally saturated solutions of sodium chloride in water, the speed of precipitation by alcohol is decreased and larger particles are formed, as illustrated in Fig. 1B. This variable is not critical enough for use as a major control, except in limited regions. On the other hand, this uncritical nature makes it possible to eliminate a frequent source of irregularity. The addition of 5 to 10 percent of water to the saturated salt solution, which introduces no great change in size range, prevents supersaturation or preprecipitation due to evaporation of the salt solution before combining with the alcohol. This is of special importance at high temperatures, where evaporation is rapid, and at low temperatures, where decreasing solubility leads to supersaturation.

(*3*) *Excess of water added to the alcohol.*—In sharp contrast to the previous case, Fig. 1A

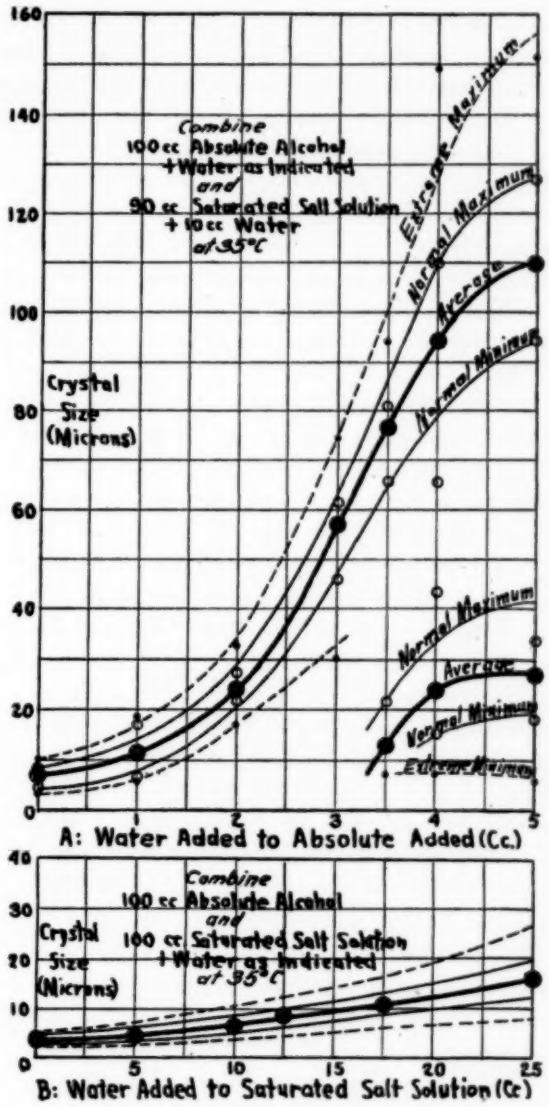

FIG. 1. Characteristic precipitation curves.

shows that as increasing quantities of water are added to commercial absolute alcohol (about 99.5 percent by volume), the size of the crystals precipitated increases rapidly. Note that the abscissa scales of Fig. 1A and 1B are different: the addition of 3 cc of water to 100 cc of salt solution causes a negligible change in the particle size, while the addition of the same 3 cc of water to the absolute alcohol multiplies the particle size by a factor of six!

As the dilution of the alcohol is extended beyond 3 percent, subsizes appear, mixed with the main large size—one subsize at first, probably several later on, although it is very difficult to

discriminate between size ranges as the curves advance. As the other variables are manipulated in this multiple region, the several mixed ranges change greatly in their average size and proportion, and occasionally they seem to converge toward a common intermediate range. But in no case has a successful precipitation been performed in which one single size resulted, uncluttered by another size range. Thus it is essential to the formation of uniform crystals that only 97 percent or higher concentration alcohol be used.

(*4*) *Temperature.*—In general, the higher the temperature of the solutions used in precipitation, the larger the crystals produced. Under some conditions, temperature seems to be a critical variable; but under the conditions recommended for the other five variables, temperature can be used to control particle size only by a factor of about five. However, for exact reproducibility of results and, in particular, for the maximum degree of uniformity of crystals, it appears to be essential that the alcohol and salt solution be at the same temperature when combined, and that there be no large variation of temperature during the precipitation process. For this reason, precipitations from test-tube quantities of solutions rarely are as satisfactory as from larger quantities. The thick walls of milk bottles have been found to provide a desirable degree of insulation from rapid temperature changes, making temperature control after combination unnecessary.

Temperatures ranging from the boiling point of alcohol to well below freezing were used. For small crystals, temperatures approaching the eutectic point of the salt solution were used. The smallest crystals were produced by the unusual procedure of dry-ice freezing the salt solution to a solid, then melting it in absolute alcohol.

(*5*) *Thoroughness of shaking during precipitation.*—Size and uniformity of powders can be greatly influenced by the degree of agitation of the combined solutions during the precipitation process. This would seem to be partly a matter of originally mixing the two solutions uniformly, partly a matter of maintaining uniform mixing on a microscopic scale while the growth of crystals continues. Little or no agitation causes non-uniformity, with the formation of larger crystals mixed with assorted smaller sizes. Results were most consistent and reproducible when the combined solutions were shaken vigorously throughout the precipitation, and this routine was finally adopted for all cases.

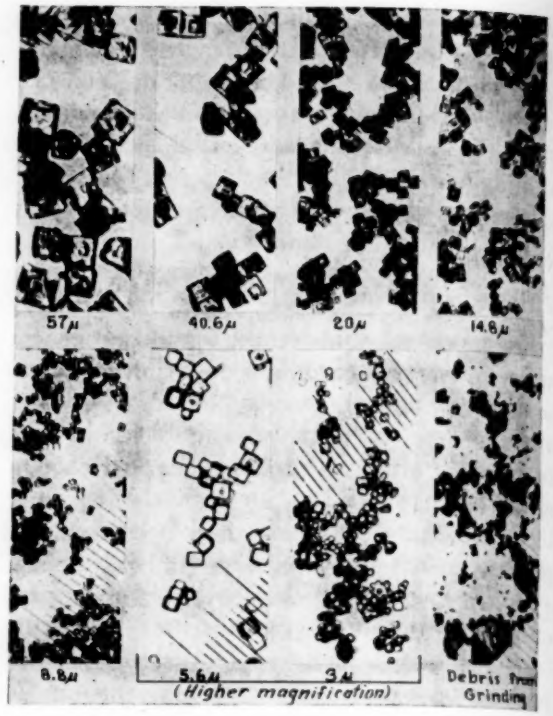

FIG. 2. Photomicrographs of crystals.

(*6*) *Time.*—Crystal sizes are highly dependent on the elapsed time between combining the two solutions and stopping the precipitation process by vacuum filtration. Since the time required for completion of growth varies from five seconds to about four minutes, five minutes from the time of mixing to pouring into the vacuum filter assured that growth would be checked only at an advanced stage. Fast vacuum filtration (aspirator) assured a minimum of "undecided" time during which no further shaking was possible.

Miscellaneous experimental details

Commercial filter papers failed to stop the smallest crystals produced. Various other types of filters were tried—Jena fused-glass filters, porous porcelain filters, etc. Some of these stopped the particles, either immediately or after the larger openings were clogged by crystals, but

the rate of flow was too slow. It was found that filter papers cut from ordinary typewriter bond stopped the small particles and filtered rapidly!

For measuring the size of crystal particles, a fifty-division scale was used in the eyepiece of a microscope (without micrometer attachment). The sample was passed back and forth in the field of vision until the smallest particle was ascertained. The linear dimension of this was measured and recorded as the "extreme minimum." The "extreme maximum" was similarly found, followed by the "normal minimum" and "normal maximum" crystals, roughly the extremes in any typical field. This preview of the sample aided in the final selection of a single crystal representing an "average."

The reproducibility of averages thus obtained, without size distribution analysis, was usually 3 percent or better. The uniformity of size can be judged from the curves of Fig. 1 and from the photomicrographs of Fig. 2. A sample prepared by grinding is included for contrast; measured sizes vary by more than one thousand to one.

For x-ray purposes, it was necessary to pack the powders into briquets in small brass frames. In the past this has usually been accomplished by mechanical compression, as with a vise. Since such a method fractures the crystals, it could not be used for the present experiment. This difficulty was avoided by allowing the powder to settle directly into the frame during filtration and pressing gently to compact. After desiccation, the excess powder was shaved off flush with the frame with a razor blade. The last few strokes were taken as lightly as possible, and microscopic examination showed no cutting or scratching of individual crystals.

Uniform powders of very large crystals, above 30 microns, fail to adhere under the conditions just described, although smaller particles form almost marble-hard masses. But these larger particles can be made to stick together by rinsing them in the filter with salt-saturated 90 percent alcohol. Evidently a droplet of this liquid is left at each point of contact between crystals and on drying deposits enough salt to bind them. The salt-saturation of the alcohol rinse is very important: 90 percent alcohol without salt saturation noticeably dissolves and disfigures the crystals; even 70 percent alcohol, when salt saturated, leaves no microscopic evidence of imperfection in the crystals. There may be some x-ray evidence that this process disturbs the crystalline surface.

The question has frequently arisen as to whether sodium chloride crystals continue to grow when suspended in absolute alcohol, the larger crystals at the expense of the smaller ones. When fresh absolute alcohol is used, there is no microscopically detectable growth of crystals, 3 microns or larger, even over time intervals of twelve hours or more. The increase in the settling rate of much smaller crystals is evidence that they do grow. A slight amount of water in the alcohol causes measurable growth of all sizes. For this reason, the smallest crystals, involving long filtration time, must be precipitated with such large excesses of alcohol that the water in the salt solution lowers the absoluteness of the alcohol by only negligible amounts. Growth is less rapid in cold solutions.

Simplified procedure for obtaining various size ranges

(1) For the smallest crystals, 1 to 5 microns, a 25-cc portion of saturated salt solution, with 5 percent of water added, is frozen in a test tube to dry-ice temperature. The test tube is cracked off and the frozen mass dropped into 500 to 2500 cc of absolute alcohol. This mixture is shaken vigorously until the melting is complete. Vacuum filtration is started immediately, using a filter paper cut from typewriter bond. As soon as filtration is complete, the powder is vacuum desiccated. The size of crystals may be controlled slightly by varying the volume or temperature of the alcohol. Apparently no irregularity is introduced by over-chilling the alcohol with dry ice and letting it warm up until melting occurs.

(2) Crystals from 5 to 15 microns are precipitated by combining equal volumes of absolute alcohol and salt solution, with varying amounts of water up to 25 percent added to the saturated salt solution, as determined from Fig. 1B. Higher or lower temperatures give larger or smaller crystals. The solutions are handled in milk bottles, for heat insulation, and are poured together when they are exactly at the same temperature. The combined solutions are vigorously shaken for five minutes, vacuum filtered (using commercial filter paper), and vacuum desiccated immediately.

(3) For crystals from 10 to 70 microns, the same general procedure as for (2) is used, except that varying amounts of water, up to 3 percent, are added only to the absolute alcohol, in accordance with Fig. 1A. To prevent supersaturation from evaporation, 10 percent of water is added in all cases to the saturated salt solution. Temperature variations cause size variations as before.

Other methods tried and possible methods for extending the size range

Small particles were produced by pouring salt solution chilled to about 0°C into a filter already filled with absolute alcohol at dry-ice temperature. A sherbet was formed instantaneously as the salt solution entered the alcohol and was filtered as it melted.

Salt solution was sprayed from an atomizer under compressed air over a pan of absolute alcohol. The idea was that droplets of salt solution from the fine spray might precipitate individually to produce ultra-fine particles. It was difficult to keep irregular crystals from forming at the edges of the pan, and the process was tedious.

Various precipitants other than ethyl alcohol were tried: other alcohols, hydrochloric acid, ether, and combinations such as ether and alcohol. These gave interesting variations in several cases, but failed under preliminary examination to reveal possibilities beyond those of ethyl alcohol.

By deliberately working beyond the multiple range region of Fig. 1A, adding three to ten percent of water to the absolute alcohol, large crystals, mixed with distinct smaller crystals, were produced and separated by screening. No detailed study of the precipitation curves involved was made since large crystals were not needed for the present x-ray experiment.

Another method for accomplishing the same results as screening, and applicable to smaller ranges, was tried with considerable success. This was based upon Stokes' law for rate of fall of particles in suspension. Powder was placed in the lower end of a long glass tube, and a constant flow of absolute alcohol up through the column was maintained to separate all particles smaller than a certain size. The flow was then increased to obtain the next size, etc. The separation was better than from the usual precipitations but was very time-consuming, particularly for small crystals.

II. The Effect of Crystal Size upon X-Ray Powder Reflection

Introduction[2]

Powdered crystals have been used in preference to single large crystals for many intensity measurements on x-ray reflections. No assumption of perfect crystalline structure is necessary, and there remains only the assumption that the powder particles are so small that extinction is negligible in them. Havighurst[1] early showed that as powders were ground finer, reflection intensities increased to limiting values in agreement with theory; and indeed that, due to fracturing of crystals in grinding, the particles were effectively smaller than their physical dimensions. Subsequent standard practice has been to grind powders as fine as possible, and no effort has been made to study systematically the effects of using powders of crystals definitely larger than allowed by simple theory.

The simple method of preparing size-graded powders, presented in the first part of this paper, now makes possible such a study for sodium chloride without the complications of irregularities in ground crystals. In this direction, the intensity of the 200-reflection of Cu $K\alpha$ radiation has been measured as a function of particle size.

Apparatus

The x-ray reflection intensities were measured on the vacuum ionization spectrometer previously used by Allison and Jesse[3] for determinations of structure factor decrements. The vacuum chamber, useful primarily to maintain the desiccation of the powders, is a part of the fore-vacuum line leading to the mercury pumps for the Dershem[4] type x-ray tube. Both tube and mercury pumps are mounted on the removable cover of the vacuum chamber. The radiation is collimated to a 0.04×1.5-cm beam by parallel steel plates and received after reflection by a 6.5-cm ionization chamber with fixed 0.15×1 cm slit. The ionization current is amplified by an external FP-54 Pliotron circuit and read as deflections of a sensitive galvanometer. A screw turned through reduction gears by an electric motor moves the top of the spectrometer table, so that either of two powder briquets may be brought into the beam (without disturbing the vacuum) with a linear motion reproducible to 0.0001 in. The primary radius arm is 9 cm, from

[2] For a more complete introduction, the reader is referred to Chapter 6 of A. H. Compton and S. K. Allison, *X-Rays in Theory and Experiment* (D. Van Nostrand, 1935).

[3] S. K. Allison and W. P. Jesse, Phys. Rev. **49**, 483 (1936). W. P. Jesse, Phys. Rev. **52**, 443 (1937).

[4] E. Dershem, Rev. Sci. Inst. **7**, 86 (1935).

central axis to either slit, but the long collimating slit prevents effective Bragg focusing.

For the present experiment, a copper target was installed, and the ionization chamber was filled with argon at 5 atmospheres. The $K\beta$ component was filtered out by a thickness of nickel sufficient to reduce the $K\alpha$ lines by 50 percent. In order that the FP-54 circuit might be operated at low amplification for stability, the power to the x-ray tube was increased to 14–28 ma d.c. at 35 kv, supplied by a full-wave kenotron 60-cycle rectifier circuit with $\frac{1}{3}$ mf filter condenser. The high potential, read from a large quartz-suspension electrostatic voltmeter, could be controlled to 0.2 percent. The filament current was supplied by storage batteries, and Dershem's[4] positive grid arrangement was used at about 600 v d.c. The current through the x-ray tube, read from a galvanometer connected between ground and the floating filament system (including batteries and rectifier for the grid), could be controlled to 0.1 percent. A neon tube arrangement, in shunt across the galvanometer and series inductance, absorbed occasional pulses due to flash-overs in the x-ray tube, thus satisfactorily preventing null shifts of the galvanometer. Constant charging of the storage batteries supplying the Pliotron circuit, at a rate equal to the drain, eliminated gradual changes of e.m.f. during long runs and also made it unnecessary to break into the sequence of runs for charging.

In the present experiment, one of the two briquets was changed before each run, introducing a source of error not encountered in previous experiments with this vacuum spectrometer. A variation of 0.001 in. in the linear position of successive briquet faces introduced an error of about 0.1 percent in the intensity reading, and it was necessary to construct a set of frames ($\frac{1}{8}$ in. thick), ground as nearly identical in thickness as possible.

Experimental procedure

All measurements were made by the "reflection method," according to the general plan used by Allison and Jesse.[3] One powder was selected as an arbitrary standard against which all others were to be compared, and this briquet was mounted permanently throughout the experiment as one of the two powders on the spectrometer table. Thus no absolute measurements of intensity were made. A run consisted of recording four or more successive intensity curves, taken alternately for the standard and the powder under test. Each curve consisted of a set of about thirty points—always the same set—so chosen as to show the maximum detail of the intensity curve. These points, separated by crystal angle increments of from 1 to 10′ and covering a total angle interval of 3° 50′, extended about 45′ to either side of the main broad rise of the intensity curve. The last three points on either side were assumed always to represent the

TABLE I. *Observed reflection intensity as a function of particle size.*

No. (Fig. 3)	Date	Crystal Size Min.	Av.	Max.	Relative Intensity	Percent of Deviation	Remarks
1	4–6	3.4	5.6	6.7	1.040	1.1	Preliminary test run
2	4–7	(No. 1, repeated)			1.053	1.1	
3	4–8	31	40.6	43	0.745	0.2	Rinse used for binding
4	4–9	0.6	1.15	2.3	1.098	0.7	Irregular crystals
5	4–10	0.7	3.0	3.4	1.127	0.2	
6	4–11	0.6	1.25	2.5	1.179	1.3	
7	4–14	5.6	8.80	10.7	0.910	0.4	Transformer burned out
8	4–15	9.6	14.8	17.3	0.820	0.3	
9	4–17	16.0	20.0	20.6	0.870	—	Imperfections within crystal cubes
10	4–19	1.7	3.55	3.8	1.116	0.9	
11	4–20	(No. 5, repeated)			1.121*	0.5	High frequency disturbance
12	4–22	(No. 5, repeated)			1.135*	0.6	
13	4–27	(No. 6, repeated)			1.173*	0.2	
14	4–28	3.7	6.0	7.0	1.160*	0.0	Redesiccated crystals
15	4–29	0.9	1.47	1.7	1.146*	0.4	
16	4–30	0.7	1.65	3.1	1.133*	0.8	Slightly irregular crystals
17	5–2	0.7	1.5	2.4	1.148*	0.4	Slightly irregular crystals
18	5–3	(No. 7, repeated)			0.951*	0.5	

* Values have been increased by a correction factor of 2.23 percent.

background base line, thus reducing any error from base line choice. The area under each intensity curve above the base line was determined, and the ratio of the areas for the two powders under test was computed as the final numerical result of each run, by averaging the two ratios, $B/\frac{1}{2}(A+C)$ and $\frac{1}{2}(B+D)/C$,[5] where A, B, C, and D are the four areas. Areas were obtained by adding ordinates times half the abscissa increments on either side of each point.

The four coarsest powders tested contained crystals of sizes no longer negligible as compared to the slit widths, causing the intensity curves to be irregular. In these instances, an extra run was made with as many additional points as necessary to resolve the entire detail. Two areas were computed—one from the usual set of thirty points abstracted from the larger number, the other from all the points. The ratio of these was considered to be an accurate correction factor by which the areas from the other runs were to be multiplied. The largest value of this correction was 1.4 percent.

The spread of ratios for any one run was usually less than 1 percent, and the average was considered precise to 0.5 percent. This was borne out by repeating runs on successive days without changing the powder under test. However, discrepancies of the order of 1.5 percent occurred when briquets once removed from the spectrometer table were replaced and tested again. These shifts were found to be due to some play in the supports of the steel plates against which the briquets were mounted. Only a major redesign of this portion of the apparatus would have eliminated this greatest source of error. In view of the irregularities which variations from the crystals themselves were found to produce, this seemed unnecessary.

Experimental results

Table I and Fig. 3 present the final experimental results. The determinations were made in random order to avoid systematic error from gradual changes in the apparatus. The values in the table marked with an asterisk have been obtained by multiplying the original values by the correction factor, 1.0223, to account for a shift in the alignment of the apparatus when the set screw on one of the briquet supports was jarred. This was obtained by comparing values for 11, 12, and 13 with those for 3 and 6. Large circles, dark or open centers, are used in the figure for determinations involving no irregularities in the crystals or in the behavior of the x-ray equipment.

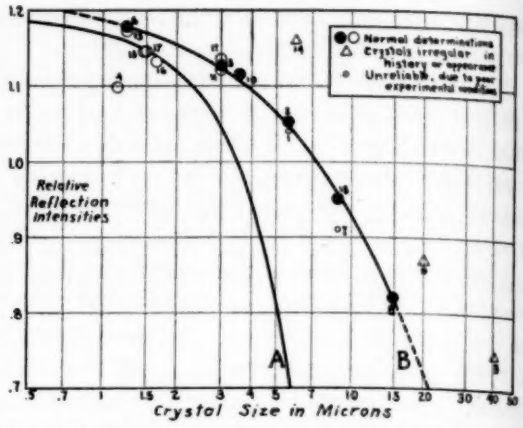

FIG. 3. Experimental observations and related theoretical curves. Curve B has been adjusted to fit the dark-centered points.

The three determinations indicated in Fig. 3 by triangles involve powders of such definite irregularity in history or appearance that their wide deviation from the general curve might almost be anticipated. The powder for No. 14 had undergone a previous desiccation and had been shaken again in absolute alcohol, packed into the briquet frame, and redesiccated. Although there was no mechanical action involved which would have been expected to produce fracturing or scratching, the crystal structure seems to have been changed. The powders of No. 9 and No. 3, corresponding to the 20μ and 40.6μ crystals of Fig. 2, contained many internal imperfections; and No. 3, too coarse to adhere in the briquet frame under the usual conditions, had to be treated with salt-saturated 80 percent alcohol before desiccation. Internal imperfection is evident to a smaller degree for all the larger crystals, but is almost absent in small crystals, as can be seen for the 5.6μ and 3μ crystals of Fig. 2. The intensity of reflection is abnormally high for each of the three points represented by triangles, as might be expected from decrease of

[5] The "Percent of Deviation" column of Table I represents the difference between these two ratios.

extinction effects with increase of imperfection in the crystalline structure.

There is little doubt that the intensity values are accurate to 1 or 2 percent. It must be stressed, however, that the crystal sizes cannot be fixed with comparable accuracy. This is caused, first, by the range of crystal size within a powder, making the average size dependent upon the type of average. The type of average attempted here was based on total *volume* of crystals within each size increment; an average based on *number* would be considerably lower.[6] Since no distribution measurements were attempted, it is unlikely that the averages shown express exactly the ideal. An error of this type might shift the curve to the right or left by a factor of as much as 15 percent. But secondly, the extreme limit of resolution of the microscope did not allow measurement of a dimension difference less than 0.3μ. Thus the six points in the 1 to 2μ range may be in error by as much as 40 percent. However, it is likely that the sizes are in the order shown,[7] and a more accurate determination of sizes would probably not bring these points into a smooth curve. It might be mentioned that oil immersion decreased rather than increased the resolution of detail because of the high index of refraction of rocksalt. Several powders of crystals larger than those for which points are shown were prepared, but intensity curves from runs on these were too irregular to be considered valid.

Theory

A detailed comparison of the experimental results with theory will not be attempted here, but certain obvious conclusions can be pointed out. The relative intensities observed are proportional to values which, due to extinction, are less than the standard theoretical reflection power from a briquet of ultra-fine crystals:[8]

$$P = P_0 \frac{jl}{16r \sin\theta} \frac{\rho'}{\mu_p \rho}. \qquad (1)$$

P is the power intercepted by a broad slit of length l at a distance r from the powder; P_0 is the incident power; j is the permutation constant, 6 for the 200-reflection of NaCl; θ is the Bragg angle of reflection; μ_p is the effective linear absorption coefficient of the powder, and ρ' and ρ are, respectively, the density of the powder and the density of the crystalline material in unpowdered solid form.

Since $\mu_p = \rho' \mu_m$, where μ_m is the mass absorption coefficient of NaCl, and since μ_m and ρ are constant, Eq. (1) reduces to

$$P = kP_0, \qquad (2)$$

where k is a constant of the apparatus and the reflection, independent of density of packing.

There are two assumptions involved in obtaining Eq. (1) which may not be fulfilled in the present experiment. First, it is assumed that there is negligible decrease in irradiation intensity within those few individual crystals aligned for Bragg reflection, whether due to normal absorption or to extinction. The present crystals were so large as to violate this assumption, definitely resulting in shielding of the deeper reflection planes by the upper planes, with consequent decrease of total power of reflection. The second assumption is that the decrease of irradiation intensity through the powder as a whole, because of normal absorption in individual crystals, is sufficiently continuous for integration according to a simple absorption curve based on a constant μ_p. Since even large irregularities probably tend to average out, it would seem that this assumption is much less critical than the first. It should be mentioned, however, that normal linear absorption in the largest crystals used was of the order of 40 percent.

Returning to the first assumption, if the particles could be considered perfect crystals, full primary extinction would occur and result in large shielding effects. While there is no theoretical equation available exactly expressing the average effects from uniform cubes, some idea of the variation to be expected can be obtained from Waller's[9] expression for the ratio R_A of the power as reduced by primary extinction to the power given by Eq. (2), in the case of

[6] The averages shown in Table I, thus stressing volume, are slightly higher than those of Fig. 1, and "maximum" and "minimum" are slightly more inclusive than the previous "normal maximum" and "normal minimum."

[7] Re-measurements on No. 4 indicate that this powder varies in size at different parts of the sample.

[8] Derived in full in A. H. Compton and S. K. Allison, *X-Rays in Theory and Experiment* (D. Van Nostrand, 1935), Eq. (6.85), p. 419.

[9] I. Waller, Ann. d. Physik **79**, 261 (1926).

crystal slabs of thickness t:

$$R_A=\frac{1}{\pi A}\int_0^{\pi/2}\frac{\sin\,(2A\,\sin\,\varphi)}{\sin\,\varphi}d\varphi, \qquad (3)$$

where

$$A=\frac{e^2\lambda}{mc^2}\frac{F}{V}\frac{t}{\sin\,\theta}.$$

e, m, c, and λ have the usual significance; F and V are the structure factor and the volume, respectively, of the unit NaCl crystal cell; θ is the Bragg reflection angle.

This equation has been plotted as curve A of Fig. 3, from unpublished simplifications by W. A. Zachariasen, with t considered equivalent to the linear dimension of the cubes as an approximation. From comparison of this curve with the experimental points, one logically concludes that the crystals are somewhat imperfect, as though constructed of smaller perfect crystals. This would be expected from the internal imperfections evident in Fig. 2, although no direct correlation as to the exact size of these inner crystals should be attempted. The points for intensities observed for small crystals, characteristically more perfect than large crystals (Fig. 2), lie very close to curve A.

Since Bragg, James, and Bosanquet[10] obtained consistent results for transmission through varying thicknesses of large single crystals by considering secondary extinction as a constant addition to the ordinary absorption coefficient, it was thought that such a treatment might be applicable to the present case. Computations were made (without approximation) of R_B, the ratio of the intensity reflected from Bragg-aligned cubes, averaged over various possible angular positions (about an axis perpendicular to reflecting planes), to the intensity that would be reflected if no absorption were taken into account. Curve B of Fig. 3, showing the best fit to the dark-centered points, which represent a series of powders thought to be similar in preparation and appearance, corresponds to an absorption coefficient thus computed to be in excess of the normal absorption coefficient (130) by about 300. That this is considerably higher than the approximately 50 percent excess found by Bragg, James, and Bosanquet[10] for large single crystals suggests that the present small crystals are more perfect than most large crystals. A more precise significance than this should not be attached to the numerical value 300, since the extinction excess to the absorption coefficient cannot be treated as a constant for perfect crystals or for crystals in which the mosaic blocks are large. It should be noted that the appearance of close agreement between curve B of Fig. 3 and the experimental points has little significance, since the curve was adjusted (in both coordinates) to fit the points. On the other hand, the abscissas of curve A are fixed at absolute values; and the ordinates, although adjusted, permit of little variation.

Thus from this incomplete theoretical analysis of the x-ray data, it appears that the crystals are imperfect but are more perfect than large crystal specimens.

[10] Bragg, James and Bosanquet, Phil. Mag. **41**, 309 and **42**, 1 (1921).

Conclusion

Powders of well-formed, uniform sodium chloride crystals in a variety of sizes may easily be produced by the method described in the first part. The intensity of x-ray reflection from these powders indicates that the crystals, although imperfect, are composed of mosaic blocks which are larger or better aligned than is usual for large single crystal specimens. These intensities are affected by the method of preparing the crystal powders.

It would be of great interest to develop a similar method for producing uniform size-graded crystals of calcite, which has been found almost unique in its tendency to form perfect large crystals. It might very well be expected that reflection intensities would correspond to full primary extinction effects.

The author wishes to express his most sincere appreciation to Dr. S. K. Allison, who sponsored this research and made valuable suggestions, and to Dr. W. A. Zachariasen for his helpful suggestions and criticisms relating to crystal structure theory.

Cloud-Chamber Studies of Fission Fragment Tracks

K. J. BROSTRØM, J. K. BØGGILD AND T. LAURITSEN
Institute of Theoretical Physics of the University of Copenhagen, Copenhagen, Denmark
(Received July 9, 1940)

SHORTLY after the discovery of the fission phenomenon, cloud-chamber photographs of tracks of fission particles were published by Joliot[1] by Corson and Thornton[2] which illustrated the intense ionization and large tendency to branch by nuclear collisions of the fission particles with the gas in the chamber. Because of the great theoretical interest connected with the passage of such heavy and highly charged particles through matter, a more complete study of the phenomenon was taken up in this Institute.

For this purpose a 25-cm Wilson chamber was constructed with a special arrangement to permit use in the chamber of various gases at low pressure (~5 cm). A large number of photographs of tracks of fission fragments were obtained, partly from thick uranium targets within the cloud chamber and partly from targets thin enough to allow the tracks of the two fragments emitted in a fission process to be photographed simultaneously. These photographs, of which a few typical examples are reproduced here (Figs. 1 and 2), show striking differences from proton- and alpha-particle tracks in several respects. Branching by nuclear collision, instead of occurring only once in several thousand tracks, here occurs many times in a single track. Instead of pursuing a straight course to the end of their range, these particles show large irregular curvature, due to numerous collisions in which the momentum transfer in any single interaction is insufficient to give an observable branch. An analysis of the measurable branches indicates a range velocity relation radically different from that for light particles.

The histograms of Fig. 3 are the result of the measurement of branch lengths at various intervals along the ranges for about 40 fission tracks. All branches with length (in the chamber) greater than 1 mm were measured, and their lengths added together in groups. The ordinate in Fig. 3 represents the sum of the lengths of branches occurring in the interval given on the axis of abscissae. In all, some 400 branches are so classified. Since the ordinate can be taken to be a function of the energy loss due to branching, one would expect such a curve to give some indication of the variation of the velocity along the range. It seems, in a rough way at least, from these curves that a proportionately much larger number of branches are obtained in the region from 4 to 6 mm from the end of the range than one would expect if the velocity fell as rapidly in the last part of the range as does that of an alpha-particle. The steep falling off at the end is a result of the arbitrary minimum limitation on the lengths of the branches counted.

In a series of 150 fission fragment tracks taken in argon at low pressure, measurements on the

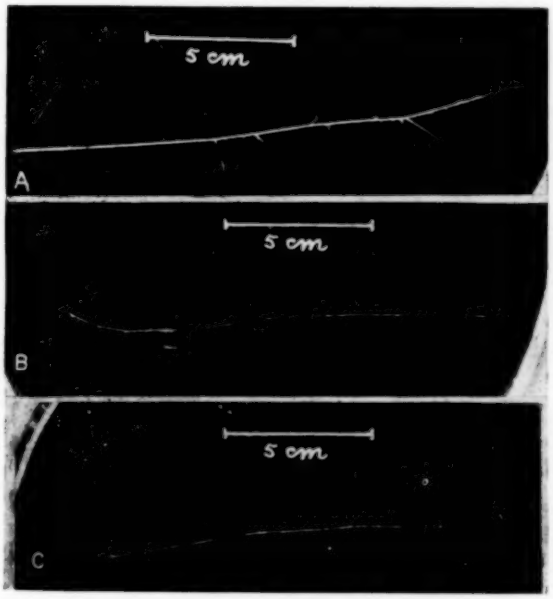

FIG. 1. A, Typical track in hydrogen, showing numerous collisions both with hydrogen and with oxygen or carbon atoms even relatively early in the range. The last $\frac{3}{4}$ of the total range is in the chamber. ($H_2+C_2H_6O$ and H_2O vapor, press. 14.5 cm, ~8 cm air.) B, Track in argon showing typical irregular curving. (Argon+20 percent oxygen+alcohol and water vapor, press. 7.5 cm, ~8 cm air.) C, Track in low pressure hydrogen, showing large number of fine proton branches. (H_2+H_2O vapor, press. 16 cm, ~6 cm air.)

[1] F. Joliot, Comptes rendus **208**, 647 (1939).
[2] D. R. Corson and R. L. Thornton, Phys. Rev. **55**, 509 (1939).

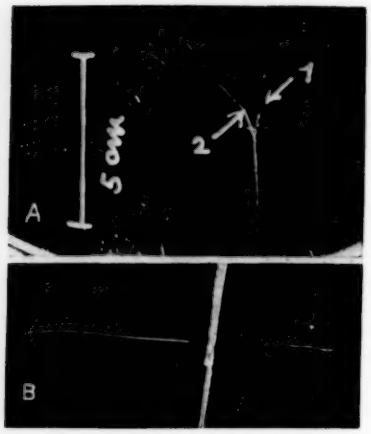

FIG. 2. A, Close encounter in argon; the end of fission fragment's track is indicated by arrow 1: at arrow 2, the projected argon nucleus collides with another, making an angle of 90°. (Argon+H_2O vapor, press. 7.5 cm, ~7 cm air.) B, Tracks of two fragments expelled simultaneously from a fission occurring in a layer of uranium evaporated on a 1μ aluminum foil. (Argon+alcohol and water vapor, press. =31 cm, ~30 cm air.)

angle of bending were made. On a photographic reproduction of each track, tangents were drawn through points at 5, 45, 85 and 125 mm from the end—(or through as many as the length of the track would permit). The angles between these tangents were measured and plotted as angles *a*, *b*, *c*, etc., referring to the various pairs of tangents. In all cases where the track suffered sharp bends due to measurable branches, the corresponding angular deflections were subtracted. As is clearly seen in Fig. 4, the last 45 mm (~$\frac{1}{4}$ of the range) suffers very large deviations, about half of the material lying outside 15°. The angles "*b*" show a considerably smaller deviation and angles "*c*" are barely measurable.

In general, the curvatures exhibited by tracks in hydrogen are considerably smaller, although the tendency is certainly present. An interesting point which has appeared is that argon branches traveling in argon gas are themselves often branched and also exhibit this general curvature. This effect, together with the haphazard curvature of the main track, makes angle and range measurements extremely unreliable except for special cases; it seems impossible, for example, to obtain any measure of the mass sufficiently precise to distinguish the two types of fragments.

In the examination of about 300 fission fragment tracks in various gases, about 30 branches have been obtained which are suitable for a direct determination of the velocity-range function by simple application of conservation of momentum and energy considerations. In all these cases, the tracks were examined stereoscopically and measurements made as nearly as possible in the plane of the branch. In the computations, the range-velocity curves for argon and for oxygen of Blackett and Lees[3]

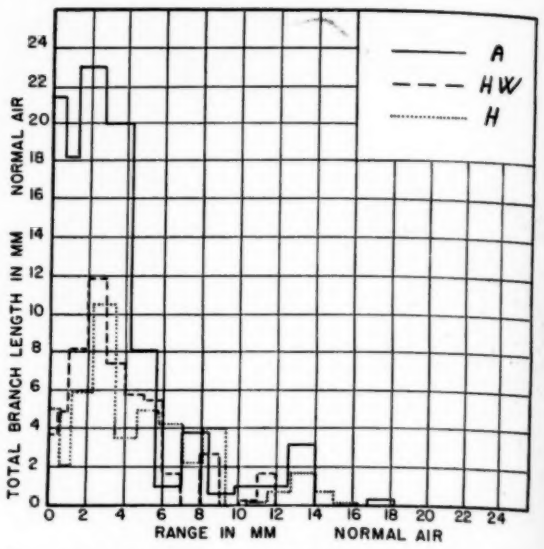

FIG. 3. Sum of lengths of all branches >1 mm long in various intervals along track. *A* = tracks in argon+alcohol and water vapor; press. = 8.8 cm, ~11 cm air, *H* = hydrogen +alcohol and water vapor; press. 14.5 cm, ~8 cm air, *HW* = hydrogen+water vapor 16 cm, ~6 cm air.

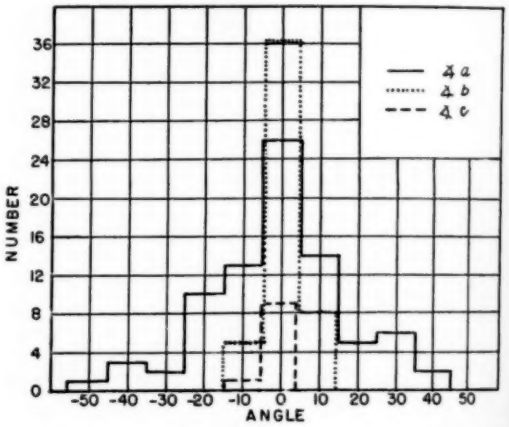

FIG. 4. Turning of fission fragment tracks. Angle "*a*" is the angle between tangent at 5 mm and that at 45 mm, from end of range. "*b*" is the corresponding angle at 45 and 85 mm and "*c*" refers to the region 85–125 mm. (Argon +alcohol and water vapor; press. 8.5 cm, ~11 cm air.)

[3] P. M. S. Blackett and D. S. Lees, Proc. Roy. Soc. 134, 658 (1931).

were used. The ranges were reduced to normal air, with the factors for alpha-particle stopping.[4] The resulting range-velocity relation is shown in Fig. 5, with that of an alpha-particle for comparison.[5] Inasmuch as it is impossible to separate the effects of the two types of fission fragments, this curve must be considered as a representation of some mean value, mass ~120, charge 45.

It has appeared from direct measurement that the total ranges of the two types of particles do not differ greatly and have a value of about 25 mm, corresponding to starting velocities of 14 and 9×10^8 cm/sec. From this it would seem that the curve of Fig. 5 should pass through a point at 25 mm range and velocity $\sim11\times10^8$ cm/sec. The general course of the curve would thus seem to be like that sketched in the figure, with a relatively rapid decrease in velocity from about 2×10^9 to a velocity in the neighborhood of 3×10^8 cm/sec., a more gentle slope down to perhaps 1×10^8 and then a steep fall at the end. It does not seem possible, with our present material to obtain more information in the range above 3×10^8 cm/sec., but just the fact that

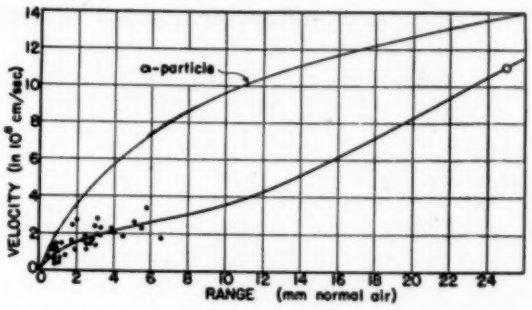

FIG. 5. Velocity *vs.* range for fission fragments. (Argon+alcohol and water vapor, press. = 8.5, ~11 cm air.)

branches become so rare here would indicate the starting of a more rapid increase of velocity with range at about this value.

A full account of this work will be published in the Communications of the Danish Academy of Science, where the photographs will be discussed in more detail.

It is a source of no little gratification to the authors to take this opportunity to express their most heartfelt appreciation of the advice and encouragement of Professor Niels Bohr, under whom this work was consummated. One of us (T. L.) is indebted to the Rockefeller Foundation for a stipend permitting his visit to Copenhagen.

[4] R. W. Gurney, Proc. Roy. Soc. **107**, 340 (1925).
[5] Cornell University curves, 1938.

Scattering and Stopping of Fission Fragments

N. BOHR
Institute of Theoretical Physics, University of Copenhagen, Copenhagen, Denmark
(Received July 9, 1940)

THE cloud-chamber pictures of tracks of uranium fission fragments in gases obtained by Brostrøm, Bøggild and Lauritsen[1] have revealed a number of interesting differences between such tracks and those of protons and alpha-particles. These differences may be simply shown to be caused by the comparatively high charge and mass of the fission fragments, which imply that nuclear collisions play a much greater part in the phenomenon than is the case for the ordinary light particles.

For such particles as protons and α-particles, measurable scattering in nuclear collision is comparatively rare, and practically all the stopping is caused by the interaction between the particles and the electrons in the gas atoms. For the fission tracks not only are branches due to close nuclear collisions the rule rather than the exception, but also the scattering and stopping effect of numerous less violent collisions is clearly shown in the irregular gradual bending of the tracks as well as in the peculiar form of the range velocity curve. Moreover, the contribution by the electrons to the stopping is greatly reduced by the fact that the fission fragments during their entire range will carry with them a large number of bound electrons, which, without essentially affecting the nuclear collisions, will in large part neutralize the effective charge of the fragments in electron collisions.

The continual capture and loss of electrons by the high speed fragments is a rather complex phenomenon, but, to a first approximation, we may assume that the fragment will possess an average effective charge equal to the ratio of its velocity V to the "orbital" velocity $V_0 \sim 10^8$ cm/sec. of the least tightly bound electron in the neutral atom. Since the orbital velocity of any electron is roughly proportional to the effective nuclear charge in the region concerned of the atom, this follows, in fact, if we assume that all the electrons carried with the fragment will have orbital velocities greater than or equal to V.

In an encounter between the fragment and a heavy atom possessing electrons lightly bound and also electrons with velocities greater than V, we may, moreover, assume that only the former electrons, in approximate number V/V_0, will be effective in the stopping. This is true since the faster electrons, just as the electrons carried with the fragment, will be merely adiabatically influenced during the encounter and will therefore have no retarding effect.

The calculation of the stopping power under such conditions, is particularly simple since, because of the comparatively high effective atomic charges, classical mechanics can be directly applied in calculating the energy and momentum transfer during the collisions. Using the above estimates of the effective charges and denoting by μ and ϵ the mass and charge of the electron, we get for the average rate of velocity loss for the fragment of mass M and charge number Z in a gas with N atoms per unit volume, each with nuclear mass m and charge number z,

$$\frac{dV}{dx}=\frac{4\pi\epsilon^4 N}{M\mu V_0^2}\left\{\ln\left(\frac{V}{V_0}\right)^2+\frac{Z^2z^2\mu(M+m)}{Mm}\left(\frac{V_0}{V}\right)^2 \times\ln\left[\frac{Mm(Z+z)}{\mu(M+m)Z^2z^2}\left(\frac{V}{V_0}\right)^2\right]\right\}, \quad (1)$$

where the first term in the bracket originates from electronic interaction, while the second is due to direct nuclear collisions.

In the case of a fission fragment of mass and charge numbers 140 and 50, traveling through argon gas with mass and charge numbers 40 and 18, the constant factor before the logarithm in the second term is about 10. This term, which, for the initial part of the range, where the velocity is about $20V_0$, is much smaller than the first term, will thus be the greater near the end of the range when the velocity has fallen to

[1] K. J. Brostrøm, J. K. Bøggild, T. Lauritsen, preceding paper.

about $2V_0$. From formula (1), we shall therefore expect the range-velocity curve to have essentially different features at the beginning and at the end of the range. Neglecting the slow variation of the logarithms, we shall, in fact, expect the rate of velocity decrease to be practically linear at the beginning of the range and to vary as the inverse cube of the velocity at the end of the range.

A curve of just this character would seem to fit the experimental data and the agreement would seem to be quite satisfactory also in a quantitative respect. For a comparison between theory and experiment at the very end of the range, it is essential to note that it is a condition for the approximation concerned that the arguments of the logarithms in both terms are greater than 1. While this means that the first term can be used only for $V > V_0$, the second term will hold with some approximation even for $V < V_0$, since the constant factor in the logarithm argument will be about 10.

Since, according to (1), the rate of velocity loss is, in the major part of the range, independent of Z, and inversely proportional to M, it follows further that two highly charged nuclei with the same initial momentum will have approximately equal ranges. This fits in well with the experimental finding that the tracks of the two fragments resulting from a single fission process in a thin uranium target have nearly the same length, although their masses and charges should in general differ considerably. In this connection, it may also be noted that, because of the preponderant effect of the nuclear collisions in the end part of the range, one should expect a straggling far greater than for protons and α-particles. While for light particles, the mean square value of the fractional straggling in range is of the same order of magnitude as the ratio of the mass of the stopping electrons to that of the moving particle,[2] we shall, in fact, expect that this value will be of the order of m/M for a considerable part of the range of fission particles.

Furthermore, the characteristic curving of the fragment tracks revealed by the cloud-chamber pictures can be shown to be a simple consequence of the scattering effect of the numerous nuclear collisions too small to give rise to detectable branching. In fact, it is easily shown that the mean square of the deviation in angle within a part of the range where the energy is changed by ΔE is given by

$$\Phi^2 = \frac{m}{M} \cdot \frac{\Delta E}{E} \left[\frac{\Delta_N E}{\Delta_N E + \Delta_e E} \right], \qquad (2)$$

where $\Delta_N E$ and $\Delta_e E$ are the fractional contributions to ΔE of the nuclear and electronic collisions respectively. While the bracketed term is small in the beginning of the range, it is, near the end of the range, almost equal to 1, and here, where the bending is easily measurable, formula (2) agrees quite satisfactorily with the experiments.

The calculations here indicated will be given in greater detail in a paper to be published in the *Communications of the Copenhagen Academy of Science.*

[2] N. Bohr, Phil. Mag. **30**, 581 (1915).

LETTERS TO THE EDITOR

Prompt publication of brief reports of important discoveries in physics may be secured by addressing them to this department. Closing dates for this department are, for the first issue of the month, the eighteenth of the preceding month, for the second issue, the third of the month. Because of the late closing dates for the section no proof can be shown to authors. The Board of Editors does not hold itself responsible for the opinions expressed by the correspondents.

Communications should not in general exceed 600 words in length.

$(d, 2n)$ Reaction in Copper

Recently a stack of one-mil copper foils was bombarded with 16-Mev deuterons from the 60-inch Berkeley cyclotron. The activity of each foil was followed with an electrometer. Fig. 1 shows the results obtained.

A strong activity apparently assignable to the reaction $Cu^{63}(d, 2n)Zn^{63}$ (half-life 38 minutes)[1] was observed. Further study verified this assignment and revealed several properties of the reaction.

Curve 1 (Fig. 1) gives the relative cross section (in arbitrary units) for the formation of Zn^{63} at various bombarding energies. (Zn^{63} activity at highest point plotted in Fig. 1 is of the order of a half-millicurie.) The energy plotted is that at the center of the respective foils (~10 cm air equivalent each). The maximum energy of the cyclotron beam was fixed as 16 Mev by the frequency and geometry of the cyclotron. The energy was calculated for each foil from the residual range, measured visually with the aid of a ZnS screen, and the formula of Livingston and Bethe. The inhomogeneity of the beam, and the fact that the maximum energy of the beam measured visually is about 7 percent less than that calculated by the frequency and geometry makes the energy scale somewhat uncertain.

The threshold of the reaction $Cu^{63}(p, n)Zn^{63}$ is variously reported as 3.6 Mev[2] and 4.1 Mev.[3] The threshold of the $Cu^{63}(d, 2n)Zn^{63}$ reaction should be higher than this value by an amount equal to the binding energy of the deuteron (2.2 Mev), or approximately 6 Mev. Qualitatively one would expect the yield curve to be flat near the threshold because (1) the Oppenheimer-Phillips process competes to give active Cu^{64}, (2) the Coulomb barrier is ~8 Mev, and (3) on Bohr's compound nucleus model of disintegration, the probability near the threshold for the emission of two neutrons is very much smaller than that for the emission of a proton or single neutron. The ratio $\sigma(d, 2n)/\{\sigma(d, n)+\sigma(d, 2n)\}$ can be calculated from the theory of Weisskopf[4] and indicates that the $(d, 2n)$ reaction should be observable first at about 7 Mev. Activated contaminants in the copper limited the measurements of Zn^{63} activity near the threshold. Even with chemical separation of the zinc, activity could be established definitely only as low as 7.5 Mev. These latter data were obtained by bombarding 0.1-mil copper foils with 8.5-Mev deuterons produced by the 37-inch Berkeley cyclotron (the beam energy being varied by aluminum absorbers). The use of the smaller cyclotron increased considerably the accuracy of measurements of the beam energy near the threshold.

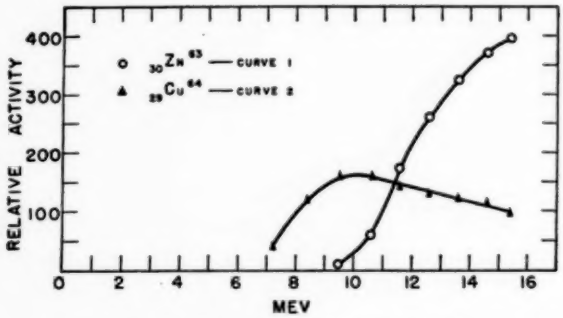

FIG. 1. Relative cross sections of Zn^{63} and Cu^{64}.

Absorption curves in aluminum indicated that the energy of the electrons was in agreement with previously reported values.

Curve 2 (Fig. 1) gives the relative cross section on the same scale for the production of Cu^{64} (half-life 12.8 hours) obtained by following the activities in the same stack of foils. The maximum observed can be explained qualitatively as follows. Cu^{64} can be formed by the Oppenheimer-Phillips process or by the (d, p) process with the deuteron entering the nucleus. The excited Zn^{65*} may disintegrate by emission of (p), (n), $(2n)$, $(n$ and $p)$, etc., the last two becoming more probable as the excitation energy increases. The Oppenheimer-Phillips process will gradually decrease above the barrier (~8 Mev) and competition between the above processes will become more important.

Clearly these processes can account for the same effect (falling off of Cu^{64} yield near 9 Mev) observed by Krishnan and Banks[5] and attributed by them to competition of $Cu^{63}(d, 2n$ and $p)Cu^{62}$. The latter reaction has been shown to be energetically impossible at 9 Mev by Goldhaber.[6]

We are indebted to Professor E. O. Lawrence and to the staff of the Radiation Laboratory for their valuable advice and assistance in this study, and to Professor V. F. Weisskopf for a helpful discussion.

R. S. LIVINGSTON
B. T. WRIGHT

Radiation Laboratory,
University of California,
Berkeley, California,
September 7, 1940.

[1] J. J. Livingood and G. T. Seaborg, Rev. Mod. Phys. 12, 36 (1940).
[2] L. A. Delsasso, *et al.*, Phys. Rev. 55, 116 (1939).
[3] C. V. Strain, Phys. Rev. 54, 1021 (1938).
[4] V. F. Weisskopf and D. H. Ewing, Phys. Rev. 57, 472 (1940).
[5] R. S. Krishnan and T. E. Banks, Nature 145, 777 (1940).
[6] M. Goldhaber, Nature 146, 167 (1940).

The Magnetic Properties of Metallic Cerium*

The magnetic behavior of cerium has been studied as a function of field strength and temperature. Several unusual characteristics were found. The cerium had the following analysis: Ce 97 percent, Fe 0.5 percent, CeO_2 0.7 percent, and the remainder other earths. The measurements were made by a method previously described.[1] The experimental results are shown in Figs. 1 and 2, where σ is the magnetization per gram, χ is the high field strength differential susceptibility $(d\sigma/dH)$ per gram, and all temperatures are °K. The intercept values plotted in Fig. 2 represent the value of σ found from Fig. 1 by a linear extrapolation back to zero field of the high field portion of the magnetization curve. If the magnetic behavior of cerium is considered as

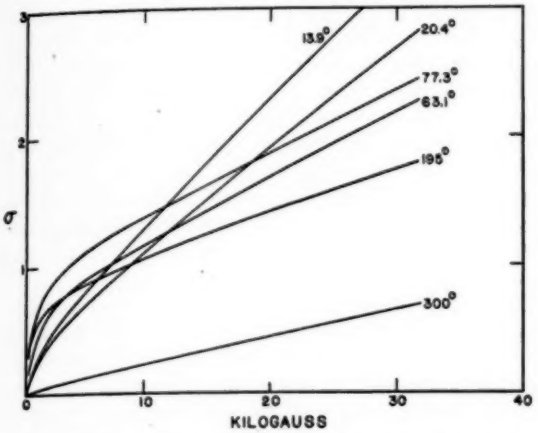

FIG. 1. The magnetization per gram as a function of the field strength for various °K.

a combination of paramagnetic and ferromagnetic terms, the magnitude of the intercept represents the saturation magnetization of the ferromagnetic term. The paramagnetic term χ appears to follow a Curie-Weiss law at high temperatures, becoming somewhat anomalous at low temperatures. The observed intercept values shown in Fig. 2 differ from that expected from the usual ferromagnetic impurity in that they decrease with decreasing temperatures at low temperatures, instead of approaching a maximum value.

The 0.5 percent Fe in the cerium may be in solution, precipitated, or as a Ce—Fe intermetallic compound. If the Fe were completely precipitated, it would be sufficient to account for the maximum observed intercept, but the effect should begin at the Curie point of Fe, 1043°K, be almost at its maximum at 300°K, and should not decrease at lower temperatures. Extension of the measurements to 800°K revealed no appreciable change in the room temperature value of the intercept, which is therefore probably due to a small amount of precipitated iron. The intermetallic compound $CeFe_2$ is reported to be ferromagnetic with a Curie temperature of 389°K, but no evidence of its presence was found. Apparently, whatever the cause of the unusual intercept characteristic, it is not due to a ferromagnetic impurity of the customary type.

The experimental results are reproducible and are not

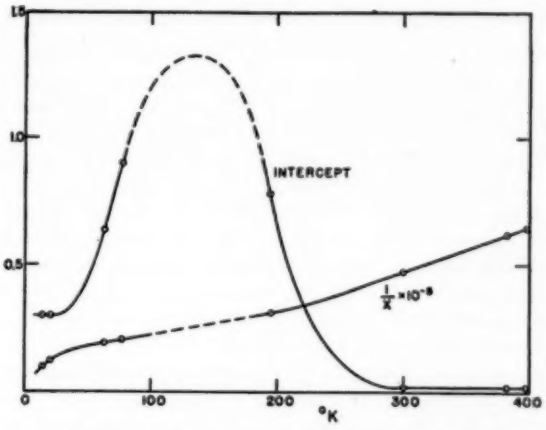

FIG. 2. The magnetization intercept and the reciprocal high field susceptibility as a function of temperature.

affected by repeated cooling and warming cycles below room temperature. There was no difference in the measurements at 20.4°K when the specimen was rapidly cooled (1 minute) from 300°K or slowly cooled (30 minutes). Since the rate of cooling has no effect, the results cannot be attributed to a sluggish phase transition occurring over a range of temperature. Prolonged aging at room temperature or high temperature heat treatment produces quantitative changes but not qualitative. A high temperature anneal at 500°C for one hour and 300°C for 12 hours resulted in an increase of the intercept at 300°K and a decrease at 77.3°K. It has been shown[2] that cerium has at least three stable phases, β (hexagonal) at room temperature, γ (cubic) above 393°C, δ above 440°C. Because of the sluggishness of the phase transitions the cerium has a mixture of these phases at any temperature, and the proportions of this mixture would be influenced by heat treatment. Trombe[3] made measurements on an impure cerium specimen down to 99°K where he found a dependence of susceptibility upon the field strength. He also reports a temperature-susceptibility hysteresis between 100 and 200°K, which may indicate another phase, α at low temperatures. In the present measurements at 13.9° and 20.4°K, the magnetization measured with increasing fields was several percent less than with decreasing fields. This magnetic hysteresis disappeared at higher temperatures.

In order to determine whether these unusual properties are characteristic of pure cerium or are caused by the presence of the iron impurity, an attempt will be made to obtain an iron-free sample of metallic cerium for further study.

The authors express their appreciation for the valuable suggestions and cooperation given by Professor F. Bitter.

C. STARR
A. R. KAUFMANN

Massachusetts Institute of Technology,
Cambridge, Massachusetts,
September 9, 1940.

* Contribution No. 466 from the Research Laboratory of Physical Chemistry.

[1] F. Bitter and A. R. Kaufmann, Phys. Rev. **56**, 1044 (1939).
[2] F. M. Jaeger, J. A. Bottema and E. Rosenbohm, Rec. trav. chim. **57**, 1137 (1938).
[3] F. Trombe, Comptes rendus **198**, 1592 (1934).

A Precise Determination of the Fine Structure Constant

About a year ago, R. T. Birge[1] suggested the possibility of an experimental determination of the fine structure constant based on measurements of the x-ray spin doublet splitting ($L_{II}-L_{III}$ levels). A direct determination of this quantity is of interest because of the discrepancies existing in the values of the atomic constants, and because of controversial ideas as to the value of this constant itself. Birge assembled data on the doublet splitting as obtained in several different x-ray lines, and in elements varying in atomic number from $Z=29$ to 92. He showed that these data formed a body of material of sufficient accuracy and consistency for such a determination.

We have recently completed calculations giving the theoretical behavior of the spin doublet splitting for elements of high atomic number. The Sommerfeld formula for the energy difference between the $2P_{1/2}$ and $2P_{3/2}$ levels (in units of mc^2),

$$S(\alpha Z)=\tfrac{1}{2}\{4-(\alpha Z)^2\}^{\frac{1}{2}}-\tfrac{1}{2}\{2+2[1-(\alpha Z)^2]^{\frac{1}{2}}\}^{\frac{1}{2}} \quad (1)$$

gives the splitting due to the Coulomb field of the nucleus alone. The effect of the electrons on the splitting is of order $1/Z$ compared to that of the nuclear charge because only those few electrons lying close to the nucleus contribute essentially. Thus we can calculate the effect of the electrons by perturbation theory, where $1/Z$ is the parameter of expansion. We have carried out this calculation, using the Dirac wave functions in a Coulomb field of charge Ze for our zero-order wave functions. Complete interactions of electrons of the K and L, and direct interactions of the M shell on the $2P_{1/2}$ and $2P_{3/2}$ states have been carried out in first order, with the use of the Breit Hamiltonian.

We thus get the interaction energy of the electrons as a function of αZ. The first-order term can be obtained to an arbitrary accuracy, both in magnitude and in its functional dependence on αZ. In the higher order terms in $1/Z$, the lowest term in αZ could in principle be determined by higher order perturbation calculation. Further terms in αZ cannot be so determined because of fundamental limitations of present quantum-electrodynamic theory. But these terms are of order α^2 times the splitting and are negligible. Actually, we do not calculate even the coefficient of the leading terms in αZ of the second and higher order perturbation terms, but consider it sufficient to introduce arbitrary coefficients, which will be determined by fitting the experimental data.

Assuming that the Rydberg constant is given correctly by $R=2\pi^2me^4/h^3$, we represent the experimental data in the form

$$\frac{\Delta\nu}{RZ^4}=\frac{2}{\alpha^2Z^4}S(\alpha Z)-\frac{2g\alpha^2f(\alpha Z)}{Z}+\frac{B\alpha^2}{Z^3}. \quad (2)$$

$f(\alpha Z)$ is the first-order term we have calculated. Because we have neglected interactions of electrons beyond the M shell, we have introduced the constant g, whose value is nearly unity. We estimate that g may differ from unity by at most one percent. Taking g as unity, we have made a least-squares solution based on Eq. (2), using data from $Z=60$ to 92. We obtain a value of $1/\alpha=136.95$, with a statistical probable error of 0.019. An error of one percent in g would produce an error of 0.068 in $1/\alpha$. To obtain an over-all limit of error, we take three times our statistical error and add to it the possible error arising from the uncertainty in g. *This gives us* $1/\alpha=hc/2\pi e^2=136.95$, *which we believe correct to within 0.13.*

We are indebted to Professor J. R. Oppenheimer for pointing out to us this method of calculating the splitting, and for continual encouragement.

R. F. CHRISTY
J. M. KELLER

Department of Physics,
University of California,
Berkeley, California,
September 16, 1940.

[1] R. T. Birge, Phys. Rev. **55**, 1119 (1939).

The Values of e, e/m, h/e and α

There has existed for several years a fundamental discrepancy between the directly measured values of e, e/m and h/e, namely, that the "best" numerical values of these three quantities do not satisfy the Bohr formula for the Rydberg constant. The writer emphasized this point some time ago,[1] and the situation has since been frequently discussed, particularly by DuMond. Unfortunately there has not been available, thus far, any fourth quantity whose value appeared to be known with sufficient reliability to throw any real light on the discrepancy.

A year ago I showed[2] that the then available data on the $L_{II}L_{III}$ interval, as determined from x-ray wave-lengths, were sufficiently extensive and precise to give a reliable value of the fine structure constant. It was, however, immediately pointed out to me by J. R. Oppenheimer that a really trustworthy value could be obtained only from a detailed study of the matter, on the basis of modern quantum mechanics. Such a study has now been made, under his direction, by J. M. Keller and R. F. Christy, and is reported in the preceding letter. The result is $1/\alpha=136.95$, with a probable error that I take to be ±0.05. This probable error is about one-tenth that of the best previous determination. The new value of $1/\alpha$ thus constitutes the desired fourth quantity.

In August, 1939, I prepared a mimeographed list of the general constants, and submitted it to many persons for suggestions and criticism. In preparing the list I used the latest values of all auxiliary constants, and in particular I *assumed* that the directly observed values of e and e/m were correct, and that the Rydberg constant formula was valid. All recent theoretical work seems to justify this last assumption. The correlated conclusion is then that the seemingly most reliable measurements of h/e (from the Duane-Hunt limit of the continuous x-ray spectrum) give a result much too low. The relevant adopted values on my 1939 list are $e=(4.8022\pm0.0010)\times10^{-10}$ e.s.u., $e/m=(1.7591\pm0.0005)\times10^{7}$ e.m.u., $R_\infty=109{,}737.45\pm0.06$ cm^{-1}. On the basis of subsequent work by Miller and DuMond,[3] I deem it best to increase the probable error of e to ±0.002, but for the present I shall not modify the actual value of e. One then calculates, from the Rydberg constant formula, $h/e=(1.37929\pm0.00040)\times10^{-17}$, as contrasted with DuMond and Bollman's directly observed[3] 1.3765 ± 0.0003. This is the fundamental discrepancy.

There have already appeared some indications of possible sources of error in the experimental values of h/e, but quite aside from this point, the new experimental value of $1/\alpha$ furnishes strong evidence that the indirectly calculated value of h/e (1.3793), rather than the observed value, is substantially correct. Thus, again using the observed values of e and e/m, and the Rydberg constant formula, one obtains $1/\alpha=137.036\pm0.023$, which is in very fair agreement with the new observed value. But if one uses the observed values of e and h/e (the Rydberg formula not being then involved), the result is $1/\alpha=136.758\pm0.065$, which is in significant disagreement with the observed value.

It thus appears now that the values adopted in my August, 1939, list of constants are at least substantially correct, but it seems to me preferable to await the results of experimental work on h/e now in progress, before preparing any extended discussion of the general constants.

RAYMOND T. BIRGE

University of California,
Berkeley, California,
September 16, 1940.

[1] R. T. Birge, Nature **137**, 187 (1936).
[2] R. T. Birge, Phys. Rev. **55**, 1119 (1939).
[3] P. H. Miller, Jr., and J. W. M. DuMond, Phys. Rev. **57**, 198 (1940).
[4] J. DuMond and V. Bollman, Phys. Rev. **51**, 400 (1937). Revised auxiliary constants are used to get the quoted value.

Some Experiments on the Relative Cross Sections of the (n, α) and (n, p) Reactions Produced by Fast Neutrons

Some elements become radioactive when they are bombarded by fast neutrons according to the reactions (n, α) and (n, p). The half-periods of these induced activities are already determined by many authors. We can therefore study some properties of these reactions by measuring the intensities of the induced activities of these elements.

To determine relative cross sections of these reactions we bombarded some elements with fast neutrons produced from a lithium or beryllium target by deuterons of energies about 3 Mev obtained in our cyclotron.

Since the energies of neutrons are not homogeneous in this case, the results obtained are somewhat complicated and not easily interpreted. But some rough idea about the relative cross sections of these reactions may be obtained from these results.

TABLE I. *Relative cross sections for (n, p) reactions.*

Active Substance	Period	Sample	σ_{rel} Li+D Neutron	σ_{rel} Be+D Neutron
$_{11}Na^{24}$	15 hr.	Mg	1.6	0.13
$_{12}Mg^{27}$	10 min.	Al	1	1
$_{13}Al^{28}$	2.36 min.	Si	2.7	1.4
$_{14}Si^{31}$	2.5 hr.	P	2.4	5.5
$_{15}P^{32}$	14.5 day	S	6.0	13
$_{18}A^{41}$	110 min.	KCl	0.83	—
$_{19}K^{42}$	12.4 hr.	$CaCO_3$	5.3	1.5
$_{25}Mn^{56}$	2.5 hr.	Fe_2O_3	0.88	0.29
$_{26}Fe^{59}$	47 day	CoO	1.1	1.6
$_{27}Co^{60}$	11 min.	Ni	—	(0.022)
$_{28}Ni^{62}$	2.6 hr.	Cu	0.19	—
$_{29}Cu^{64}$	12.8 hr.	Zn	2.6	5.3

TABLE II. *Relative cross sections for (n, α) reactions.*

Active Substance	Period	Sample	σ_{rel} Li+D Neutron	σ_{rel} Be+D Neutron
$_{11}Na^{24}$	15 hr.	Al	1	1
$_{13}Al^{28}$	2.36 min.	P	—	0
$_{15}P^{32}$	14.5 day	KCl	2.5	122
$_{21}Sc^{48}$	41 hr.	V_2O_4	0.052	—
$_{25}Mn^{56}$	2.5 hr	CoO	0.20	0.38

The relative cross sections were determined by the following method. As the standard for comparison we have chosen the activities induced in aluminum foil by (n, α) and (n, p) processes. When aluminum is bombarded by fast neutrons, there are produced, as is well known, two radioactive substances, namely, Na^{24} (15 hr.) and Mg^{27} (10.5 min.). The activity 2.3 min. (Al^{28}) produced by slow neutrons can be almost suppressed by shielding the aluminum foil with cadmium of thickness about 2 mm. The elements to be studied were enclosed with aluminum foil of standard size in a small cadmium case of thickness of about 2 mm, and placed near the Li or Be target of our cyclotron. After bombarding them for a suitable time with fast neutrons, the activities induced in the samples as well as in the aluminum foil were measured by a Lauritsen electroscope. By brief calculations one can compute the relative cross section from the ratio of the intensities of the initial activities of the samples.

Now to see the order of the fluctuation of the neutron intensity and to check the reliability of the standard (Al), we measured the ratio of the intensities of the two activities (15 hr. and 10 min.) induced in aluminum by changing the length of bombarding time. In the case of Be+D the maximum error was 30 percent, and in the case of Li+D 10 percent.

The activity 10 min. (N^{13}) which might be produced in aluminum from occluded air and might cause an error in the ratio of 10 min. (Mg^{27}) and 15 hr. (Na^{24}) could be reduced by washing the aluminum samples with nitric acid before bombardment. With this method we determined the relative cross sections of several elements which are lighter than Zn.

The results are shown in Tables I and II, where the cross sections Al^{27} (n, p) Mg^{27} and Al^{27} (n, α) Na^{24} are taken as unity for the (n, p) and (n, α) reactions, respectively.

These figures are of course corrected for the absorption of β-rays in the source itself and the aluminum window of the electroscope, except for Co^{60}, since its energies of β-rays are not known. From the tables we can see the wide range of variation in these cross sections far exceeding the error of measurements.

In conclusion we wish to express our best thanks to Dr. Y. Nishina for his kind interest throughout this work.

TOSHIO AMAKI
ASAO SUGIMOTO

Nuclear Research Laboratory,
Institute of Physical and Chemical Research,
Tokyo, Japan,
August 24, 1940.

Secondary Emission and Electron Diffraction on the Glass Surface

The optical surfaces of some optical glasses especially those containing a high percentage of barium and lead often show stain or interference hues due to very thin films of compounds formed on the glass surface as a result of attack by moisture or by various vapors contained in the atmosphere.

Because of the minute quantities involved, these compounds can hardly be analyzed chemically or by x-rays. We have succeeded, however, in obtaining electron diffraction patterns of such surfaces.

The difficulty with obtaining diffraction photographs from the surface of a good insulator results from the charging up of this surface. The method here used has obviated that difficulty. Measurements[1] show that the secondary emission of electrons from a glass surface increases from 1 to a maximum of about 2 as the velocity of the primary electron beam increases to a few hundred volts. As the velocity is further increased the emission factor decreases and becomes smaller than 1.

In the present experiments a beam of high velocity electrons (40–50 kv) which is to be diffracted was projected on the surface. At the same time a beam of low velocity electrons (~300v) was projected on the same surface in a direction perpendicular to the high velocity beam and at about 30° to the surface normal. By adjusting the intensity of this beam the resulting secondary emission factor for the two beams could be made zero and as a consequence the surface would remain electrically neutral.

With this technique it was found that a freshly polished surface of glass shows amorphous halos as indicated in Fig. 1A at $\sin \frac{1}{2}\theta/\lambda = 0.13, 0.20, 0.37$. These values differ somewhat from previous results of transmission experiments on an amorphous silica film.[2] This suggests that the polished layer has a structure different from that of the base glass.[3]

Surfaces which have become tarnished give various diffraction rings which differ according to atmospheric conditions, time, and kind of glass. Polished surfaces of optical glass containing a high percentage of BaO (e.g., SK_4, $BaLF_4$) and a high percentage of PbO (e.g., SF_2, SF_5) after being kept about two months in an atmosphere rich in humid SO_2 gas at room temperature show interference colors produced by a film the thickness of which is of the order of the wave-length of light. Investigation shows that this film is $BaSO_4$ in the case of barium glass (Fig. 1B) and that it is a mixture of PbS and $PbSO_4$ in the case of the lead glass (Fig. 1C). A detailed account will be reported in a Japanese journal.

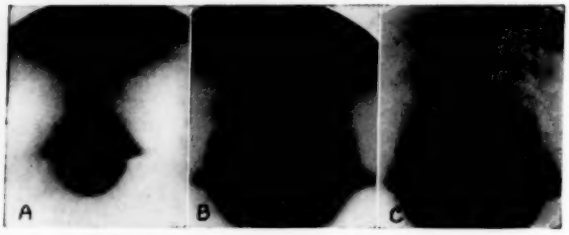

FIG. 1. A, Amorphous diffraction halos from a polished glass surface. B, Diffraction rings from the surface of a tarnished barium optical glass ($BaLF_4$). C, Diffraction rings from a tarnished lead optical glass (SF_2).

We wish to express thanks to Dr. K. Fuwa, Director of our Research Laboratory, under whose guidance this experiment was carried out and to Professor Y. Shibata, Dr. S. Tanaka, Mr. M. Nagaoka, and Mr. K. Harai, the members of the committee of the Japan Society for the Promotion of Scientific Research for their valuable suggestions and cordial assistance.

HIROSI KAMOGAWA

Research Laboratory,
Tokyo Shibaura Electric Company,
Matsuda Division,
Kawasaki, Japan,
August 1, 1940.

[1] H. Salow, Zeits. f. Physik **21**, 8 (1940).
[2] L. R. Maxwell and V. M. Mosley, Phys. Rev. **47**, 331 (1935); H. Kamogawa, *ibid.* **54**, 91 (1938).
[3] Beilby, Proc. Roy. Soc. **A72**, 220 (1903); Lord Rayleigh, *ibid.* **A156**, 329 (1936).

Fission Products of Uranium by Fast Neutrons

Under the above title we reported[1] the results of investigations on silver, cadmium and indium isotopes obtained from uranium by bombardment of fast neutrons. In continuing our experiments we found that palladium isotopes are also produced by fission, and one of them is the mother substance of the 3.5-hour silver isotope, Ag^{112}, which was mentioned in the above note. The experimental procedure was as follows.

The palladium fraction, which was separated as dimethylglyoxime salt from an irradiated sample and was carefully freed from the known fission products of uranium such as silver, antimony, tellurium, iodine, molybdenum, barium, lanthanum, cadmium, indium, etc., as well as from uranium itself, was examined for its activity. The decay curve, which was obtained from samples of long exposure, shows two periods, the longer one being 17 hours and the shorter one 26 minutes.

Under the supposition that the 17-hour palladium probably forms the mother substance of the 3.5-hour silver isotope mentioned above, we tried the search for this daughter product in the following manner. After 15 hours from the time of separation, the palladium compound was ignited, the residue was fused with sodium bisulphate and the melt was dissolved in water. From this solution, after adding silver nitrate as carrier, silver was precipitated as silver chloride. From the filtrate, palladium was precipitated with hydrogen sulphide. Both precipitates were then tested for the activity. The decay curve of the silver chloride showed a half-value period of 3.5 hours, which was ascribed to Ag^{112} as mentioned in the above note in *Nature*. A similar method was tried to see if any silver isotope is produced from the 26-min. palladium but the result was negative. It is thus clear that the 3.5-hour silver grows from the 17-hour palladium, which therefore is identified with Pd^{112}. On the other hand, the identification of mass number of the 26-min. palladium is not yet certain.

The results of our investigations on the fission products of uranium so far obtained by fast neutrons are summarized in Table I.

TABLE I. *Summary of the identifications of fine products of uranium bombarded by fast neutrons.*

ELEMENT	HALF-PERIOD	ISOTOPE	RADIATION	MAXIMUM ENERGY (MEV)
Pd	26 min. 17 hr.	112	electrons	
Ag	7.5 day 3.5 hr.	111 112	electrons electrons	0.8 2.0
Cd	56 hr. 3 hr. 50 min.	115 117		
In	4.5 hr.	115*	γ-rays conversion electrons	0.31–0.35 0.28
	2 hr.	117	electrons	1.8

* Radioactive isomer of stable nucleus.

The above investigations were carried out as a part of the work of the Atomic Nucleus Sub-Committee of the Japan Society for the Promotion of Scientific Research. We acknowledge the assistance given by our laboratory colleagues in connection with the irradiation of samples and by Messrs. N. Saito and N. Matuura regarding the chemical separations.

Y. NISHINA
T. YASAKI

Nuclear Research Laboratory,
Institute of Physical and Chemical Research,

K. KIMURA
M. IKAWA

Chemical Institute,
Faculty of Science,
Imperial University of Tokyo,
Tokyo, Japan,
August 10, 1940.

[1] Y. Nishina, T. Yasaki, H. Ezoe, K. Kimura and M. Ikawa, Nature, in press (1940).

On the Temperature Assignments of Experimental Thermal Diffusion Coefficients

When one calculates coefficients of thermal diffusion from viscosity data on the basis of a particular molecular model, the isothermal nature of viscosity measurements enables one to evaluate theoretically the coefficients at definite temperatures. The thermal diffusion coefficient can only be directly measured, however, when a temperature gradient exists. Comparison of theory with experiment then becomes rather difficult, because the measured value is essentially the "effective" value of the coefficient over a temperature range that is usually quite large. The problem then arises as to what definite temperature to assign an experimentally determined value.

The fundamental equation of thermal diffusion is

$$\text{grad } c_1 = -(K_T/T) \text{ grad } T, \tag{1}$$

where c_1, is the concentration (mol-fraction) of one of the constituents, T is the absolute temperature, and K_T is a quantity that for isotopes reduces to the form

$$K_T = \frac{105}{118}\frac{M_2-M_1}{M_2+M_1}R_T c_1 c_2, \tag{2}$$

the M's being the molecular weights and R_T being the ratio of the thermal diffusion coefficient for the given gas to that for rigid elastic spheres.

Assuming R_T independent of temperature, we then have from Eqs. (1) and (2)

$$\frac{118}{105}\frac{M_2+M_1}{M_2-M_1}\ln\frac{(c_1/c_2)_1}{(c_1/c_2)_2} = R_T \ln\frac{T_2}{T_1}. \tag{3}$$

If one then measures the concentrations of the constituents in the hot and cold sides of the apparatus, the value of R_T that one calculates from Eq. (3) will be an "effective" value of R_T over the temperature range T_1 to T_2, that we shall hereafter designate as R_e to distinguish it from the true value of R_T at a given temperature.

Let us now take into consideration the fact that R_T varies with temperature by assuming that the variation can be described approximately by an equation of the form

$$R_T = R_\infty - B/T. \tag{4}$$

R_∞ is the value approached by R_T as T increases, and B is a constant for a given gas. We see that if $R_\infty = 1$ we have the equation derivable from Sutherland's model neglecting terms of higher order in ϵ/KT.[1] R_∞ is used in this case instead of unity in order to make our result more general.

We have from Eqs. (1), (2), and (4)

$$\frac{118}{105}\frac{M_2+M_1}{M_2-M_1}\ln\frac{(c_1/c_2)_1}{(c_1/c_2)_2} = R_\infty \ln\frac{T_2}{T_1} - B\frac{T_2-T_1}{T_1T_2}. \tag{5}$$

We now want to find the temperature T_r at which our measured value, R_e becomes equal to the true value R_T. From Eqs. (3), (4) and (5), we find this to be

$$T_r = \frac{T_1T_2}{T_2-T_1}\ln\frac{T_2}{T_1}. \tag{6}$$

Actually one should use instead of Eq. (4) the equation derived from the particular model that one is comparing. However, Eq. (4) has two advantages. First, having two adjustable parameters, it can be made to represent with sufficient accuracy for our purpose the variation of R_T with temperature. Second, as we see from Eq. (6), the final result comes out independent of our constants R_∞ and B. For example, if one were to use the equation for the Sutherland model derived recently by Jones,[2] the final result, besides being much more complicated is dependent on the Sutherland constant, while at the same time values of T_r calculated in this manner differ but slightly from those calculated from Eq. (6).

In comparing the values for methane and neon measured by Nier[3, 4] with those calculated from viscosity, Brown[5] and Jones[1] have taken the measured value R_e to be roughly the value at the mean temperature $T_m = \frac{1}{2}(T_1+T_2)$. However, inspection of Eq. (6) shows that T_r is often considerably smaller than T_m, and if R_T falls at all rapidly with the temperature, serious error can result.

Nier[4] has measured R_e for neon over three temperature ranges. Jones calculates from Eq. (54) of his paper values of R_T at the mean temperature of the above temperature ranges, that are in rough agreement with experiment. For comparison, corresponding values of R_T calculated from Jones' equation at temperatures T_r as well as T_m are shown in Table I. We see that they are in somewhat better agree-

TABLE I. *Experimental values of R_s for neon and R_T values calculated from the Sutherland model.*

TEMPERATURE RANGE	T_m	T_r	R_s(NIER)	R_T AT T_m	R_T AT T_r
283°–617°K	450°K	407°K	0.71±0.02	0.77	0.75
90°–294°K	192°K	153°K	0.44±0.01	0.54	0.45
90°–195°K	142°K	129°K	0.39±0.03	0.42	0.38

ment with experiment, although this should not be taken too seriously at the present time, for as Jones points out, many difficulties still face the Sutherland model. The important point is that using values calculated at T_m instead of at T_r can lead one to errors of as much as 25 percent.

It is a pleasure to acknowledge the friendly interest of Dr. Robert Dudley Fowler, with whom the writer is engaged on an isotope separation project for which financial aid has been kindly given by Dr. H. A. B. Dunning.

HARRISON BROWN

Chemical Laboratories,
The Johns Hopkins University,
Baltimore, Maryland,
August 8, 1940.

[1] R. C. Jones, Phys. Rev. **58**, 111 (1940), Eq. (43).
[2] Reference 1, Eq. (54).
[3] A. O. Nier, Phys. Rev. **56**, 1009 (1939).
[4] A. O. Nier, Phys. Rev. **57**, 338L (1940).
[5] Harrison Brown, Phys. Rev. **57**, 242L (1940).

On the Fine Structure Pattern of Cosmic Rays at Mexico City

In August, 1940, a preliminary survey of directional cosmic-ray intensity was carried out at Mexico City, in search of a fine structure pattern analogous to that found at St. Louis, Missouri, by Ribner[1] and at Columbia, Missouri, by Cooper.[2] As in the Missouri experiments, the procedure here was to explore repeatedly a succession of zenith angles z at a given azimuth φ, and in this manner to determine the zenith angle intensity distribution $I(z, \varphi)$ for a predetermined set of azimuthal orientations φ. In the experiment described here, the four principal azimuths $\varphi=0°$, 90°, 180°, 270° (N, E, S, W) were explored in the zenith angle range $0° \leqq z \leqq 54°$ at angular intervals of 6°. The cosmic-ray telescope employed has been briefly described elsewhere.[3]

Before proceeding to our results, it should first be remarked that the fine structure pattern found in Missouri, $\lambda=50°$N, $h_0=10.6$ meters,[4] may be represented throughout the sky by an intensity surface $I(z, \varphi)$ possessing loci of prominences of very nearly circular form, concentric about the zenith.[2] There appear to be at least three such loci, at zenith angles $z=7°$, 20°, 35°. The possibility had been contemplated by one of us[5] that a pattern of this simple form might arise from the absorption of lines or bands inherent in the cosmic-ray spectra at infinity, provided that such spectral lines or bands were unaffected by the earth's magnetic field. This simple explanation has not been substantiated thus far by direct absorption measurements,[6] and so the possibility remains that the phenomena may have a geomagnetic or other origin. This peculiar circumstance added further incentive to undertake the present experiment at a lower geomagnetic latitude.

TABLE I. *Inner and outer prominences z_1 and z_2 (in degrees) for different azimuths φ.*

φ	z_1	z_2
N	(18)	42
E	18	42
S	12	48
W	12	42

Our present results at Mexico City, $\lambda=29°$N, $h_0=7.5$ meters,[4] are summarized in Fig. 1, where we have plotted $I(z, \varphi)$ directly,[7] in two curves. The top curve shows the variation of $I(z, \varphi)$ (that is, the total number of counts normalized to unity at the zenith) in the western and eastern azimuths; and the bottom curve shows the variation of $I(z, \varphi)$ in the southern and northern azimuths. It may be noted, in passing, that the top curve shows a marked west-east excess and the bottom curve an almost equally pronounced south-north excess, both agreeing well with those established by Johnson[8] at the same locality. The features of the curves which are of primary interest to us are the two prominences in each of the three azimuths E, S, W and the prominence (possibly two) in the N azimuth. Their positions are summarized in Table I. These results suggest, as the simplest hypothesis, that there are two oval loci of prominences, enclosing the zenith but slightly eccentric with respect to it. Whether or not this is the proper connectivity of the prominences remains to be decided by further exploration at smaller intervals of both azimuth and zenith angle. Such further exploration is now being undertaken with this object in view.

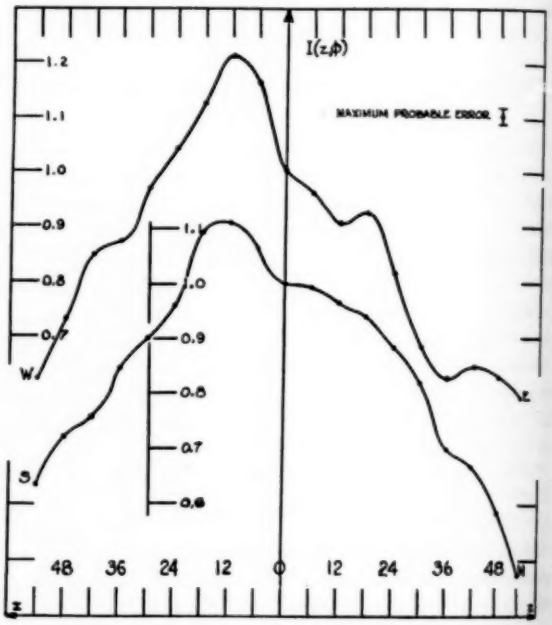

FIG. 1. Normalized directional cosmic-ray intensity $I(z, \varphi)$ at Mexico City, as a function of zenith angle z, for the four azimuths W, E (top curve) and S, N (bottom curve). The maximum probable error is about 1.5 percent, and the average probable error about 1.0 percent, of the zenith intensity.

To what extent the variations between the two patterns at Mexico City and Missouri are due, respectively, to changes of magnetic latitude and of altitude, and to what extent their loci of prominences are due, respectively, to particles of positive and of negative sign, are questions which must await further experimental results. The preliminary results which we have just described are presented at this time as a further confirmation of the existence and detectability of a fine structure pattern of cosmic rays, and of its potential value in the analysis of the primary radiations. A more extensive experimental program is now under way at Mexico City, the results of which we hope to report upon shortly.

This work was made possible by grants to one of us (E. J. S.) from the Penrose Fund of the American Philosophical Society and from the Rumford and Permanent Science Funds of the American Academy of Arts and Sciences, and by means of apparatus provided by Washington University. The National University of Mexico very generously provided facilities in Mexico City. Mr. J. E. Nafe cooperated in the shipment of apparatus to Mexico City and in the field work there.

E. J. SCHREMP

Washington University,
St. Louis, Missouri,

ALFREDO BAÑOS, JR.

Institute of Physics,
National University of Mexico,
Mexico City, Mexico,
September 14, 1940.

[1] H. S. Ribner, Phys. Rev. **56**, 1069 (1939).
[2] D. M. Cooper, Phys. Rev. **58**, 288 (1940).
[3] E. J. Schremp, Phys. Rev. **57**, 1061A (1940).
[4] Cf. E. J. Schremp and H. S. Ribner, Rev. Mod. Phys. **11**, 149 (1939) for definitions.
[5] Cf. E. J. Schremp and H. S. Ribner, reference 4, p. 150.
[6] Professor N. S. Gingrich and Mr. D. M. Cooper have privately communicated to us that their preliminary attempts at such direct measurements appear to give negative results.
[7] Rather than its deviation $\Delta(z)$ from the $\cos^2 z$ distribution, employed in references 1, 2 and 4.
[8] T. H. Johnson, Phys. Rev. **47**, 91 (1935); **48**, 287 (1935).